Photon-resolved Floquet theory approach to spectroscopic quantum sensing

Georg Engelhardt [1,*] Konstantin Dorfman,[2,3,†] and Zhedong Zhang [4,5,‡]
[1]*Shenzhen International Quantum Academy, Shenzhen 518048, China*
[2]*Center for Theoretical Physics and School of Physics and Optoelectronic Engineering, Hainan University, Haikou 570228, China*
[3]*Himalayan Institute for Advanced Study, Unit of Gopinath Seva Foundation, MIG 38, Avas Vikas, Rishikesh, Uttarakhand 249201, India*
[4]*Department of Physics, City University of Hong Kong, Kowloon, Hong Kong SAR, China*
[5]*Shenzhen Research Institute, City University of Hong Kong, Shenzhen, Guangdong 518057, China*

(Received 12 June 2025; accepted 5 November 2025; published 22 December 2025)

Spectroscopic methods play a vital role in quantum sensing, which uses the quantized nature of atoms or molecules to reach astonishing precision for sensing of, e.g., electric or magnetic fields. In the theoretical treatment, one typically invokes semiclassical methods to describe the light-matter interaction between quantum emitters, e.g., atoms or molecules, and a strong coherent laser field. However, these semiclassical approaches struggle to predict the stochastic measurement fluctuations beyond the mean value, necessary to estimate the sensitivity of spectroscopic quantum sensing protocols. Here, we develop a theoretical framework based on the recently developed photon-resolved Floquet theory (PRFT), which is capable of predicting the measurement statistics describing higher-order cumulants of coherent quantum states of light. The PRFT constructs flow equations for the cumulants of the photonic measurement statistics utilizing only the semiclassical dynamics of the matter system. We apply the PRFT to spectroscopic quantum sensing using dissipative two-level and four-level systems (describing electric-field sensing with Rydberg atoms), and demonstrate how to calculate the Fisher information of the measurement statistics with respect to various system parameters. In doing so, we demonstrate that the PRFT is a flexible tool allowing for improving the sensitivity of spectroscopic quantum sensing devices by several orders of magnitude.

DOI: 10.1103/btrr-bd3q

I. INTRODUCTION

Having tremendous importance in science and technology [1–4], spectroscopy studies atomic and molecular processes, such as isomerization [5], photo dissociation [6], conical intersections [7], polariton dynamics [8–10], as well as free-space superradiance [11–13] with astonishing precision. Moreover, spectroscopic methods find vital applications in quantum sensing [14–16], e.g., for the definition of the time-standard [17,18], the measurement of the gravitational field [19–21], and the detection of gravitational waves [22]. Protocols deploying entangled photons can improve spectroscopic precision [23,24] by circumventing the time-frequency uncertainty relation [25–27].

In particular, spectroscopic quantum sensing protocols utilizing coherent laser light, as sketched in Fig. 1, feature a simple design, robustness against high temperatures, and outstanding sensitivity. Two important examples are optical magnetometry [28–33] and electric-field sensing using Rydberg atoms [34–43], which usually deploy protocols based on the Faraday effect and electromagnetically induced transparency effect, respectively, to infer the strength of an external stimulus from the statistics of the measured intensity, polarization direction, or phase of the probe light. Both setups are currently deployed in the search for dark matter [44–47].

Crucially, the theoretical sensitivity estimation of spectroscopic sensing protocols using coherent light requires the modeling of the photonic measurement statistics: The mean value of spectroscopic signals can be calculated using the celebrated Maxwell-Bloch theory [48,49], which can be readily combined with analytical expansion methods for weak laser fields [50]. To predict high-order moments of the measurement statistics, more advanced methods such as phase-space methods [48], quantum trajectories [51], the input-output theory [52], Maxwell-Bloch-Langevin theory [53–55], Stokes operators for the description of Raman processes [56–58], or approaches based on the Heisenberg equations [59] can be employed. However, these methods invoke either drastic simplification on the matter system (e.g., neglect atomic memory effects) or are costly to numerically evaluate.

The shortcomings of the aforementioned theoretical methods motivate to develop a flexible, yet accurate framework for spectroscopic quantum sensing featuring the following properties: (i) The framework shall be based on a semiclassical approach, which allows for an efficient numerical evaluation and analytical analysis to gain insight into the underlying dynamics shaping the detected probability distribution. (ii) It shall generalize the Maxwell-Bloch theory in such that it is capable to predict the measurement statistics of time-integrated

*Contact author: georg-engelhardt-research@outlook.com
†Contact author: dorfmank@hainanu.edu.cn
‡Contact author: zzhan26@cityu.edu.hk

Published by the American Physical Society under the terms of the Creative Commons Attribution 4.0 International license. Further distribution of this work must maintain attribution to the author(s) and the published article's title, journal citation, and DOI.

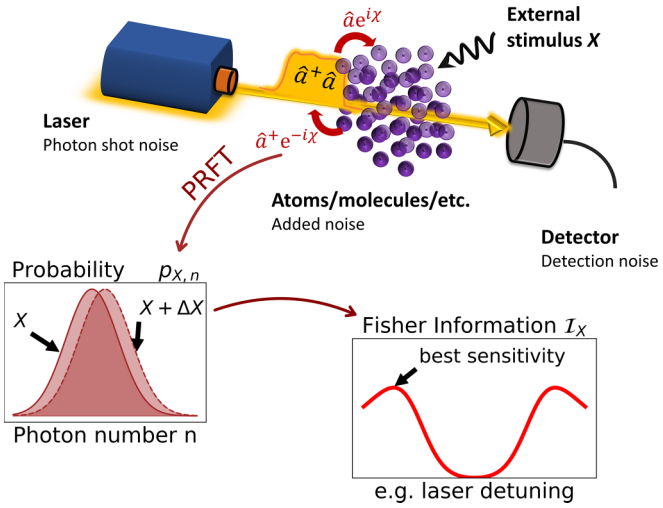


FIG. 1. Sketch of the spectroscopic setup, in which laser light interacts with an atomic ensemble, before it is finally measured by a detector. The PRFT includes counting fields χ in the semiclassical dynamics, allowing the prediction of the measured photonic probability distribution. The presence of an external stimulus X changes the measurement statistics from which one can estimate the strength of X. The Fisher information predicted by the PRFT assists in finding experimental parameters (e.g., the laser detuning) that optimize the measurement sensitivity.

spectroscopic observables (in particular, intensity, polarization direction and phase shifts), relevant for the sensitivity estimation within a finite measurement duration. Based on such a framework, it is then possible to predict the sensitivity in terms of the Fisher information, which can assist in the optimization of experimental control parameters, such as the laser detuning, as illustrated in Fig. 1.

To this end, we develop here a framework to predict the measurement statistics for quantum sensing devices using strong coherent light based on the recently developed photon-resolved Floquet theory (PRFT). This is a semiclassical method of light-matter interaction, originally developed in the realm of Floquet theory [60–62], not only capable of predicting the state of the driven matter system, but also the detailed photon statistics of the driving field. The PRFT takes advantage of the rich methodologies of full-counting statistics of electron transport through mesoscopic structures [63–76] and heat transport through quantum systems [77–81] by including counting fields into the semiclassical equations of motion of the quantum emitters, which trace the photon exchange with coherent driving fields. Crucially, as our framework makes the same prediction for the photonic mean value as the Maxwell-Bloch equation, it can be viewed as a systematic extension of the Maxwell-Bloch theory to higher-order moments of time-integrated photonic statistics.

The flexibility of the PRFT approach allows us to make predictions beyond existing methods of light-matter interaction. To showcase this, we evaluate the Fisher information of a dissipative two-level model describing atoms both numerically and analytically, allowing for the analysis of the measurement sensitivity in an arbitrary parameter range. Intriguingly, the investigation of the Fisher information predicts an intriguing turnover as a function of dissipation, which arises due to a competition between coherent and incoherent dynamics. The analysis for an atomic four-level system, which models spectroscopic quantum sensing of electric fields using Rydberg atoms [36,37], reveals that the measurement precision can be improved by several orders of magnitude by invoking a phase measurement instead of the commonly used intensity measurement.

The rest of this article is organized as follows: In Sec. II, we introduce the generic system under investigation and the theoretical framework. In Sec. III, we explain how to utilize the framework to calculate the measurement statistic of important spectroscopic observables, namely, the intensity, the polarization direction, and phase shift of a coherent light field, from which one can calculate the Fisher information of spectroscopic sensing protocols. In Sec. IV, we apply the framework to analyze the spectroscopic properties of an ensemble of dissipative two-level systems. In Sec. V, we evaluate the measurement sensitivity of an ensemble of four-level atoms. In Sec. VI, we conclude and discuss our findings. Details and derivations are given in the appendixes.

II. FRAMEWORK

In this section, we introduce the generic light-matter system for which we develop methods to predict the measurement statistics in spectroscopic experiments with coherent light. Thereby, we apply the PRFT by introducing counting-fields into the semiclassical equation of motions, which predict the major characteristics of the photonic probability distribution required to calculate the Fisher information.

A. System

The spectroscopic setup investigated in this work is sketched in Fig. 2(a), in which strong laser light propagates through an ensemble of quantum emitters (e.g., atoms or molecules), to which we refer as the matter system in the following. For concreteness, we specify the discussion to atoms but remark that the framework has broader applicability. In a microscopic quantum optical description, the Hamiltonian is given by

$$\hat{H} = \sum_{m=1}^{N} \hat{H}_m + \sum_{k=1}^{D} \omega_k \hat{a}_k^\dagger \hat{a}_k + \sum_{m,k} g_{m,k} \hat{V}_m (\hat{a}_k^\dagger + \hat{a}_k), \qquad (1)$$

where $\hat{H}_m$ describes the quantum emitter m in the absence of the laser fields, and $\hat{V}_m$ denotes the corresponding polarization operator. The photonic creation and annihilation operators $\hat{a}_k^\dagger$, $\hat{a}_k$ quantize the laser light with corresponding frequencies ω_k. The light-matter interaction strength is parametrized by the couplings $g_{m,k}$. After traversing the atomic ensemble, the transmitted light is measured by a detector setup.

More precisely, we assume that the laser light consists of a sequence of pulses with duration t_P within the total measurement time t_M. A specific pulse is quantized by a set of photonic operators $\hat{a}_k^\dagger$, $\hat{a}_k$ whose statistics is measured afterward in the detection setup. These photonic operators might quantize, e.g., different frequencies of the laser light, the polarization direction of linearly polarized light, or some

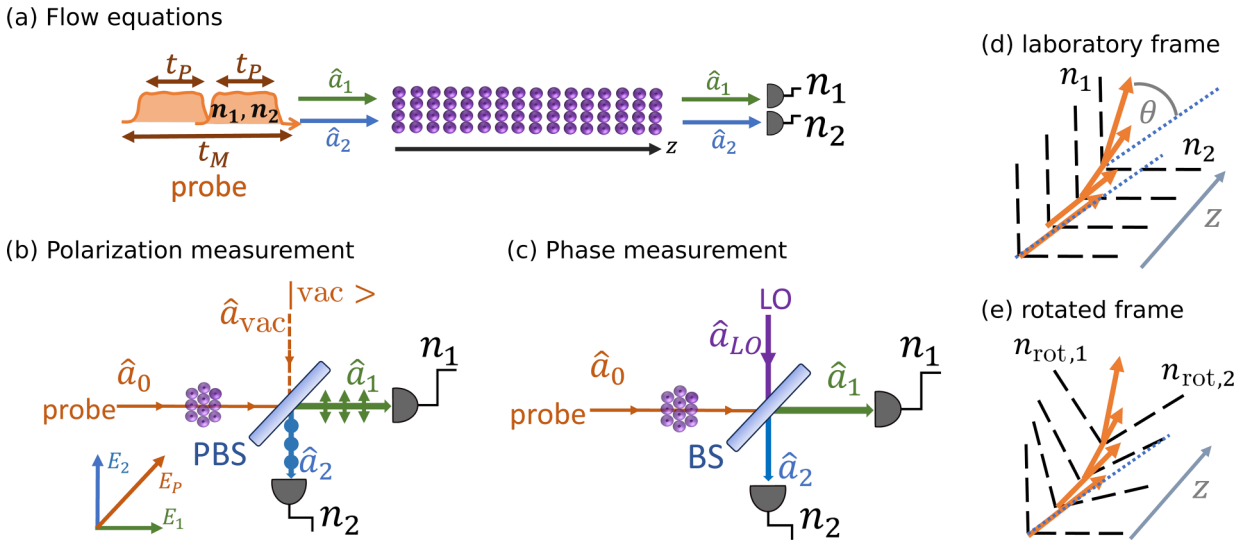


FIG. 2. (a) Sketch of the setup: A probe field, which can be quantized in terms of the operators $\hat{a}_k$ for $k = 1, 2$ propagates through a cloud of atoms (or any other kind of quantum emitters). This generic setup can, e.g., represent a polarization direction measurement as sketched in panel (b), or a phase measurement as sketched in panel (c). (d) Illustration of the fixed laboratory frame used to measure linearly polarized light. The polarization direction rotates by an angle of $\overline{\theta}$. (e) Rotated measurement basis, in which the polarization direction always encloses an angle of $\pi/4$ with the two measurement directions.

other quantized photonic observables. We envision that the laser pulses interact with a particular atom m, during which photons can be either absorbed by the atom or redistributed between the photonic modes. This interaction process can be parametrized by time-dependent coupling parameters $g_{m,k}(t)$, whose time dependence is determined by the amplitude and shape of the pulse.

Prior to the interaction of a pulse with the ensemble of atoms, the joint system is assumed to be in the product state

$$\rho_{\text{tot}}(t=0) = \rho_{\text{M}}(0) \otimes |\alpha\rangle\langle\alpha|, \tag{2}$$

in which the matter state

$$\rho_{\text{M}}(t=0) = \bigotimes_{j=1}^{N} \rho_{\text{M},j}(0) \tag{3}$$

is a tensor product of the density matrices of the individual atoms. The initial state of the photonic modes is assumed to be a pure coherent state, which is parametrized by

$$\begin{aligned} |\alpha\rangle &= \sum_{\boldsymbol{n}} a_{\mathbf{n}} |\boldsymbol{n}\rangle, \\ a_{\mathbf{n}} &= \frac{1}{(2\pi)^{\frac{D}{4}}\sqrt{\det \boldsymbol{\Sigma}}} e^{-\frac{1}{4}(\mathbf{n}-\overline{\mathbf{n}})\boldsymbol{\Sigma}^{-2}(\mathbf{n}-\overline{\mathbf{n}})^T} e^{i\overline{\boldsymbol{\varphi}}\cdot\boldsymbol{n}}, \end{aligned} \tag{4}$$

where we have introduced the vector notation $\boldsymbol{n} = (n_1, \ldots, n_D)$ for the photon numbers n_k, which label the Fock states $|\boldsymbol{n}\rangle = \bigotimes_{k=1}^{D} |n_k\rangle$. The photonic state is assumed to have well-defined mean photon numbers $\overline{\mathbf{n}}$ and mean phases $\overline{\boldsymbol{\varphi}} = (\overline{\varphi}_1, \ldots, \overline{\varphi}_D)$. The covariance matrix $\boldsymbol{\Sigma}^2$ parametrizes the photon shot noise and mutual correlations between the photonic modes.

In the semiclassical limit, the photonic creation and annihilation operators in Eq. (1) can be approximated by their values at the mean-photon numbers $\overline{\mathbf{n}}$. More precisely, after a transformation of the Hamiltonian in Eq. (1) into a rotating frame defined by $U^{(\text{free})} = \exp(-i\sum_k \omega_k \hat{a}_k^\dagger \hat{a}_k t)$, we replace the photonic operators in the Hamiltonian with complex-valued numbers, i.e.,

$$\hat{a}_k \to \sqrt{\overline{n}_k} e^{i\varphi_k - i\omega_k t}. \tag{5}$$

The corresponding Hamiltonian in the semiclassical limit is given by

$$\begin{aligned} \hat{\mathcal{H}}_{\boldsymbol{\varphi}}(t) &= \sum_{m=1}^{N} \hat{\mathcal{H}}_{m,\boldsymbol{\varphi}}(t), \\ \hat{\mathcal{H}}_{m,\boldsymbol{\varphi}}(t) &= \hat{H}_m + \sum_k \Omega_{m,k}(t) \hat{V}_m \cos(\omega_k t - \varphi_k), \end{aligned} \tag{6}$$

which acts only on the matter system. Thereby, we have introduced the time-dependent Rabi frequencies $\Omega_{m,k}(t) = 2g_{m,k}(t)\sqrt{\overline{n}_k}$. As we assume noninteracting quantum emitters, the Hamiltonian can be expressed as a sum over the quantum emitter index m. For each quantum-emitter Hamiltonian $\hat{\mathcal{H}}_{m,\boldsymbol{\varphi}}(t)$, the time-evolution operator given by

$$\hat{\mathcal{U}}_{\overline{\boldsymbol{n}},m,\boldsymbol{\varphi}}(t) = \hat{\mathcal{T}} e^{-i\int_0^t \hat{\mathcal{H}}_{m,\boldsymbol{\varphi}}(t')dt'} \tag{7}$$

describes the time evolution of the matter system in the semiclassical regime. As we assume identical quantum emitters in this paper, we neglect the index m hereafter. For later purposes, we have added the mean-photon number vector $\overline{\boldsymbol{n}}$ as an index to the time-evolution operator. Despite the absence of the photonic operators in Eq. (6), the PRFT can predict the detailed information about the photonic state solely based on the semiclassical time-evolution operator Eq. (7), as we show in the remaining part of this paper.

B. PRFT approach to spectroscopy

The key quantity within the PRFT is the cumulant-generating function

$$K_{\boldsymbol{\chi}} \equiv \log\left(\sum_{\boldsymbol{n}} p_{\boldsymbol{n}} e^{-i\sum_k \chi_k n_k}\right), \tag{8}$$

which is an alternative way to store the information about the photonic probability distribution $p_{\boldsymbol{n}}$ of the laser field. The χ_k are the counting fields which are conjugated to the photon numbers n_k, and represented as a vector $\boldsymbol{\chi} = (\overline{\chi}_1, \ldots, \overline{\chi}_D)$. The cumulants of the probability distribution (e.g., the mean, the variance, skewness, kurtosis) can be obtained by deriving the cumulant-generating function with respect to the counting fields, as reviewed in Appendix A 1.

In Appendixes A 2–A 4, we apply the methods of the PRFT to the spectroscopic setup in Fig. 2(a), by including counting fields into the semiclassical time evolution of the matter system to keep track of the photon-number statistics. In doing so, we derive a flow equation, which describes the evolution of the cumulant-generating function in Eq. (8) as a function of propagation distance z

$$\frac{d}{dz}K_{\boldsymbol{\chi}}(z) = \rho_A \mathcal{A} K_{\mathrm{aux},\overline{\boldsymbol{n}},\boldsymbol{\chi}}(z), \tag{9}$$

where ρ_A denotes the density of the quantum emitters and $\mathcal{A}$ is the (effective) cross section of the laser. The initial condition is given by the cumulant-generating function of a Gaussian probability distribution [cf., Eq. (A2)]. The function $K_{\mathrm{aux},\overline{\boldsymbol{n}},\boldsymbol{\chi}}$ will be denoted as the auxiliary-generating function and is defined as

$$K_{\mathrm{aux},\overline{\boldsymbol{n}},\boldsymbol{\chi}}(z) = \sum_{r=0}^{\infty} \sum_{\iota_1+\ldots\iota_D=r} \left\{ \frac{\partial_{\overline{n}_1}^{\iota_1} \cdots \partial_{\overline{n}_D}^{\iota_D}}{\iota_1! \cdots \iota_D!} \mathcal{K}_{\overline{\boldsymbol{n}},\boldsymbol{\chi}}(z) \right\} \times \prod_{k=1}^{D} \left[\partial_{-i\chi_k} K_{\boldsymbol{\chi}}(z) - \overline{n}_k\right]^{\iota_k}. \tag{10}$$

The central building block appearing in the auxiliary-generating function is the dynamical cumulant-generating function

$$\mathcal{K}_{\overline{\boldsymbol{n}},\boldsymbol{\chi}}(z) = \log\left\langle \hat{\mathcal{U}}^{\dagger}_{\overline{\boldsymbol{n}},\overline{\boldsymbol{\varphi}}-\frac{\boldsymbol{\chi}}{2}}(t_{\mathrm{M}}) \hat{\mathcal{U}}_{\overline{\boldsymbol{n}},\overline{\boldsymbol{\varphi}}+\frac{\boldsymbol{\chi}}{2}}(t_{\mathrm{M}}) \right\rangle_0, \tag{11}$$

where the semiclassical time-evolution operator is given in Eq. (7). It encodes the information about the light-matter interaction of the laser field with a single quantum emitter. The time-evolution operator is evaluated at the measurement time t_{M}. In Eq. (10), we express the dynamical cumulant-generating function as a function of the propagation distance z to highlight a possible position dependence. More details about the terms in the flow equations are discussed in Appendix A 5. Of note, the dynamical-cumulant-generating function plays a vital role in the PRFT, as it allows us to accurately describe a macroscopic light-matter entanglement effect in the Floquet-state basis of the semiclassical system [60].

The flow equation Eq. (9) is reminiscent of the semiclassical Maxwell-Bloch theory, yet, for the cumulant-generating function instead of the electric field. The derivation of Eq. (9) in Appendix A also relies on the same assumptions as the Maxwell-Bloch equations, both for the matter and the photonic subsystems: (i) The matter system shall not exhibit correlation between the atoms. (ii) The coherent photonic modes shall be highly occupied, such that the photon number uncertainty and the phase uncertainty are small.

C. Mean and variance

In general, the flow equation for the cumulant-generating function in Eq. (9) cannot be integrated. However, it can be considered as an *equation-generating equation*, as we demonstrate here. More precisely, by deriving Eq. (9) with respect to the counting fields, we can generate flow equations for low-order cumulants. Here, we discuss the first two cumulants, which will dominate the probability distribution, as the derivation of Eq. (9) assumed independent quantum emitters.

(i) Deriving Eq. (9) with respect to each counting field χ_k, we obtain the flow equation for the mean photon numbers

$$\frac{d}{dz}\overline{\boldsymbol{n}} = \boldsymbol{I}_{\overline{\boldsymbol{n}}}, \tag{12}$$

where the coefficient on the right-hand side is explicitly given by

$$[\boldsymbol{I}_{\overline{\boldsymbol{n}}}]_k = \rho_A \mathcal{A} \partial_{\chi_k} \mathcal{K}_{\overline{\boldsymbol{n}},\boldsymbol{\chi}=0}(z). \tag{13}$$

Importantly, this flow equation is a nonlinear differential equation, as $\boldsymbol{I}_{\overline{\boldsymbol{n}}}$ depends on the mean photon numbers in a nonlinear fashion. Thus, we have to continuously update $\overline{\boldsymbol{n}} = \overline{\boldsymbol{n}}(z)$ when (numerically) solving Eq. (12). Crucially, the mean-photon-number flow equation is equivalent to the semiclassical Maxwell-Bloch equation, as shown in Appendix A 6.

(ii) Deriving Eq. (9) twice with respect to the counting fields χ_k, we obtain the flow equation for the covariance matrix

$$\frac{d}{dz}\boldsymbol{\Sigma}^2 = \boldsymbol{D}_{\overline{\boldsymbol{n}}} + \boldsymbol{C}_{\overline{\boldsymbol{n}}}\boldsymbol{\Sigma}^2 + \boldsymbol{\Sigma}^2\boldsymbol{C}_{\overline{\boldsymbol{n}}}, \tag{14}$$

where

$$[\boldsymbol{D}_{\overline{\boldsymbol{n}}}]_{k_1,k_2} = \rho_A \mathcal{A}\, \partial_{\chi_{k_1}} \partial_{\chi_{k_2}} \mathcal{K}_{\overline{\boldsymbol{n}},\boldsymbol{\chi}=0}(z),$$
$$[\boldsymbol{C}_{\overline{\boldsymbol{n}}}]_{k_1,k_2} = \rho_A \mathcal{A}\, \partial_{\overline{n}_{k_1}} \partial_{\chi_{k_2}} \mathcal{K}_{\overline{\boldsymbol{n}},\boldsymbol{\chi}=0}(z). \tag{15}$$

This equation has to be solved with $\boldsymbol{\Sigma}^2$ of the photonic state in Eq. (4) as the initial condition. Noteworthy, the coefficient matrices $\boldsymbol{D}_{\overline{\boldsymbol{n}}}$ and $\boldsymbol{C}_{\overline{\boldsymbol{n}}}$ depend on the mean photon numbers. Of note, as the mean-photon-number flow equation in Eq. (12) is equivalent to the semiclassical Maxwell-Bloch theory, the covariance flow equation in Eq. (14) can thus be interpreted as an extension of this established framework.

The matrix $\boldsymbol{D}_{\overline{\boldsymbol{n}}}$ is obtained by a twofold derivation of the dynamical cumulant-generating function with respect to the counting fields. Using similar methods as in Ref. [61], it is possible to show that $[\boldsymbol{D}_{\overline{\boldsymbol{n}}}]_{k_1,k_2} \geqslant 0$, i.e., its contribution enhances the variance. In the following, we refer to this term as the diffusion matrix: The analysis of $\boldsymbol{D}_{\overline{\boldsymbol{n}}}$ reveals that it asymptotically scales linearly in time (see Appendix A 6). This thus resembles the linear growth of the mean-square displacement in diffusive transport [82,83], but here in the photon-number domain instead of space. Moreover, the flow equation in Eq. (14) shows that the covariance matrix increases linearly as a function of position z due to the diffusion coefficient, which

can be interpreted as a diffusion process with position being viewed as a generalized time.

The other coefficient matrix $\boldsymbol{C}_{\bar{\boldsymbol{n}}}$ incorporates the photon number dependence of the photonic creation and annihilation operators into the dynamical equation and describes the resulting deformation of the photonic probability distribution. We denote it as the phase-space matrix in the following.

III. SPECTROSCOPIC QUANTUM SENSING

In Sec. II, we established a theoretical framework that is capable of predicting the photon exchange between pulses of light and an ensemble of quantum emitters without further specifying the physical meaning of the photonic operators. In this section, we now link the photonic operators in the Hamiltonian in Eq. (1) to relevant observables in spectroscopic quantum sensing, namely, the intensity of a laser, the polarization direction of linearly polarized light, and the phase shift of the laser-light imposed by the light-matter interaction. In doing so, we provide practical guidelines on how to best integrate the flow equations in Eqs. (12) and (14), and explain how this can be utilized to estimate the measurement precision in spectroscopic quantum sensing.

A. Intensity

A vital observable in spectroscopic experiments is the optical intensity of the laser field, which is defined as the radiation energy traversing a unit area $\mathcal{A}$ within a unit time. In contrast, the PRFT counts the number of photons contained in a laser pulse. The laser intensity of a pulse with frequency ω, duration t_{P}, and cross section $\mathcal{A}$ can be estimated by

$$I_{\mathrm{L}} = \frac{\hbar\omega}{t_{\mathrm{P}}\mathcal{A}} n, \tag{16}$$

where n is the measured photon number. Thus, from the statistics of the photon number n (as predicted by the PRFT), we can obtain the statistics of the intensity.

To improve the signal-to-noise ratio of the intensity measurement, one can invoke longer measurement times t_{M} by recording the measurement outcomes for the continuous train of pulses. Quantizing the pulses with the photonic operators $\hat{a}_k$, we denote the measured photon number by n_k. Crucially, the n_k cannot be regarded as independent random variables. Rather, the photon numbers are highly correlated because of the memory effects of the atoms, which the pulses interact with. For example, the correlation time of the atomic dynamics can be determined by relaxation processes with rate γ such that $t_{\mathrm{P}} \ll 1/\gamma$.

To estimate the mean intensity of this pulse train, we employ the cumulative photon number $\sum_k n_k$ as a random variable. Comparing with the definition of the cumulant-generating function in Eq. (A1), we see that we can simply obtain the statistics of the cumulative photon number by setting all counting fields equally, $\chi_k = \chi$. We then evaluate the flow equations in Sec. II B for χ and $t = t_{\mathrm{M}}$ in Eq. (10). The intensity of the radiation field can thus be estimated as

$$I_{\mathrm{L}} = \frac{\hbar\omega}{t_{\mathrm{M}}\mathcal{A}} \sum_{k=1}^{D} n_k, \tag{17}$$

where the statistics of the cumulative photon number $\sum_{k=1}^{D} n_k$ can be obtained using the dynamical cumulant-generating function in Eq. (10) with integration time t_{M}. Noteworthy, in principle it is possible to construct more precise estimators for the intensity based on the joint photonic measurement probabilities $p_{n_1,\ldots,n_D}$ using, e.g., a Markov-chain approach. However, this would exceed the scope of this work and will be considered elsewhere.

B. Polarization direction

In this section, we assume that the laser pulse is initially polarized in the direction

$$\boldsymbol{E}_{\mathrm{in}}(\boldsymbol{r}, t) \propto \boldsymbol{e}_x + \boldsymbol{e}_y, \tag{18}$$

where $\boldsymbol{e}_x$ and $\boldsymbol{e}_y$ denote the unit vectors in the x and y directions as shown in the inset of Fig. 2(b). Accordingly, we introduce the operators $\hat{a}_1$ and $\hat{a}_2$ which quantize the electromagnetic field of the laser pulse in the x and y directions, respectively. Thus, initially, both occupation number operators $\hat{n}_\alpha = \hat{a}_\alpha^\dagger \hat{a}_\alpha$ with $\alpha = 1, 2$ have the same mean value,

$$\langle \hat{n}_1 \rangle_{\mathrm{in}} = \langle \hat{n}_2 \rangle_{\mathrm{in}} = \frac{\overline{n}_+^{(\mathrm{in})}}{2}, \tag{19}$$

where $\overline{n}_+^{(\mathrm{in})}$ is the initial total number of photons in the pulse, which is a function of its shape, duration, and frequency. The choice of the basis direction in Eq. (18) is, in principle, arbitrary as long as the photonic field in both directions is macroscopically occupied. Yet, the initial symmetric occupation in both measurement directions is advantageous for the evaluation of the flow equations.

When the light pulse is propagating through an ensemble of quantum emitters, the polarization direction can be changed, e.g., because of the Faraday effect [28]. The change in the polarization direction manifests itself in an imbalance in the photonic occupations of $\hat{n}_1$ and $\hat{n}_2$. The photon numbers can be measured using a polarization beam splitter and two photon detectors, as sketched in Fig. 2(b), from which we can infer the mean value of the polarization rotation $\overline{\theta}$ via

$$\sin\overline{\theta} = \frac{\sqrt{\overline{n}_2} - \sqrt{\overline{n}_1}}{\sqrt{2\overline{n}_+}}, \tag{20}$$

where $\overline{n}_\alpha$ is the mean photon number at detector $\alpha = 1, 2$, and $\overline{n}_+ = \overline{n}_1 + \overline{n}_2$.

C. Phase

Even though the PRFT is a framework that counts the number of photons, it is also capable of predicting the statistics of phase measurements. This assertion becomes clear when recalling that it is only possible to measure intensities in optical experiments. A phase measurement is typically carried out by superposing the probe field (whose phase is to be measured) with a local oscillator, and then inferring the phase information from the intensity change of the resulting light field.

The corresponding experimental setup is depicted in Fig. 2(c), where the probe field is quantized by $\hat{a}_0$ and the local oscillator is quantized by $\hat{a}_{\mathrm{LO}}$. Using a beam splitter, we create the two superposition output fields $\hat{a}_1$, $\hat{a}_2$, which are related to

the input fields $\hat{a}_0$, $\hat{a}_{\mathrm{LO}}$ via

$$\hat{a}_1 = \frac{1}{\sqrt{2}}(\hat{a}_{\mathrm{LO}} + i\hat{a}_0), \quad \hat{a}_2 = \frac{1}{\sqrt{2}}(\hat{a}_{\mathrm{LO}} - i\hat{a}_0). \tag{21}$$

For illustration, let us assume that the probe pulse is in a coherent state with complex amplitude $\sqrt{\overline{n}_0}e^{i\overline{\varphi}_0}$, where $\overline{n}_0$ is the mean photon number and $\overline{\varphi}_0$ is the phase to be measured. Likewise, the local oscillator is in a coherent state with complex amplitude $\sqrt{\overline{n}_{\mathrm{LO}}}e^{i\overline{\varphi}_{\mathrm{LO}}}$. Denoting the mean occupations of the operators by $\overline{n}_\alpha = \langle \hat{a}_\alpha^\dagger \hat{a}_\alpha \rangle$ for $\alpha = 1, 2$, we find relations for the sum and difference of the mean photon numbers

$$\begin{aligned} \overline{n}_1 + \overline{n}_2 &= \overline{n}_0 + \overline{n}_{\mathrm{LO}}, \\ \overline{n}_1 - \overline{n}_2 &= 2\sqrt{\overline{n}_0 \overline{n}_{\mathrm{LO}}} \sin(\overline{\varphi}_0 - \overline{\varphi}_{\mathrm{LO}}), \end{aligned} \tag{22}$$

from which we can infer the phase of the probe field via

$$\sin(\overline{\varphi}_0 - \overline{\varphi}_{\mathrm{LO}}) = \frac{\overline{n}_1 - \overline{n}_2}{2\sqrt{\overline{n}_0 \overline{n}_{\mathrm{LO}}}}. \tag{23}$$

Thus, we obtain the phase information via a photon number measurement, which is closely related to the intensity.

Based on these considerations, we can now establish a connection to the PRFT. To this end, we assume that originally the quantum emitters interact with the probe field via the operator $\hat{a}_0$ in the Hamiltonian. Now we invert Eq. (21), i.e.,

$$\hat{a}_0 = \frac{1}{\sqrt{2}i}(\hat{a}_1 - \hat{a}_2), \tag{24}$$

and insert this into the Hamiltonian. As a consequence, the quantum emitters interact now with the two modes $\hat{a}_1, \hat{a}_2$, for which we can use the formalism in Sec. II to calculate the projected measurement statistics. The replacement in Eq. (24) is a unitary transformation into the basis of measurement. Thus, we express the Hamiltonian in exactly the basis in which we finally measure the photon statistics.

D. Rotated measurement frame

For the following explanations, we focus on a polarization measurement as introduced in Sec. III B. Nevertheless, the following considerations also apply to phase measurements, as polarization rotation and phase shifts are closely related via the Faraday effect, as reviewed in Appendix B 1.

The flow equations in Eqs. (12) and (14) predict the measured photonic probabilities in a basis that is fixed in the laboratory frame. While this setup is intuitive, it is beneficial to consider a measurement basis, which rotates along with the polarization direction of the light pulse. The two different measurement setups are sketched in Figs. 2(d) and 2(e), showing the fixed and rotated measurement directions for various positions z, respectively. In the rotated basis, the instantaneous direction of the electric-field polarization is depicted by the orange arrow, and encloses a $\pi/4$ angle with both rotated basis directions for all positions z.

To parametrize the rotation, we utilize the position-dependent mean polarization angle $\overline{\theta} = \overline{\theta}(z)$ defined in Eq. (20). In terms of $\overline{\theta}$, the rotated photonic operators are defined by

$$\hat{a}_{\mathrm{rot},1} = \cos\overline{\theta}\hat{a}_1 - \sin\overline{\theta}\hat{a}_2, \quad \hat{a}_{\mathrm{rot},2} = \sin\overline{\theta}\hat{a}_1 + \cos\overline{\theta}\hat{a}_2. \tag{25}$$

The angle $\overline{\theta}$ is chosen such that for all positions z the mean occupations of the photonic modes $\hat{n}_{\mathrm{rot},\alpha} = \hat{a}_{\mathrm{rot},\alpha}^\dagger \hat{a}_{\mathrm{rot},\alpha}$ with $\alpha = 1, 2$ are equal, i.e.,

$$\langle \hat{n}_{\mathrm{rot},1} \rangle = \langle \hat{n}_{\mathrm{rot},2} \rangle \equiv \frac{\overline{n}_+(z)}{2}, \tag{26}$$

where $\overline{n}_+(z)$ denotes the total number of photons in both modes.

As shown in Appendix B 2, the rotation angle and the total number of photons can be calculated using the following differential relations:

$$\frac{d\overline{\theta}}{dz} = \frac{\partial_z \overline{n}_{\mathrm{rot},2} - \partial_z \overline{n}_{\mathrm{rot},1}}{2\overline{n}_+}, \quad \frac{d\overline{n}_+}{dz} = \partial_z \overline{n}_{\mathrm{rot},2} + \partial_z \overline{n}_{\mathrm{rot},1}. \tag{27}$$

Thereby, $\partial_z \overline{n}_{\mathrm{rot},\alpha}$ refers to the derivatives of the mean photon number $\overline{n}_{\mathrm{rot},\alpha}$ in the fixed measurement basis and can be evaluated via

$$\partial_z \overline{n}_{\mathrm{rot},\alpha} = \left[\boldsymbol{I}_{\overline{\boldsymbol{n}}_{\mathrm{rot}}}\right]_\alpha, \tag{28}$$

where $\boldsymbol{I}_{\overline{\boldsymbol{n}}_{\mathrm{rot}}}$ is the photon flux vector in Eq. (13) for the semiclassical Hamiltonian, in which the photonic mode occupations satisfy the rotation condition in Eq. (26).

The differential equation for the covariance matrix, measured in the rotated measurement basis, is given by

$$\begin{aligned} \frac{d}{dz}\boldsymbol{\Sigma}^2_{\mathrm{rot}} &= \boldsymbol{D}_{\overline{\boldsymbol{n}}_{\mathrm{rot}}} + \tilde{\boldsymbol{C}}_{\overline{\boldsymbol{n}}_{\mathrm{rot}}}\boldsymbol{\Sigma}^2_{\mathrm{rot}} + \boldsymbol{\Sigma}^2_{\mathrm{rot}}\tilde{\boldsymbol{C}}_{\overline{\boldsymbol{n}}_{\mathrm{rot}}}, \\ \tilde{\boldsymbol{C}}_{\overline{\boldsymbol{n}}_{\mathrm{rot}}} &= \boldsymbol{C}_{\overline{\boldsymbol{n}}_{\mathrm{rot}}} - \frac{d\overline{\theta}}{dz}\hat{\Xi}, \end{aligned} \tag{29}$$

where we have introduced $\hat{\Xi} = i\hat{\sigma}_y + \hat{\sigma}_z$ ($\hat{\sigma}_\alpha$ with $\alpha = x, y, z$ denoting the common Pauli matrices). Thereby, $\boldsymbol{D}_{\overline{\boldsymbol{n}}_{\mathrm{rot}}}$ and $\boldsymbol{C}_{\overline{\boldsymbol{n}}_{\mathrm{rot}}}$ refer to the diffusion and phase-space matrices as defined in Eq. (15), but evaluated under the rotation condition in Eq. (26). Typically, the entries of $\tilde{\boldsymbol{C}}_{\overline{\boldsymbol{n}}_{\mathrm{rot}}}$ are significantly smaller than those of $\boldsymbol{C}_{\overline{\boldsymbol{n}}_{\mathrm{rot}}}$, enabling a more efficient numerical and analytical treatment.

Conversely, in terms of the observables $\overline{n}_+$ and $\overline{\theta}$, it is also straightforward to retrieve the means and covariances for the measurement in the original measurement basis in the laboratory frame by evaluating

$$\begin{pmatrix} \overline{n}_1 \\ \overline{n}_2 \end{pmatrix} = \overline{n}_+ \begin{pmatrix} \cos^2\left(\frac{\pi}{4} + \overline{\theta}\right) \\ \sin^2\left(\frac{\pi}{4} + \overline{\theta}\right) \end{pmatrix}, \tag{30}$$

and

$$\boldsymbol{\Sigma}^2_{\alpha,\beta} = \frac{2\sqrt{\overline{n}_\alpha}\sqrt{\overline{n}_\beta}}{\overline{n}_+}\left(e^{i\overline{\theta}\hat{\sigma}_y}\boldsymbol{\Sigma}^2_{\mathrm{rot}}e^{-i\overline{\theta}\hat{\sigma}_y}\right)_{\alpha,\beta}, \tag{31}$$

for $\alpha, \beta = 1, 2$. The detailed derivation is given in Appendix B 2.

E. Fisher information

The celebrated Cramér-Rao bound is an indispensable tool to bound the sensitivity $\langle \Delta X^2 \rangle$ of the physical parameter X to be estimated [84,85] via

$$\langle \Delta X^2 \rangle \geqslant \frac{1}{\mathcal{I}_X}, \tag{32}$$

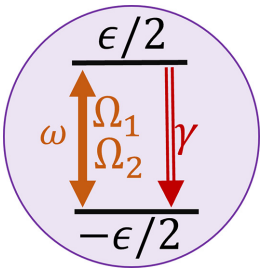


FIG. 3. Level structure of the two-level systems, which are probed by a coherent laser field with Rabi frequencies Ω_k and subject to dissipation γ.

where the Fisher information

$$\mathcal{I}_X = \sum_{\boldsymbol{n}} p_{X,\boldsymbol{n}} (\partial_X \ln p_{X,\boldsymbol{n}})^2 \tag{33}$$

quantifies the dependency of the measured probability distribution $p_{X,\boldsymbol{n}}$ on X. Under the assumption of a Gaussian probability distribution, the leading-order term of the Fisher information is given by

$$\mathcal{I}_X = (\partial_X \overline{\boldsymbol{n}}_X) \boldsymbol{\Sigma}_X^{-2} (\partial_X \overline{\boldsymbol{n}}_X)^T, \tag{34}$$

which can be interpreted as a generalized signal-to-noise ratio [86]. Thus, it can be expressed in terms of the mean values and covariance matrix of the probability distribution of $\boldsymbol{n}$. As the photonic probability distribution approaches a Gaussian distribution when interacting with a macroscopic number of independent quantum emitters, we use Eq. (34) in the following calculations.

When working in the rotated measurement basis introduced in Sec. III D, the measurement statistics and the Fisher information can be conveniently expressed in terms of

$$n_+ = n_1 + n_2, \quad n_- = n_1 - n_2. \tag{35}$$

The total photon number n_+ carries information about the total intensity of a laser pulse, while the photon-number difference n_- is related to the polarization rotation $\overline{\theta}$ via Eq. (23). We recall that, by definition, the mean value $\overline{n}_- = 0$ in the rotated measurement basis, such that the information about the polarization rotation is expressed by $\overline{\theta}$. In the rotated measurement picture, $\partial_X \overline{\boldsymbol{n}}_X$ can be simply evaluated via

$$\partial_X \overline{\boldsymbol{n}}_X = \overline{n}_+ \frac{d\overline{\theta}}{dX} \begin{pmatrix} 1 \\ -1 \end{pmatrix} + \frac{d\overline{n}_+}{dX} \begin{pmatrix} 1 \\ 1 \end{pmatrix}, \tag{36}$$

as can be shown using Eq. (30) for $\overline{\theta} = 0$.

IV. TAVIS-CUMMINGS MODEL

To demonstrate the theoretical concepts in Secs. II and III for a concrete example, we consider here a dissipative version of the celebrated Tavis-Cummings model, whose level structure is sketched in Fig. 3. The corresponding light-matter Hamiltonian reads

$$\hat{H} = \hat{H}_{\mathrm{TC}} + \hat{H}_{\mathrm{Bath}}. \tag{37}$$

Thereby, the closed Tavis-Cumming model is given by

$$\hat{H}_{\mathrm{TC}} = \omega \hat{a}_0^\dagger \hat{a}_0 + \sum_m \frac{\epsilon}{2} \hat{\sigma}_{m,z} + \sum_m g_m(t) (\hat{\sigma}_{m,-} \hat{a}_0^\dagger + \hat{\sigma}_{m,+} \hat{a}_0), \tag{38}$$

where the photonic operators $\hat{a}_0, \hat{a}_0^\dagger$ quantize a laser pulse with frequency ω, and $\hat{\sigma}_{m,z}$ describes the two levels of atom m, which has level splitting ϵ. The coupling operators of the quantum emitters are given by the Pauli operators $\hat{\sigma}_{m,-}$, $\hat{\sigma}_{m,+}$, whose time-dependent coupling to the photonic field is parametrized by $g_m(t)$. We recall that the time-dependence of $g_m(t)$ is determined by the pulse shape and quantum emitter location.

Moreover, each quantum emitter is coupled to its own bath, which gives rise to dissipation. The bath and the coupling operators are described by

$$\hat{H}_{\mathrm{Bath}} = \sum_{m,q} \omega_q \hat{b}_{m,q}^\dagger \hat{b}_{m,q} + \sum_{m,q} v_q (\hat{\sigma}_{m,-} b_{m,q}^\dagger + \mathrm{H.c.}), \tag{39}$$

where the bosonic bath modes $\hat{b}_{m,q}$ with frequency ω_q are coupled to the quantum emitters with strength v_q. We assume that the baths are in a thermal state with temperature $k_B T \ll \hbar\omega$.

A. Cumulant-generating function

In the following, we apply the methods introduced in Secs. II and III to predict the statistics for the phase measurement of the probe pulse quantized by $\hat{a}_0$, using the measurement sketched in Fig. 2(c). The first step is to obtain an expression for the dynamical cumulant-generating function defined in Eq. (10). To accurately implement the counting fields related to the phase mesurement depicted in Fig. 2(c), we represent the photonic field in the measurement basis using Eq. (24), such that the Hamiltonian reads

$$\hat{H}_{\mathrm{TC}} = \sum_{k=1,2} \omega \hat{a}_k^\dagger \hat{a}_k + \sum_m \frac{\epsilon}{2} \hat{\sigma}_{m,z} + \sum_{m,k=1,2} \left[\frac{g_m(t)}{\sqrt{2}} i \hat{\sigma}_{m,-} \hat{a}_k^\dagger + \mathrm{H.c.} \right]. \tag{40}$$

Next, we consider the Hamiltonian in the semiclassical limit by replacing $\hat{a}_k \to \sqrt{\overline{n}_k} e^{i\overline{\varphi}_k}$, such that

$$\hat{\mathcal{H}}(t) = \sum_m \hat{\mathcal{H}}_{m,\boldsymbol{\varphi}}(t) + \hat{H}_{\mathrm{Bath}}, \tag{41}$$

where the semiclassical light-matter interaction of two-level system m is described by

$$\hat{\mathcal{H}}_{m,\boldsymbol{\varphi}}(t) = \frac{\epsilon}{2} \hat{\sigma}_{m,z} + \sum_{k=1,2} \left[\frac{\Omega_{m,k}(t)}{2} e^{i(\omega t - \varphi_k)} \hat{\sigma}_{m,-} + \mathrm{H.c.} \right], \tag{42}$$

in which the effective Rabi frequencies are given by $\Omega_{m,k}(t) = \sqrt{2\overline{n}_k} i g_{m,k}(t)$. In the following, we omit the index m, as the quantum emitters are formally decoupled in the semiclassical Hamiltonian and assumed to be identical.

As each quantum emitter is coupled to a continuum of bath modes, we cannot exactly construct the semiclassical time-evolution operator in Eq. (7). Instead, we use an open

quantum system approach of the PRFT to construct the dynamical cumulant-generating function in Eq. (10). To this end, we deploy a generalized quantum master equation, which describes the system-bath coupling in second-order perturbation theory as introduced in Ref. [62]. To obtain the dynamical cumulant-generating function, we first have to integrate the generalized master equation

$$\frac{d}{dt}\rho_{\boldsymbol{\chi}} = \mathcal{L}_{\bar{\boldsymbol{n}},\boldsymbol{\chi}}\rho_{\boldsymbol{\chi}}, \tag{43}$$

and then use the generalized density matrix of the quantum-emitter system $\rho_{\boldsymbol{\chi}}$ to construct the dynamical moment-generating function via

$$\mathcal{K}_{\bar{\boldsymbol{n}},\boldsymbol{\chi}}(z) = \log \mathrm{tr}[\rho_{\boldsymbol{\chi}}(t_\mathrm{M})] \to \lambda_{\bar{\boldsymbol{n}},\boldsymbol{\chi}} t_\mathrm{M}. \tag{44}$$

The information about the laser pulse properties (i.e., the occupations of the photonic modes) is expressed by the subscript $\bar{\boldsymbol{n}}$ of the generalized Liouvillian. For long enough measurement times t_M, the generating function becomes proportional to the dominating eigenvalue of the Liouvillian, i.e., the eigenvalue which is $\lambda_{\bar{\boldsymbol{n}},\boldsymbol{\chi}} \to 0$ for $\boldsymbol{\chi} \to 0$ [61], which leads to the simple expression for the generating function in Eq. (44).

For the Hamiltonian in Eq. (42) under the influence of the dissipative bath modes, the generalized Liouvillian is time-independent and given by

$$\begin{aligned}\mathcal{L}_{\bar{\boldsymbol{n}},\boldsymbol{\chi}}\rho = &-i\big[\hat{\mathcal{H}}_{\boldsymbol{\varphi}+\frac{\boldsymbol{\chi}}{2}}\rho - \rho\hat{\mathcal{H}}_{\boldsymbol{\varphi}-\frac{\boldsymbol{\chi}}{2}}\big] \\ &+\gamma\big[\hat{\sigma}_-\rho\hat{\sigma}_+ - \tfrac{1}{2}\{\rho, \hat{\sigma}_+\hat{\sigma}_-\}\big],\end{aligned} \tag{45}$$

where the Hamiltonian acting on the quantum emitters reads

$$\hat{\mathcal{H}}_{\boldsymbol{\varphi}} = \frac{\epsilon_\Delta}{2}\hat{\sigma}_z + \sum_{k=1,2}\left[\frac{\Omega_k}{2}e^{i\varphi_k}\hat{\sigma}_- + \mathrm{H.c.}\right], \tag{46}$$

where $\epsilon_\Delta = \epsilon - \omega$ denotes the laser detuning. For simplicity, we consider a Rabi frequency that is constant during the pulse duration t_M. The dissipation term can be microscopically derived using a generalized master-equation approach [62]. The dissipation parameter γ quantifies the coupling strength of the atoms to the bath modes and describes the relaxation within the two-level system. For the description of realistic atomic systems, the value of γ can be obtained via tables, software packages such as ARC [87], the Wigner-Weisskopf theory [88,89], or from data fitting of optical experiments.

Of note, the Tavis-Cummings model describes the light-matter interaction within a rotating-wave approximation, which gives rise to the time-independent master equation in Eq. (45), enabling the analytical expressions of the measurement statistics. Yet, we emphasize that the methods developed in this work are also applicable to models beyond the rotating-wave approximation. In this situation, counterrotating wave terms give rise to a periodic-time dependence of the semiclassical Liouvillian, for which one can evaluate the dynamical cumulant-generating function in Eq. (10) using the tools of the PRFT in Ref. [62]. This flexibility in the light-matter description highlights the broad scope of applicability of the spectroscopic framework introduced here.

B. Flow equations

We are now in a position to construct the flow equations for the mean and the covariance matrix in Eqs. (12) and (14), respectively, using the generating function in Eq. (44). The following formulas are represented by a vector notation in the basis (n_1, n_2). Details of the step-by-step calculations are given in Appendixes C 1 and C 2.

The photon flux coefficients defined in Eq. (13) read

$$\begin{aligned}\boldsymbol{I}_{\bar{\boldsymbol{n}}} = \frac{t_\mathrm{M}\rho_A\mathcal{A}}{4\epsilon_\Delta^2 + 2\Omega_{\tilde{\varphi}}^2 + \gamma}\Bigg[&\Omega_1\Omega_2\epsilon_\Delta \sin(\tilde{\varphi})\begin{pmatrix}1\\-1\end{pmatrix} \\ &-\gamma\begin{pmatrix}\Omega_1^2\\ \Omega_2^2\end{pmatrix} - \gamma\Omega_1\Omega_2\cos(\tilde{\varphi})\begin{pmatrix}1\\1\end{pmatrix}\Bigg],\end{aligned} \tag{47}$$

where we have introduced

$$\Omega_{\tilde{\varphi}}^2 = \Omega_1^2 + 2\Omega_1\Omega_2\cos(\tilde{\varphi}) + \Omega_2^2. \tag{48}$$

This is the effective Rabi frequency which the two-level system experiences due to the driving by the two modes. Moreover, we have defined $\tilde{\varphi} = \overline{\varphi}_1 - \overline{\varphi}_2$. The term proportional to ϵ_Δ gives rise to a mean-photon number imbalance between modes $k = 1$ and $k = 2$, which can be associated with a phase shift according to the explanations in Eq. (23). The terms proportional to γ describe absorption of photons by the dissipative two-level systems.

The diffusive matrix defined in Eq. (15) can be represented as

$$\boldsymbol{D}_{\bar{\boldsymbol{n}}} \approx \rho_A\mathcal{A}t_\mathrm{M}\frac{32\Omega_1^2\Omega_2^2\Omega_{\tilde{\varphi}}^4\sin^2(\tilde{\varphi})}{\gamma\big[4\epsilon_\Delta^2 + 2\Omega_{\tilde{\varphi}}^2\big]^3}\begin{pmatrix}1 & -1\\ -1 & 1\end{pmatrix} + O(\gamma^0), \tag{49}$$

which we have expanded for small dissipation γ. The full expression can be found in Eq. (C9). Interestingly, the lowest order contribution scales with γ^{-1}. The matrix has two eigenvectors. The first one is (1,1) and has a vanishing eigenvalue, and thus does not contribute to the diffusive dynamics. The second one is $(1, -1)$ and has a finite eigenvalue and thus contributes to the diffusion. As the eigenvector $(1, -1)$ is proportional to the first line in Eq. (47), and the leading order of the diffusion matrix is proportional to $\sin^2(\tilde{\varphi})$, we conclude that the leading order of $\boldsymbol{D}_{\bar{\boldsymbol{n}}}$ describes phase diffusion.

Finally, the phase-space matrix defined in Eq. (15) can be calculated by deriving the photon fluxes with respect to the mean photon numbers $\overline{n}_1, \overline{n}_2$. In doing so, we obtain

$$\begin{aligned}\boldsymbol{C}_{\bar{\boldsymbol{n}}} = \frac{\rho_A\mathcal{A}t_\mathrm{M}}{4\epsilon_\Delta^2 + 2\Omega_{\tilde{\varphi}}^2 + \gamma}\Bigg[&\frac{\Omega_1\Omega_2\epsilon_\Delta}{2}\sin(\tilde{\varphi})\begin{pmatrix}\frac{1}{\overline{n}_1} & \frac{1}{\overline{n}_2}\\ -\frac{1}{\overline{n}_1} & -\frac{1}{\overline{n}_2}\end{pmatrix} \\ &-\gamma\begin{pmatrix}\frac{\Omega_1^2}{\overline{n}_1} & 0\\ 0 & \frac{\Omega_2^2}{\overline{n}_2}\end{pmatrix} - \frac{\Omega_1\Omega_2\gamma}{2}\cos(\tilde{\varphi})\begin{pmatrix}\frac{1}{\overline{n}_1} & \frac{1}{\overline{n}_2}\\ \frac{1}{\overline{n}_1} & \frac{1}{\overline{n}_2}\end{pmatrix} \\ &-\frac{\boldsymbol{I}_{\bar{\boldsymbol{n}}}}{\rho_A\mathcal{A}t_\mathrm{M}}\otimes\left(\frac{d\Omega_{\tilde{\varphi}}^2}{d\overline{n}_1}, \frac{d\Omega_{\tilde{\varphi}}^2}{d\overline{n}_2}\right)\Bigg],\end{aligned} \tag{50}$$

where $\otimes$ denotes the tensor product of two vectors producing a matrix. The first three terms in the rectangular bracket

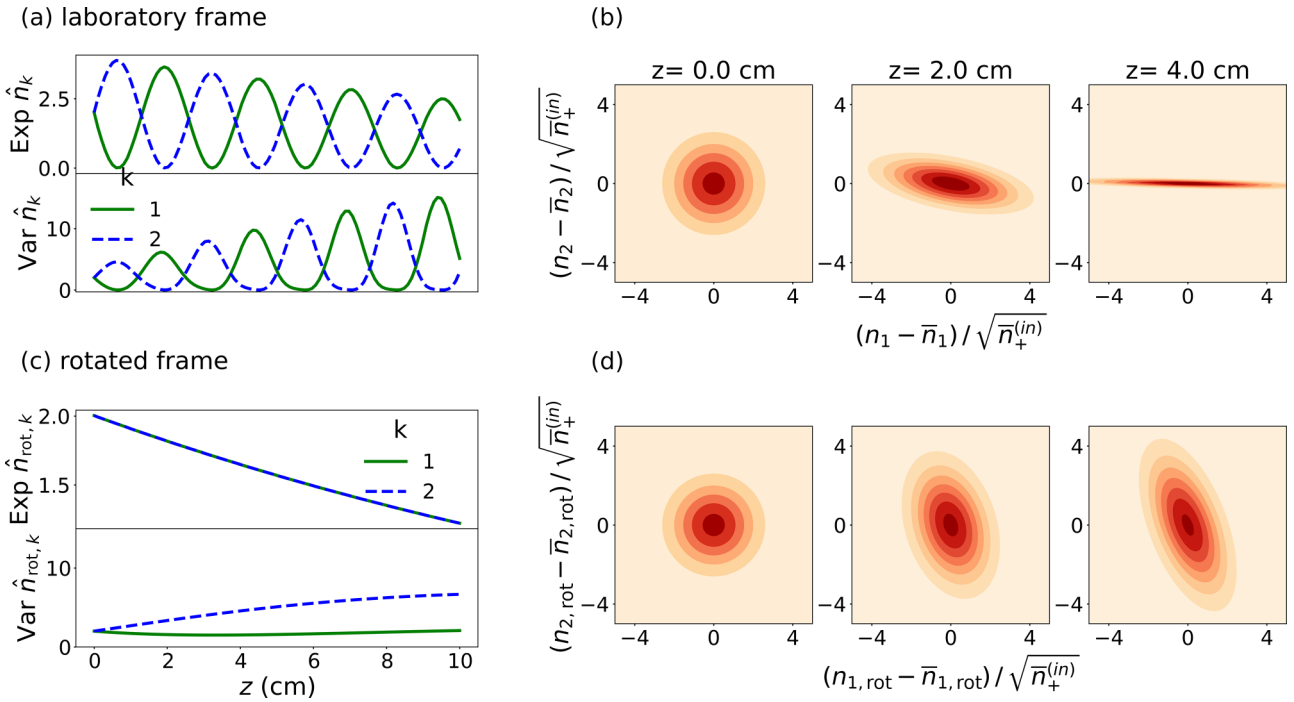


FIG. 4. (a) Mean photon number and variance as a function of propagation distance z for the mode $k = 1, 2$ in the laboratory measurement frame. (b) Probability distribution for three selected distances. (c) and (d) depict the same as (a) and (b) but in the rotated measurement basis. The dynamics in the rotated frame is obtained by integrating the flow equations in Eqs. (27) and (29) using the coefficients in Eqs. (52)–(54). The values in the laboratory frame can be obtained using Eqs. (30) and (31). Parameters are $\gamma = 1$ MHz, $z_{\max} = 10$ cm, $P = 100$ mW, $\mathcal{A} = 1$ cm^2, $\rho_A = 10^{14}$m^{-3}, $t_M = 1$ s, and atomic dipole moment $d = 5ea_0$. This gives rise to an overall Rabi frequency of $\Omega = 60$ MHz.

are the derivatives of the first three terms in the rectangular bracket in Eq. (47). The fourth term in the bracket is generated by the prefactor in Eq. (47), and has not been explicitly written down for brevity.

The mean photon numbers and the corresponding variances as a function of position z are depicted in Fig. 4(a). For small distances z, we observe that the mean value of $\hat{n}_1$ decreases while the mean value of $\hat{n}_2$ increases, representing a phase shift with propagation distance. Likewise, the variance of $\hat{n}_1$ decreases while the variance of $\hat{n}_2$ increases. This is a consequence of the phase-space terms $C_{\bar{\boldsymbol{n}}}$ in Eq. (50), which describe the deformation of the probability distribution due to the photon-number dependence of the creation and annihilation operators. The effect of the diffusion matrix $D_{\bar{\boldsymbol{n}}}$ leads to an overall increase in the variance for larger z.

In Fig. 4(b), we depict the probability distribution for three propagation distances. For $z = 2$ cm, the distribution is noticeably deformed due to the action of the phase-space terms $C_{\bar{\boldsymbol{n}}}$. This deformation is even clearer for $z = 4$ cm for which the variance $\mathrm{Var}\,\hat{n}_2$ almost vanishes. At this point, $\bar{n}_2 \approx 0$, meaning that the measurement direction is almost orthogonal to the polarization of the laser field, such that the corresponding photon mode is close to its vacuum state.

C. Rotating frame

It is beneficial to integrate the flow equations in the rotating frame introduced in Sec. III D, in which $\Omega_1 = \Omega_2 \equiv \Omega/\sqrt{2}$ and $\tilde{\varphi} = \pi/2$. In doing so, the coefficients in Sec. IV B and the equations of motion simplify drastically, enabling a theoretical analysis in limiting cases.

The photon-flux coefficients in Eq. (47) read

$$\boldsymbol{I}_{\bar{\boldsymbol{n}}_{\mathrm{rot}}} = \frac{\rho_A \mathcal{A} t_M}{4\epsilon_\Delta^2 + 2\Omega^2 + \gamma^2}\left[\epsilon_\Delta \Omega^2 \begin{pmatrix} 1 \\ -1 \end{pmatrix} - \gamma\Omega^2 \begin{pmatrix} 1 \\ 1 \end{pmatrix}\right], \quad (51)$$

which allows us to express the equations for the phase shift and the total number of photons according to Sec. III D as

$$\frac{d\bar{\varphi}}{dz} = \frac{\rho_A \mathcal{A} t_M}{\bar{n}_+} \frac{\epsilon_\Delta \Omega^2}{4\epsilon_\Delta^2 + 2\Omega^2 + \gamma^2},$$
$$\frac{d\bar{n}_+}{dz} = -\rho_A \mathcal{A} t_M \frac{\gamma\Omega^2}{4\epsilon_\Delta^2 + 2\Omega^2 + \gamma^2}. \quad (52)$$

Notably, the integration of the phase shift equation is trivial for a vanishing γ, for which $\bar{n}_+$ becomes constant: Noting that in the rotated basis $\Omega = g\sqrt{\bar{n}_+}$, we see that the right-hand side of the phase equation becomes independent of z.

Likewise, the diffusion matrix simplifies and now reads

$$\boldsymbol{D}_{\bar{\boldsymbol{n}}_{\mathrm{rot}}} \approx \frac{8\rho_A \mathcal{A} t_M \Omega^8}{\gamma[4\epsilon_\Delta^2 + 2\Omega^2]^3} \begin{pmatrix} 1 & -1 \\ -1 & 1 \end{pmatrix} + O(\gamma^0). \quad (53)$$

As for the phase-shift Eq. (52), the diffusion matrix becomes independent of position for a small dissipation γ, allowing for an analytical integration of the variance equation.

A drastic simplification appears for the phase-space matrix, which in the rotated frame becomes

$$\tilde{\boldsymbol{C}}_{\bar{\boldsymbol{n}}_{\mathrm{rot}}} = \frac{t_{\mathrm{M}}\rho_A\mathcal{A}}{\bar{n}_+}\frac{\Omega^2}{4\epsilon_\Delta^2+2\Omega^2+\gamma^2} \times\left[-4\gamma\begin{pmatrix}1&0\\0&1\end{pmatrix}-\frac{\boldsymbol{I}_{\bar{\boldsymbol{n}}_{\mathrm{rot}}}}{\rho_A\mathcal{A}t_{\mathrm{M}}}\otimes\begin{pmatrix}1\\1\end{pmatrix}\right], \tag{54}$$

i.e., the first and the third terms in Eq. (50) disappear. The first term in the bracket corresponds to the dissipative dynamics, which results in a contraction of the covariance matrix. The second term describes the photon-number dependence of the Rabi frequency.

In Fig. 4(c), we depict the means and variances of the photonic modes $k = 1, 2$ in the rotated measurement frame. By definition, $\bar{n}_{\mathrm{rot},1} = \bar{n}_{\mathrm{rot},2} = \bar{n}_+/2$ for all positions. The total mean photon number is declining because of the absorption by the atoms. The rapid oscillations of the variance, which are visible in the laboratory frame, disappear in the rotated measurement frame.

Interestingly, we find that the variances of both modes are not equal. While the variance of mode $k = 1$ decreases, the variance of mode $k = 2$ significantly increases. This asymmetry is a consequence of a distortion of the probability distribution as depicted for selected values of z in Fig. 4(d). The distortion is driven by the second term of the phase-space coefficient in Eq. (54): The vector (1,1) acts on $\boldsymbol{\Sigma}$ in the direction of $\bar{n}_+$, and distorts the covariance matrix controlled by $\boldsymbol{I}_{\bar{\boldsymbol{n}}}$.

We interpret this distortion as a result of the dependence of the energy-level splitting in the two-level system on the photon number (i.e., the laser intensity): The larger the light intensity, the larger the level splitting. This relation leads to a reduced photon transfer between the atoms and the photonic modes for larger photon numbers. As the variance of the photonic probability distribution is on the order $\sqrt{\bar{n}_k}$, and the level splitting is a function of the Rabi frequencies $\Omega_k \propto \sqrt{\bar{n}_k}$, i.e., the variance and Rabi frequencies both change on the same order of magnitude, the level splitting dependence thus results in a significant distortion of the probability distribution.

D. Mean and variance

Using the coefficients in Sec. IV C, we can integrate Eq. (29) and analyze the measurement statistics after the laser pulses have propagated through the atomic cloud at $z = z_{\max}$. The results are depicted in Fig. 5.

In Fig. 5(a), we depict the mean photon number $\bar{n}_+$ and the phase shift $\bar{\varphi}_0$ along with their corresponding variances as a function of the detuning ϵ_Δ. Note that the variance associated with the $\bar{\varphi}_0$ measurement is given by the variance of n_-. The mean total photon number $\bar{n}_+$ exhibits the common absorption dip at resonance $\epsilon_\Delta = 0$, while the mean phase shift $\bar{\varphi}_0$ resembles the well-known dispersion-relation curve. The variance of n_+ and n_- both exhibit a single peak at resonance. While the variance of n_+ hardly overcomes the photon shot noise, the variance of n_- exceeds the photon shot noise by more than two orders of magnitude.

To analyze this effect theoretically, we first note that the photon number statistics of n_+ and n_- can be obtained by expressing the cumulant-generating function in Eq. (A1) it terms of the new counting fields $\chi_+ = (\chi_1 + \chi_2)/2$ and $\chi_- = (\chi_1 - \chi_2)/2$. For theoretical purposes, we introduce the coefficients

$$\kappa_\alpha^{(\delta)} = \frac{i}{t_{\mathrm{M}}}\partial_{\chi_\alpha}\mathcal{K}_{\bar{\boldsymbol{n}}_{\mathrm{rot}},\boldsymbol{\chi}=0}, \quad \kappa_{\alpha\beta}^{(\delta)} = -\frac{1}{t_{\mathrm{M}}}\partial_{\chi_\alpha}\partial_{\chi_\beta}\mathcal{K}_{\bar{\boldsymbol{n}}_{\mathrm{rot}},\boldsymbol{\chi}=0}, \tag{55}$$

with $\alpha, \beta = +, -$, which we denote as cumulant aptitudes in the following. They describe the intrinsic ability of a single atom to modify the photonic statistics of their driving fields. The dynamical cumulant-generating function is thereby evaluated in the rotating frame (as expressed by $\bar{\boldsymbol{n}}_{\mathrm{rot}}$) for which $\bar{n}_{\mathrm{rot},-} = 0$.

Analytically, the evaluation of the cumulant aptitudes is closely related to the calculation of the flow equation coefficient matrices in the rotated measurement basis in Sec. IV C, and we obtain

$$\begin{aligned}
\kappa_+^{(\delta)} &= \frac{\gamma\Omega^2}{4\epsilon_\Delta^2+2\Omega^2+\gamma},\\
\kappa_-^{(\delta)} &= \frac{2\epsilon_\Delta\Omega^2}{4\epsilon_\Delta^2+2\Omega^2+\gamma},\\
\kappa_{++}^{(\delta)} &= \frac{\gamma\Omega^2}{4\epsilon_\Delta^2+2\Omega^2+\gamma^2}+\frac{\Omega^4\gamma(8\epsilon_\Delta^2-6\gamma^2)}{(4\epsilon_\Delta^2+2\Omega^2+\gamma^2)^3},\\
\kappa_{--}^{(\delta)} &= \frac{2\Omega^4+\gamma^2\Omega^2}{\gamma(4\epsilon_\Delta^2+2\Omega^2+\gamma^2)}-\frac{8\epsilon_\Delta^2\Omega^4(4\Omega^2+4\epsilon_\Delta^2+5\gamma^2)}{\gamma(4\epsilon_\Delta^2+2\Omega^2+\gamma^2)^3},
\end{aligned} \tag{56}$$

as shown in Appendix C 3. The cumulant aptitudes are depicted in Fig. 5(b) below the corresponding measured cumulants. We see that the aptitudes closely resemble the corresponding cumulants, which shows the importance of the aptitudes to describe the response of the matter system to an external driving field. In particular, from Eq. (56) we learn that the phase variance aptitude $\kappa_{--}^{(\delta)}$ is proportional to $1/\gamma$, which is the essential driver of the phase fluctuations. As explained in Appendix C 4, the $1/\gamma$ dependency originates from incoherent jumps between the two eigenstates of the two-level system, each of which features distinct optical properties. Between these jumps, deviations from the mean photon number are correlated and add up. The correlation time, i.e., the average time between jumps, scales thereby with γ^{-1}. Consequently, the time-integrated fluctuations diverge for a vanishing dissipation. In contrast, for a large γ, the correlation time is short, such that deviations from the mean rapidly cancel each other.

To further illustrate the large fluctuations of n_-, we depict the photonic probability distribution shown in Fig. 5(c) as a function of the photon numbers n_1 and n_2 for various detunings. The closer the detuning is to the resonance $\epsilon_\Delta = 0$, the more the probability ellipsoid extends across the antidiagonal. Thus, the variance of the photon-number difference $\Delta n_1 - \Delta n_2$ (with $\Delta n_k = n_k - \bar{n}_k$) is very pronounced, while the variance of the sum of the photon numbers $\Delta n_1 + \Delta n_2$ hardly exceeds the photon shot noise. This is in agreement with the variances in Fig. 5(a) and the cumulant aptitude $\kappa_{--}^{(\delta)}$ in Fig. 5(b). Physically, the variance of the difference can grow significantly faster, as it corresponds to energy-conserving processes between the degenerate modes $k = 1$ and $k = 2$.

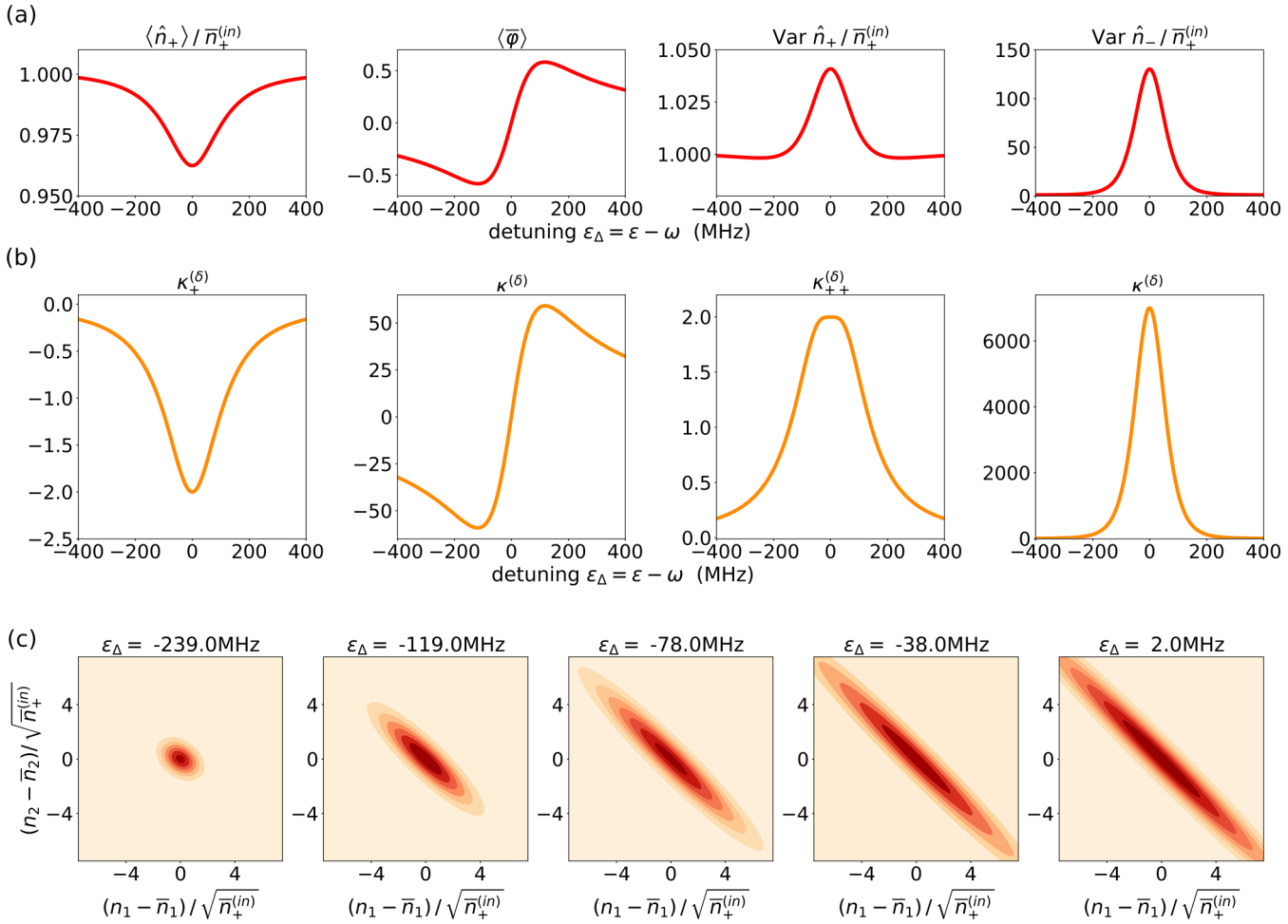


FIG. 5. Measurement statistics for the dissipative Tavis-Cummings model in Eq. (37). (a) Means and variances for the observed photon numbers n_+ and n_- obtained by integrating the flow equations in Eqs. (27) and (29) using the coefficients in Eqs. (52)–(54). (b) Corresponding cumulant aptitudes at $z = 0$ given in Eq. (56). (c) Probability distributions for selected detunings. Overall parameters are the same as in Fig. 4.

In contrast, the loss of photons is relatively unlikely for the weak dissipation in Fig. 5(c). As the photon-number difference is directly related to the phase measurement, this effect describes the tremendous fluctuations that can appear in phase measurements.

E. Fisher information

We continue to discuss the dissipative Tavis-Cummings model in Fig. 3 for its potential in spectroscopic quantum sensing. In the following, we focus on the estimation of two quantities, namely, the atomic density ρ_A, and the level splitting ϵ, which could be a function of an unknown external stimulus.

Using Eq. (34), which we evaluate using the mean values and covariance matrix obtained by the numerical integration of the flow equations, we can conveniently estimate the Fisher information for vast parameter regimes. In Figs. 6(a) and 6(b) we depict the Fisher information $\mathcal{I}_X$ for the estimation of the density $X = \rho_A$ and the energy splitting $X = \epsilon$ as a function of the detuning by a red solid line. Both Fisher informations exhibit a nontrivial dependence on the detuning. Thus, the methods introduced in this work constitute a flexible methodology to quickly find experimental parameters that optimize the sensitivity of the measurement apparatus.

To emphasize the importance of taking the added fluctuation predicted by the variance flow equation in Eq. (29) into account, we also depict a simplistic variance estimate by a dashed black line, which approximates the noise by the photon shot noise of the incoming laser pulse. We observe in Figs. 6(a) and 6(b) that this oversimplified estimate drastically fails to accurately predict the actual Fisher information by several orders of magnitude. Only far from resonance, where the variance aptitude is strongly suppressed [see Fig. 5(b)], and very close to the resonance condition, where the Fisher information is mainly carried by the total photon-number change, does the shot-noise estimate succeed in being a reliable measure.

F. Small dissipation

To better understand the functional dependence of the Fisher information on the system parameters, we investigate the Fisher information in the small-dissipation regime $\gamma \ll \Omega$. In this limit, it is safe to assume that $\overline{n}_+$ is constant, for which the integration of the flow equations in the rotating

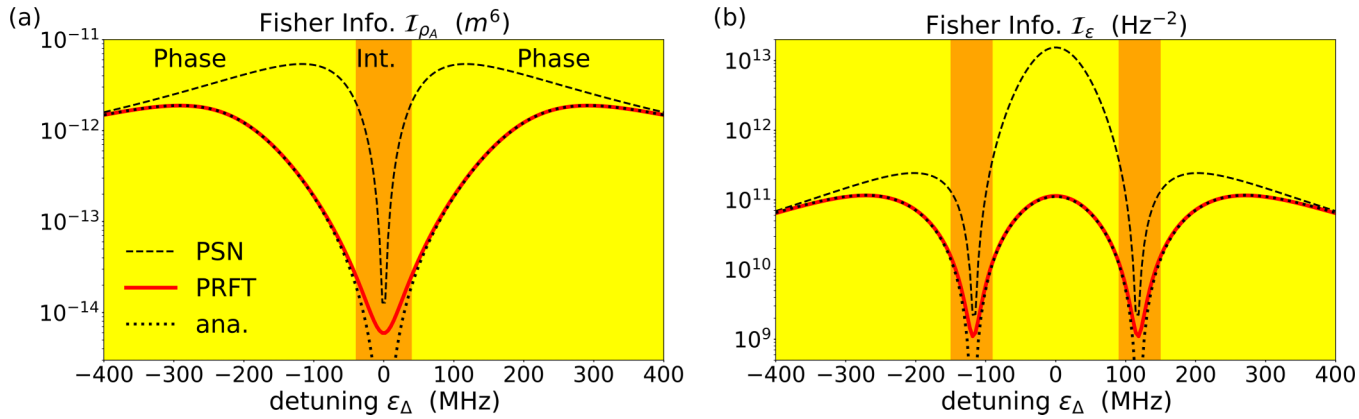


FIG. 6. (a) Fisher information for the atomic density estimation as a function of detuning. The dashed line shows the Fisher information where the photonic variance has been estimated with the initial photon shot noise (PSN). The dotted line shows the analytical result in Eq. (59). Yellow (orange) regions mark parameter regimes in which the phase (intensity) measurement dominates. (b) The same as panel (a), but for the Fisher information for the detuning. The dotted line shows the analytical result in Eq. (60). Overall parameters are the same as in Fig. 4.

measurement frame becomes trivial. Integrating Eq. (52), the total phase shift becomes

$$\overline{\varphi}_0 = \frac{t_M \rho_A \mathcal{A} z_{\max}}{\overline{n}_+} \frac{2\epsilon_\Delta \Omega^2}{4\epsilon_\Delta^2 + 2\Omega^2} + O(\gamma^0), \tag{57}$$

where we have neglected terms of order γ^0. Noteworthy, if $\Omega \ll \epsilon_\Delta$, we find that $\overline{\varphi}$ is independent of $\overline{n}_+$ as $\Omega^2 \propto \overline{n}_+$. In the opposite regime $\Omega \gg \epsilon_\Delta$, the phase shift is suppressed by a factor $\overline{n}_+^{-1}$.

Integrating Eq. (29) using Eq. (53) to obtain the covariance matrix in the weak-dissipation regime, we find

$$\boldsymbol{\Sigma}^2 = \begin{pmatrix} \frac{\overline{n}_+}{2} & 0 \\ 0 & \frac{\overline{n}_+}{2} \end{pmatrix} + 8 t_M \rho_A \mathcal{A} z_{\max} \frac{\Omega^8}{\gamma (4\epsilon_\Delta^2 + 2\Omega^2)^3} \times \begin{pmatrix} 1 & -1 \\ -1 & 1 \end{pmatrix} + O(\gamma^0, \overline{n}_+^0), \tag{58}$$

where we have neglected terms scaling with γ^0 and $\overline{n}_+^0$. The first term is the photon shot noise, while the second terms describes the noise added by the light-matter interaction. According to the explanations in Sec. IV D, it describes the fluctuations appearing in the phase measurement. The product $N_A = \rho_A \mathcal{A} z_{\max}$ is the total number of two-level systems interacting with the laser pulse.

Using Eq. (34) to calculate the Fisher information for the atom density, we obtain

$$\mathcal{I}_{\rho_A} \approx \frac{\left(t_M \mathcal{A} z_{\max} \frac{2\epsilon_\Delta \Omega^2}{4\epsilon_\Delta^2 + 2\Omega^2} \right)^2}{\overline{n}_+ + 8 t_M N_A \frac{\Omega^8}{\gamma (4\epsilon_\Delta^2 + 2\Omega^2)^3}}, \tag{59}$$

which is valid in the weak-dissipation limit. Likewise, we find that the Fisher information for the energy splitting is given by

$$\mathcal{I}_\epsilon \approx \frac{\left[t_M N_A \frac{\Omega^2 (4\epsilon_\Delta^2 - 2\Omega^2)}{(4\epsilon_\Delta^2 + 2\Omega^2)^2} \right]^2}{\overline{n}_+ + 8 t_M N_A \frac{\Omega^8}{\gamma (4\epsilon_\Delta^2 + 2\Omega^2)^3}}. \tag{60}$$

For comparison, these analytical expressions are depicted in Figs. 6(a) and 6(b), respectively, with dotted lines, which agree with the actual Fisher information for vast parameter regimes. For the detunings for which we observe deviations, the total photon number measurement n_+ contributes significantly to the Fisher information. Overall, we observe that the Fisher information contained in the phase shift is considerably larger than that in the total photon number (i.e., intensity). For this reason, it is sufficient to optimize the Fisher information related to the phase information, which is approximately given by Eqs. (59) and (60).

In Fig. 6(a), we observe that the Fisher information has a minimum at $\epsilon_\Delta = 0$, which is a consequence of the vanishing derivative of $\overline{\varphi}_0$ in Eq. (57) with respect to ρ_A. Away from the resonance, the Fisher information $\mathcal{I}_{\rho_A}$ increases and finally exhibits a turnover: For large detunings ϵ_Δ, the added noise [second term in the denominator of Eq. (59)] vanishes, and only the photon shot noise remains. In this parameter regime, the predictions of the PRFT and the naive photon shot noise approximation agree with each other. The decreasing derivative of $\overline{\varphi}_0$ in Eq. (57) for large detunings is eventually reflected in a decreasing Fisher information $\mathcal{I}_{\rho_A}$.

A similar interpretation holds for the Fisher information in Fig. 6(b) for the estimation of the level splitting ϵ. Here, we also find that the Fisher information is optimized for parameter regimes in which the phase measurement dominates, where the analytical expression in Eq. (60) agrees with the numerical result. Because of the functional dependence of the phase in Eq. (57) on ϵ, the Fisher information exhibits two minima, in which the phase sensitivity vanishes, and the Fisher information is only contained in the intensity measurement. Of note, also for the estimation of ϵ, the naive approximation of the photon shot noise (dashed line) exceeds the actual Fisher information by several orders of magnitude.

G. Dissipation dependence

In Fig. 7, we investigate the dependence of the Fisher information on the dissipation rate γ. Intriguingly, we observe that both $\mathcal{I}_{\rho_A}$ and $\mathcal{I}_\epsilon$ exhibit a turnover as a function of γ, i.e., they increase for small γ and decrease for large γ.

In the small-γ regime, we can readily explain the enhancement of the Fisher information using Eqs. (59) and (60). If $\gamma \to 0$, we can neglect the photon shot noise term in the denominator, such that $\mathcal{I}_{\rho_A} \propto \gamma$ and $\mathcal{I}_\epsilon \propto \gamma$. From

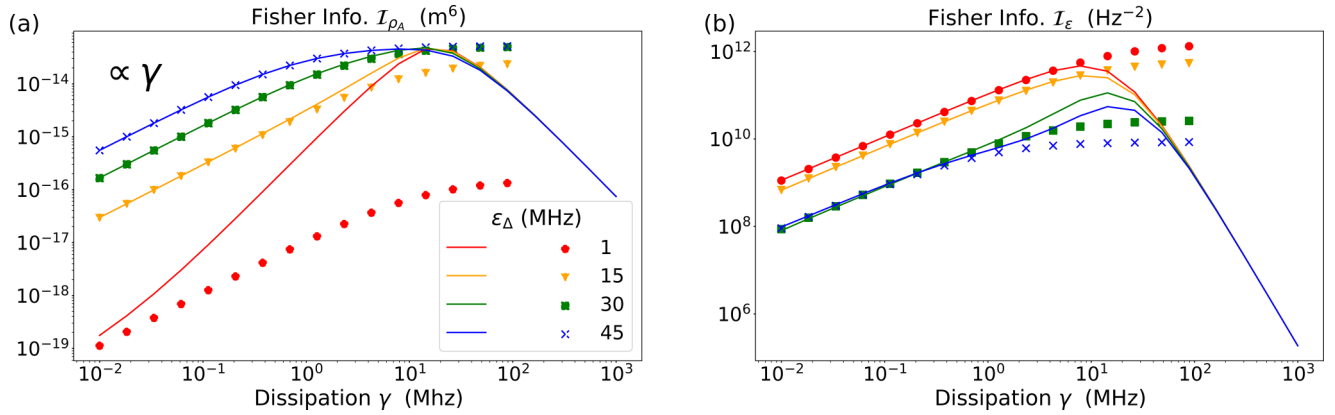


FIG. 7. Fisher information of the atom density $\mathcal{I}_{\rho_A}$ and the detuning $\mathcal{I}_\epsilon$ for the Tavis-Cummings model as a function of dissipation rate γ depicted in panels (a) and (b), respectively. The solid lines show the numerical results obtained by integrating the flow equations using the coefficients in Eqs. (51), (53), and (54). The symbols show the analytical calculations in Eq. (59) and (60). The overall parameters are the same as in Fig. 4.

these considerations, we conclude that the increase of the Fisher information in Eq. (34) is driven by a decrease of the phase fluctuation in the measurement, while the differential change of the mean phase remains almost unchanged. This is in agreement with previous investigations [90] showing that positively correlated random variables have a detrimental effect on the Fisher information: For a vanishing γ, positively correlated deviations from the mean photon number add up rapidly, instead of canceling each other, which leads to the diverging variance discussed in Sec. IV D. As an increasing dissipation γ destroys correlations in time, the Fisher information increases accordingly.

In the opposite regime of strong dissipation, we learn from Eq. (51) that the mean photon flux becomes increasingly suppressed for larger γ. This is consequently reflected in a decreasing Fisher information. In the large-dissipation regime, γ dominates the atomic dynamics such that all curves in Fig. 7 collapse on each other. Physically, the increasing γ destroys all quantum coherence in the atom, such that the system ceases to be a quantum sensor, reflected by a decreasing Fisher information.

Worthwhile, similar turnovers as a function of system-bath coupling are well known from exciton and energy transport in molecular systems [91,92] and polariton systems [93]. Thereby, the transport efficiency is optimized by an interplay of coherent and incoherent dynamics. Surprisingly, here we observe a similar turnover, yet in a genuine quantity of information science. Similar to transport in molecular systems, the optimal Fisher information requires a fine-tuned coherent dynamics, which can be controlled by an appropriately adjusted dissipation rate γ.

V. FOUR-LEVEL SYSTEM

As a more sophisticated application, we consider an ensemble of four-level systems, whose level structure is sketched in Fig. 8(a). Thereby, the four energy levels $j = a, b, c, d$ are coupled by three laser fields, namely, the probe, coupling, and signal lasers. The Hamiltonian of a single atom coupled to the light field is given by

$$\hat{H}(t) = \sum_{j=a,b,c,d} \epsilon_j |j\rangle\langle j| + \sum_{k=\mathrm{P,C,S}} \omega_k \hat{a}_k^\dagger \hat{a}_k + [g_\mathrm{P}\hat{a}_\mathrm{P}|b\rangle\langle a| + g_\mathrm{C}\hat{a}_\mathrm{C}|c\rangle\langle b| + g_\mathrm{S}\hat{a}_S|d\rangle\langle c| + \mathrm{H.c.}], \tag{61}$$

where ϵ_j and $|j\rangle$ denote the energies and the eigenstates of the atom. The probe, coupling, and signal fields are quantized by $\hat{a}_\mathrm{P}$, $\hat{a}_\mathrm{C}$, and $\hat{a}_\mathrm{S}$. The corresponding frequencies and light-matter coupling strengths are denoted by ω_k and g_k, respectively.

This and similar protocols find application in the detection of electric fields in the radio-frequency regime using Rydberg states [34–42], and have been suggested for the detection of axion dark matter in the galactic halo [94]. The signal to be

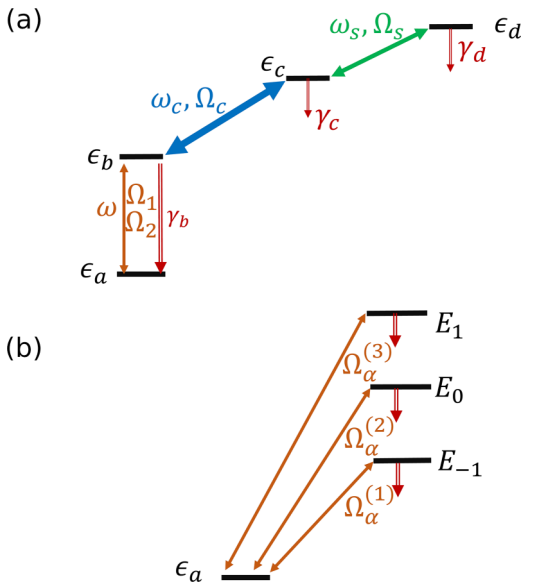


FIG. 8. (a) Sketch of the coupling structure of the four-level system in Eq. (61). (b) Representation in the partially diagonalized basis.

estimated is proportional to the Rabi frequency $\Omega_S = g_S\langle\hat{a}_S\rangle$ and typically in the range $\omega_S < 20$ GHz, which couples two Rydberg states c and d. Here, we carry out a theoretical investigation of its sensitivity by estimating the Fisher information $\mathcal{I}_X$ for $X = \Omega_S$ utilizing the methods developed in this work.

A. Semiclassical equations of motion

To estimate the measurement statistics for the four-level system, we follow the same steps introduced in Sec. IV for the two-level systems. We first express the probe field in the basis to be measured:

$$\hat{a}_P = \frac{1}{\sqrt{2}i}(\hat{a}_1 - \hat{a}_2), \tag{62}$$

according to Eq. (24). Next, we transform the Hamiltonian into an interaction frame to remove the second term of the Hamiltonian in Eq. (61). The corresponding semiclassical Hamiltonian thus becomes

$$\hat{\mathcal{H}}_{\boldsymbol{\varphi}} = \sum_{j=a,b,c,d} \epsilon_{j,\Delta}|j\rangle\langle j| + \left[\frac{\Omega_{P,\boldsymbol{\varphi}}}{2}|b\rangle\langle a| + \frac{\Omega_C}{2}|c\rangle\langle b| + \frac{\Omega_S}{2}|d\rangle\langle c| + \text{H.c.}\right], \tag{63}$$

where $\epsilon_{a,\Delta} = \epsilon_a$, $\epsilon_{b,\Delta} = \epsilon_b - \omega_P$, $\epsilon_{c,\Delta} = \epsilon_c - \omega_P - \omega_C$, and $\epsilon_{d,\Delta} = \epsilon_d - \omega_P - \omega_C - \omega_S$. The Rabi frequencies of the coupling and signal fields are denoted by Ω_C and Ω_S. We choose the corresponding driving phases to be zero. We express the Rabi frequency of the probe field in terms of the Rabi frequencies of the measured fields Ω_1 and Ω_2 as

$$\Omega_{P,\boldsymbol{\varphi}} = \frac{\sqrt{2}}{i}(\Omega_1 e^{i\varphi_1} - \Omega_2 e^{i\varphi_2}), \tag{64}$$

where φ_1 and φ_2 are the respective phases.

To construct the dynamical cumulant-generating function, we follow the same procedure as for the two-level system in Sec. IV A. To model dissipative effects, we solve the generalized Liouvillian equation

$$\frac{d}{dt}\rho_{\boldsymbol{\chi}} = -i\left[\hat{\mathcal{H}}_{\boldsymbol{\varphi}+\frac{\boldsymbol{\chi}}{2}}\rho_{\boldsymbol{\chi}} - \rho_{\boldsymbol{\chi}}\hat{\mathcal{H}}_{\boldsymbol{\varphi}-\frac{\boldsymbol{\chi}}{2}}\right] + \sum_{j=b,c,d}\gamma_j D_{|a\rangle\langle j|}\rho_{\boldsymbol{\chi}}, \tag{65}$$

where $\rho_{\boldsymbol{\chi}}(t)$ denotes the reduced density matrix of a single atom. The dynamical cumulant-generating function is then equal to the trace of $\rho_{\boldsymbol{\chi}}(t)$. In Eq. (65), we have phenomenologically added the decay from the excited states to the ground states with dissipation rate γ_j, where the dissipator is defined by

$$D_{\hat{O}}\rho = \hat{O}\rho\hat{O}^\dagger - \tfrac{1}{2}(\hat{O}^\dagger\hat{O}\rho + \rho\hat{O}^\dagger\hat{O}). \tag{66}$$

The corresponding decay rates are denoted γ_j.

B. Findings

The numerically evaluated findings for the mean and variances of the measurement statistics of the total photon number and the phase estimation are depicted in Fig. 9(a). In contrast with the findings in Fig. 5(a), the four-level system exhibits three resonances, two of which feature broad absorption dips for $\bar{n}_+$ around $\epsilon_{ba,\Delta} \approx \pm 20$MHz, and one narrow dip for $\epsilon_{ba,\Delta} = 0$. Accordingly, the dispersion of $\overline{\varphi}$ consists of three characteristic phase steps. The variance of $\hat{n}_+$ hardly deviates from the initial photon shot noise. In contrast, the variance of $\hat{n}_-$ exceeds the initial photon shot noise by several orders of magnitude for all three resonances. This is thus reminiscent of the findings in Fig. 5(a), where the variance of $\hat{n}_-$ is significantly more pronounced than that of $\hat{n}_+$.

The corresponding cumulant aptitudes are depicted in Fig. 9(b), which exhibit a close resemblance with the means and the variances in Fig. 9(a). We conclude that the main information about the measured photon statistics is directly determined by these quantities. In Fig. 9(c), we depict the probability distribution for selected detunings, which illustrates the dominance of the $\hat{n}_-$ noise over the $\hat{n}_+$ noise for parameters close to the resonance.

In Fig. 10(a), we depict the estimate for the Fisher information $\mathcal{I}_{\Omega_S}$. As the system is more sophisticated than the two-level system in Sec. IV, the overall dependence on the system parameters is more complicated. We compare the Fisher information predicted by the PRFT with the photon shot noise estimation, as we did in Fig. 6. In doing so, we find that the photon shot noise estimation would drastically overestimate the Fisher information by more than three orders of magnitude.

In Figs. 10(b) and 10(c), we depict the Fisher information in two special detuning intervals $\epsilon_{ba,\Delta} \in [-3\text{ MHz}, 3\text{ MHz}]$ and $\epsilon_{ba,\Delta} \in [10\text{ MHz}, 30\text{ MHz}]$. Notably, Figs. 10(b) and 10(c) closely resemble Figs. 6(a) and 6(b), respectively, investigating the two-level system. This close resemblance will be explained in the next section.

C. Analysis

The more advanced four-level system does not allow for a simple nonperturbative treatment as the two-level system in Sec. IV. Nevertheless, here we give some analytical arguments which explain why Figs. 6(a) and 6(b) closely resemble Figs. 10(b) and 10(c).

To this end, we assume that the probe-field Rabi frequency is significantly smaller than the Rabi frequencies of the coupling and the signal fields. In this regime, it is beneficial to represent the three excited states in their diagonal basis as sketched in Fig. 8(b). In this basis, the Hamiltonian reads

$$\hat{\mathcal{H}}_{\boldsymbol{\varphi}} = \sum_{j=a,0,\pm1} E_{j,\Delta}|j\rangle\langle j| + \sum_{j=0,\pm1}\left[\frac{\Omega_{j,\boldsymbol{\varphi}}}{2}|j\rangle\langle 0| + \text{H.c.}\right], \tag{67}$$

where $E_{a,\Delta} = \epsilon_a$,

$$E_{0,\Delta} = \epsilon_b, \quad E_{\pm1,\Delta} = \epsilon_b \pm \frac{1}{2}\sqrt{\Omega_C^2 + \Omega_S^2}, \tag{68}$$

denote the level energies, and

$$\Omega_{0,\boldsymbol{\varphi}} = \frac{\Omega_S}{2\sqrt{\Omega_C^2 + \Omega_S^2}}\Omega_{P,\boldsymbol{\varphi}}, \quad \Omega_{\pm1,\boldsymbol{\varphi}} = \pm\frac{\Omega_C}{\sqrt{\Omega_C^2 + \Omega_S^2}}\Omega_{P,\boldsymbol{\varphi}} \tag{69}$$

are the effective Rabi frequencies in the modified basis.

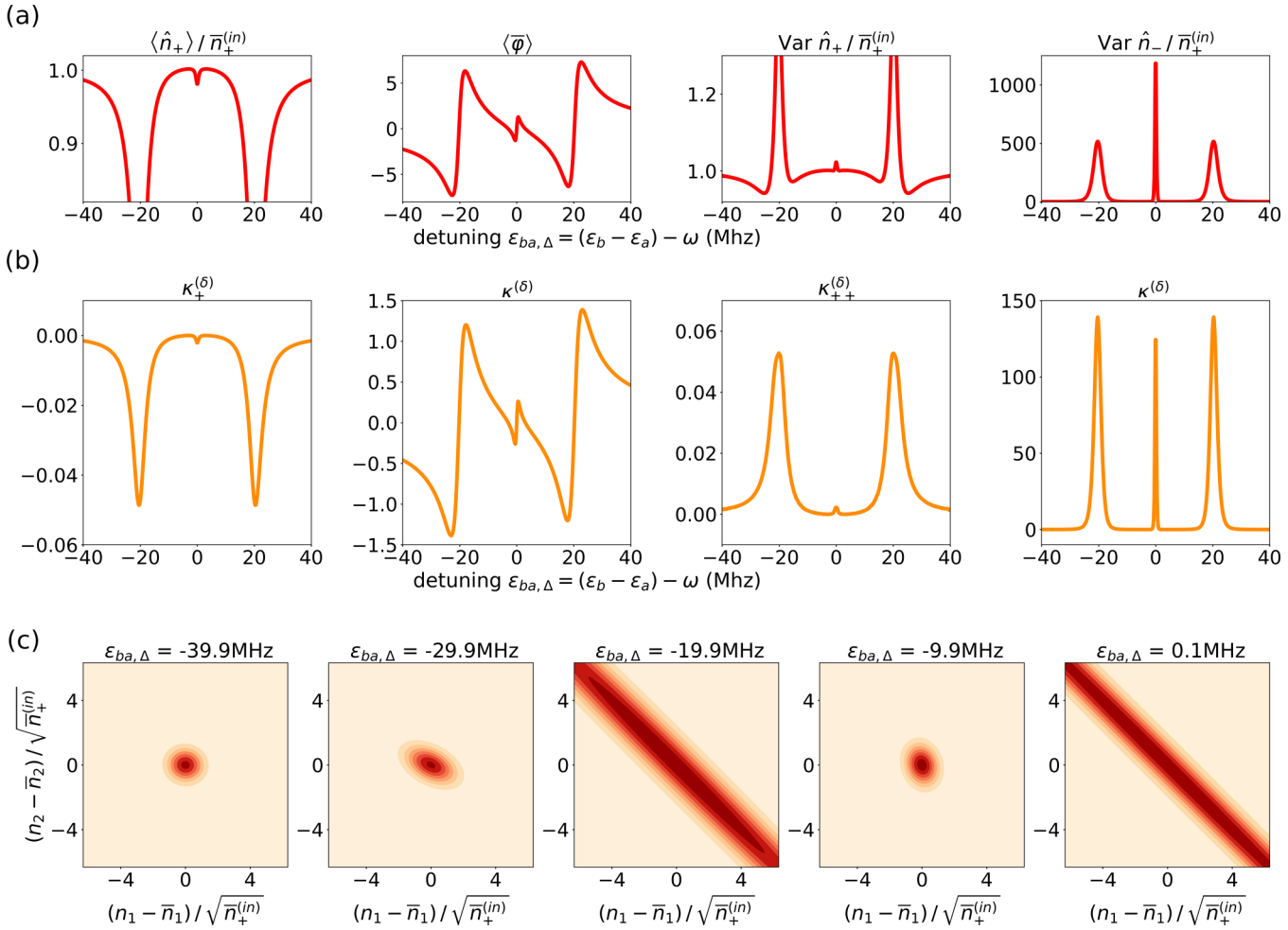


FIG. 9. Analysis of the measurement statistics for the four-level system in Eq. (61). (a) Mean values and variances of the photon measurement statistics, which are calculated in the same way as for Fig. 5. (b) Corresponding cumulant aptitudes at $z = 0$. (c) Photonic probability distribution for selected detunings. Parameters of the probe field are $P = 0.1$ mW, $\mathcal{A} = 1$ cm^2, $t_\mathrm{P} = 1$ s, $\lambda = 500$ nm, and atomic dipole moment $d = 5ea_0$, which gives rise to an Rabi frequency of $\Omega_\mathrm{P} = 1.9$ MHz. Other parameters are $\Omega_\mathrm{C} = 20$ MHz, $\Omega_\mathrm{S} = 3$ MHz $\gamma_b = 0.1$ MHz, $\gamma_c = 0.01$ MHz $= \gamma_d = 0.01$ MHz, $z_\mathrm{max} = 10$ cm, $\rho_A = 5 \times 10^{13}$ m^{-3}, and $t_\mathrm{M} = 1$ s.

Based on this representation, we can interpret the ensemble of four-level systems as consisting of three ensembles of two-level systems with distinct physical properties. The respective excitation energies and Rabi frequencies of each two-level system are given by Eqs. (68) and (69). Each ensemble of two-level systems contributes independently to the measurement properties in Fig. 9(a). For this reason, the means and variances of the total photon number measurement and the phase measurement appear to be a concatenation of three two-level-system measurements, each with a different excitation frequency.

We use this interpretation to explain the respective similarity of Figs. 6(a) and 6(b) with Figs. 10(b) and 10(c). The derivation of the mean photon numbers $\overline{n}_k$ with respect to the signal Rabi frequency Ω_S is closely related to the derivations of the Hamiltonian parameters in Eqs. (68) and (68) with respect to Ω_S: From Eq. (68), we find that only $E_{\pm1,\Delta}$ have a functional dependence on Ω_S, while from Eq. (69), we see that $\Omega_{0,\varphi}$ depends more sensitively on Ω_S than $\Omega_{\pm1,\varphi}$. In other words, a variation of Ω_S leads thus mainly to variations of $\Omega_{0,\varphi}$ and $E_{\pm1,\Delta}$.

A variation of $\Omega_{0,\varphi}$ is closely related to a variation of the atomic density, as the probe field experiences an effectively modified impact of the atomic ensemble. As $\Omega_{0,\varphi}$ is prevalent for detunings close to $\epsilon_{ba,\Delta} = 0$, the Fisher information in Fig. 6(a) for the density estimation resembles the Fisher information in Fig. 10(b). Likewise, a variation of $E_{\pm1,\Delta}$ corresponds to a variation of the level splitting in a two-level system. As the $E_{\pm1,\Delta}$ variation impact is prevalent for detunings close to $\epsilon_{ba,\Delta} = \pm 20$ MHz, the Fisher information in Fig. 6(b) for ϵ resembles the Fisher information in Fig. 10(c).

Our analysis in terms of the partially diagonalized Hamiltonian in Eq. (67) is thus capable of explaining the overall structure of the Fisher information in Fig. 10(a) in the parameter regime investigated here. The investigation of arbitrary parameter regimes of this four-level model would require a more comprehensive numerical study and a more sophisticated analytical treatment, which exceeds the scope of the present work. We expect that new quantum effects beyond these explanations in terms of a set of two-level systems can appear for a strong probe field. Moreover, for a vanishing signal $\Omega_\mathrm{S} = 0$, the emergent dark state induces

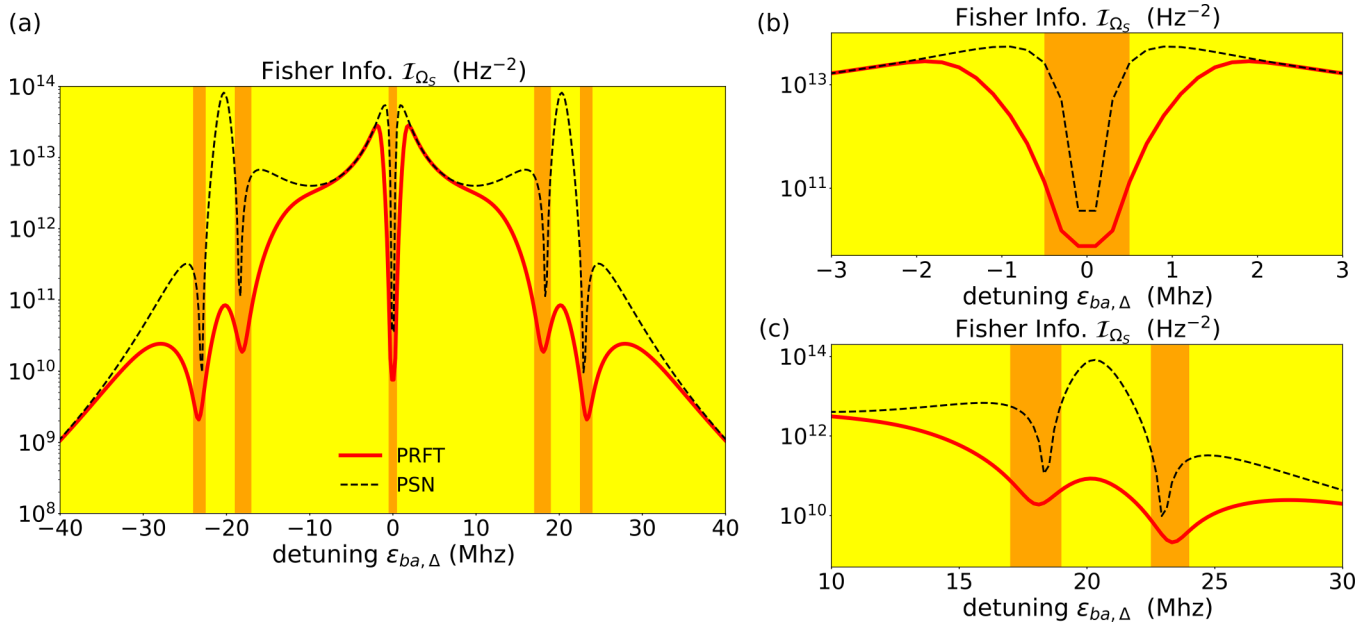


FIG. 10. Analysis of the Fisher information $\mathcal{I}_{\Omega_S}$ for the estimation of the signal amplitude Ω_S using the four-level system. Parameters are the same as in Fig. 9.

the so-called electromagnetically induced transparency effect [95,96], which will be investigated elsewhere.

VI. CONCLUSIONS

We have developed a comprehensive framework of light-matter interaction that is capable of predicting the spectroscopic measurement statistics by evaluating the semiclassical dynamics of quantum emitters, such as atoms and molecules. This allows us to predict the sensitivity of the spectroscopic quantum sensing protocol in terms of the Fisher information. The framework constructs flow equations for the mean values and the covariance matrix of relevant spectroscopic observables. In this work, we have focused on the measurement statistics related to the intensity, the polarization direction, and the phase shift. The application to dissipative two-level systems and four-level systems has demonstrated the flexibility of the developed framework.

We conjecture that the spectroscopic analysis deploying a full counting statistics approach has plenty of applications. In particular, it can optimize the operational configuration of currently existing spectroscopic quantum sensing devices, which deploy complicated level structures or periodic driving protocols [36,37,46]. As our approach is nonperturbative, it allows us to predict and interpret the statistical features close to resonance conditions, for which both the signal and the noise are strongly enhanced. This might prove advantageous when extending the current methods to investigate the dynamics of laser systems, which are naturally closely related to spectroscopy. Laser systems, which typically work close to resonance conditions to enhance the gain, often suffer from phase diffusion, which can be investigated with virtually the same methods as introduced here. Moreover, the simplicity of the semiclassical approach enables us to investigate the measurement statistics of interacting many-body systems and their potential in quantum sensing.

Furthermore, there are several relevant topics that have not been addressed in this work. In the cases studied in Secs. IV and V, we have focused on the stationary state. When assuming short pulse durations t_P, one must integrate the Schrödinger equation (or Liouville equation) to obtain the correct dynamical cumulant-generating function. This will be important for transient dynamics, for example, in the read-out of atomic interferometers. In addition, we have not considered some other effects, such as the Doppler shift or a broken rotational symmetry of the quantum emitters, for which the integration of the flow equations will become more elaborate.

Moreover, in our studies, we have assumed that the measurement time is relatively long. Modern measurement devices allow us to record spectroscopic signals with a high temporal resolution. As the PRFT accounts for the accumulated photon number (i.e., the time-integrated signal), a theoretical prediction of the joint probability distribution for the time-resolved measurement statistics will give a higher estimate for the Fisher information. As such, the Fisher information predicted by the PRFT can be interpreted as a lower bound for the Fisher information of the joint probability distribution. Given that the PRFT can also construct Kraus operators related to specific measurement outcomes [61], it is also possible to calculate the detailed joint probability distribution. These questions will be addressed in future work.

ACKNOWLEDGMENTS

G.E. acknowledges the support by the National Natural Science Foundation of China (Grant No. W2432004). Z.Z. acknowledges the Excellent Young Scientists Fund by National Science Foundation of China (No. 9240172), the General Fund by National Science Foundation of China (No. 12474364), and the National Science Foundation of China/RGC Collaborative Research Scheme (No. 9054901).

DATA AVAILABILITY

The data that support the findings of this article are openly available [97].

APPENDIX A: DERIVATION OF THE CUMULANT FLOW EQUATION

In this appendix, we provide a detailed step-by-step derivation of the flow equation for the cumulant-generating function in Eq. (9). In Appendix A 1, we first recall the basic concepts of full-counting statistics. In Appendix A 2, we derive an exact, yet formal, expression for the moment-generating function of the photonic field after interaction of the laser light with a localized quantum system using the concepts of the PRFT. In Appendix A 3, we apply a semiclassical approximation of the moment-generating function and carry out a scaling analysis to identify the leading terms. In Appendix A 4, we progress from the interaction of a localized quantum system with the laser field to the interaction of a spatially extended ensemble of atoms with the laser field by deriving the flow equation of the cumulant-generating function. In Appendix A 5, we provide some technical interpretations about the terms appearing in the flow equation. Finally, in Appendix A 6, we prove the equivalence of the first-order flow equation and the Maxwell-Bloch theory, and interpret the higher-order flow equations in this spirit.

1. Full-counting statistics

Here, we briefly review the basic concepts of full-counting statistics. The moment- and cumulant-generating functions of the photonic probability distribution are defined by

$$M_{\boldsymbol{\chi}}(t) = \langle e^{-i\sum_k \chi_k \hat{a}_k^\dagger \hat{a}_k}\rangle, \quad K_{\boldsymbol{\chi}}(t) = \log M_{\boldsymbol{\chi}}(t), \tag{A1}$$

where $\langle\bullet\rangle$ denotes the expectation value with regard to an arbitrary quantum state. For instance, for the Gaussian state in Eq. (4), the moment-generating function is given by

$$M_{\boldsymbol{\chi}} = e^{-i\overline{\boldsymbol{n}}\cdot\boldsymbol{\chi} - \frac{1}{2}\boldsymbol{\chi}\boldsymbol{\Sigma}^2\boldsymbol{\chi}}. \tag{A2}$$

For brevity, we have represented the counting fields using a vector notation $\boldsymbol{\chi} = (\overline{\chi}_1, \ldots, \overline{\chi}_D)$. The cumulants of the photonic probability distribution are defined as the derivatives of the cumulant-generating function with respect to the counting fields

$$\kappa_{l_1,\ldots,l_D} \equiv i^{l_1+\cdots+l_D} \frac{d^{l_1}}{d\chi_1^{l_1}} \cdots \frac{d^{l_D}}{d\chi_D^{l_D}} K_{\boldsymbol{\chi}=\boldsymbol{0}}, \tag{A3}$$

where the l_k are positive integer-valued numbers.

The cumulants allow for a geometric interpretation of the characteristic features of the probability distribution, and have convenient mathematical properties. For example, the first and second cumulants, which explicitly read

$$\begin{aligned}\overline{n}_k &= \kappa_{0,\ldots,l_k=1,\ldots,0} = \sum_{\boldsymbol{n}} n_k p_{\boldsymbol{n}},\\ \sigma^2_{k_1k_2} &= \kappa_{0,\ldots,l_{k_1}=1,\ldots,l_{k_2}=1,\ldots,0}\\ &= \sum_{\boldsymbol{n}} \big[n_{k_1} - \overline{n}_{k_1}\big]\big[n_{k_2} - \overline{n}_{k_2}(t)\big] p_{\boldsymbol{n}}(t),\end{aligned} \tag{A4}$$

are the means and the covariances of the probability distribution. For a notational reason, we combine the $\sigma^2_{k_1k_2}$ into the covariance matrix $(\boldsymbol{\Sigma}^2)_{k_1,k_2} = \sigma^2_{k_1k_2}$, whose diagonal elements represent the variances of the probability distribution.

2. Exact moment-generating function

Here, we derive an expression for the moment-generating function of the laser pulse operators $\hat{a}_k$ appearing in the Hamiltonian in Eq. (1) after interaction with a localized quantum system. For later purposes, we assume a more generic light-matter initial state than the one in Eq. (2), namely

$$\rho_{\mathrm{tot}}(t=0) = \rho^{(\mathrm{M})}(0) \otimes \rho^{(\mathrm{L})}(0), \tag{A5}$$

i.e., where the light field is described by a mixed state instead of a pure state. Thereby, we assume that $\rho^{(\mathrm{L})}(0)$ describes a highly occupied photonic state with a well-defined phase. This condition will be further formalized during the semiclassical approximation in Appendix A 3. The moment-generating function of the time-evolved photonic probability distribution in Eq. (A1) becomes

$$M_{\boldsymbol{\chi}}(t) \equiv \mathrm{tr}[\hat{U}^{(N)\dagger}(t) e^{-i\sum_k \chi_k \hat{a}_k^\dagger \hat{a}_k} \hat{U}^{(N)}(t) \rho_{\mathrm{tot}}(0)], \tag{A6}$$

where $\hat{U}^{(N)}(t)$ denotes the time-evolution operator corresponding to the Hamiltonian in Eq. (1). The index N refers thereby to the number of quantum emitters. In an interaction picture defined by $U^{(\mathrm{free})} = \exp(-iH_{\mathrm{L}}t)$ with $H_{\mathrm{L}} = \sum_k \omega_k \hat{a}_k^\dagger \hat{a}_k$, the time-evolution operators can be written as

$$\hat{U}^{(N)}(t) = \hat{U}^{(\mathrm{free})}(t) \hat{U}^{(N,\mathrm{int})}(t), \tag{A7}$$

where $\hat{U}^{(N,\mathrm{int})}(t)$ denotes the time-evolution operator in the interaction picture. Evaluating the time-evolution operator in the Fock basis, we find

$$[\hat{U}^{(N)}(t)]_{\boldsymbol{n},\boldsymbol{n}_1} = \langle \boldsymbol{n}|\hat{U}^{(N)}(t)|\boldsymbol{n}_1\rangle = e^{-i\boldsymbol{\omega}\cdot\boldsymbol{n}} [\hat{U}^{(N,\mathrm{int})}(t)]_{\boldsymbol{n},\boldsymbol{n}_1}. \tag{A8}$$

We can now evaluate the moment-generating function of the photonic probability distribution

$$\begin{aligned} M_{\boldsymbol{\chi}}(t) &= \sum_{\boldsymbol{n},\boldsymbol{n}_1,\boldsymbol{n}_2} \mathrm{tr}\{[\hat{U}^{(N)\dagger}(t)]_{\boldsymbol{n}-\boldsymbol{n}_1,\boldsymbol{n}} e^{-i\boldsymbol{\chi}\cdot\boldsymbol{n}} [\hat{U}^{(N)}(t)]_{\boldsymbol{n},\boldsymbol{n}-\boldsymbol{n}_2}\\ &\quad \times \rho^{(\mathrm{M})}(0)\} \rho^{(\mathrm{L})}_{\boldsymbol{n}-\boldsymbol{n}_1,\boldsymbol{n}-\boldsymbol{n}_2}\\ &= \sum_{\boldsymbol{n},\boldsymbol{n}_1,\boldsymbol{n}_2} \langle [\hat{U}^{(N,\mathrm{int})\dagger}(t)]_{\boldsymbol{n}-\boldsymbol{n}_1,\boldsymbol{n}} e^{-i\boldsymbol{\chi}\cdot\boldsymbol{n}} [\hat{U}^{(N,\mathrm{int})}(t)]_{\boldsymbol{n},\boldsymbol{n}-\boldsymbol{n}_2}\rangle_0\\ &\quad \times \rho^{(\mathrm{L})}_{\boldsymbol{n}-\boldsymbol{n}_1,\boldsymbol{n}-\boldsymbol{n}_2}\\ &= \sum_{\boldsymbol{n},\boldsymbol{n}_1,\boldsymbol{n}_2} \langle [\hat{U}^{(N,\mathrm{int})\dagger}(t)]_{\overline{\boldsymbol{n}}+\boldsymbol{n}-\boldsymbol{n}_1,\boldsymbol{n}} [\hat{U}^{(N,\mathrm{int})}(t)]_{\overline{\boldsymbol{n}}+\boldsymbol{n},\boldsymbol{n}-\boldsymbol{n}_2}\rangle_0\\ &\quad \times e^{-i\boldsymbol{\chi}\cdot(\overline{\boldsymbol{n}}+\boldsymbol{n})} \rho^{(\mathrm{L})}_{\overline{\boldsymbol{n}}+\boldsymbol{n}-\boldsymbol{n}_1,\overline{\boldsymbol{n}}+\boldsymbol{n}-\boldsymbol{n}_2}. \end{aligned} \tag{A9}$$

In the first equality, we have expressed Eq. (A6) in the Fock basis. In the second equality, we have introduced the notation $\langle\bullet\rangle_0 = \mathrm{tr}[\bullet\rho^{(\mathrm{M})}(0)]$ and deployed Eq. (A8). In the third equality, we have shifted the dummy index $\boldsymbol{n}$ by $\overline{\boldsymbol{n}}$.

Next, we carry out a Taylor series of the matter-system expectation value as a function of photon number around the

mean-photon number of the system $\overline{\boldsymbol{n}}$, guided by the intuition that the photon-number dependence of the photonic creation and annihilation operators depends only weakly on the photon number in the high-occupation regime. In doing so, we obtain

$$M_{\boldsymbol{\chi}}(t) = \sum_{r=0}^{\infty} \sum_{\iota_1+\ldots+\iota_D=r} \left\{ \partial_{\overline{n}_1}^{\iota_1} \cdots \partial_{\overline{n}_{\mathrm{D}}}^{\iota_{\mathrm{D}}} \langle [\hat{U}^{(N,\mathrm{int})\dagger}(t)]_{\overline{\boldsymbol{n}}-\boldsymbol{n}_1,\overline{\boldsymbol{n}}} [\hat{U}^{(N,\mathrm{int})}(t)]_{\overline{\boldsymbol{n}},\overline{\boldsymbol{n}}-\boldsymbol{n}_2} \rangle_0 \right\} \frac{n_1^{\iota_1} \cdots n_{\mathrm{D}}^{\iota_{\mathrm{D}}}}{\iota_1! \cdots \iota_{\mathrm{D}}!} e^{-i\boldsymbol{\chi}\cdot(\overline{\boldsymbol{n}}+\boldsymbol{n})} \rho^{(\mathrm{L})}_{\overline{\boldsymbol{n}}+\boldsymbol{n}-\boldsymbol{n}_1,\overline{\boldsymbol{n}}+\boldsymbol{n}-\boldsymbol{n}_2}, \tag{A10}$$

where r denotes the Taylor expansion order. The subscript of the second summation ($\iota_1 + \cdots + \iota_{N_{\mathrm{D}}} = r$) means that we have to sum over all combinations $\iota_1, \ldots, \iota_{N_{\mathrm{D}}}$ whose index sum equals r. The derivatives with respect to the mean photon numbers $\overline{n}_k$ are denoted by $\partial_{\overline{n}_k}^{i}$, where i denotes the order of the derivation. Physically, the higher-order terms $r > 0$ in Eq. (11) appear because of the photon-number dependence of the photonic creation and annihilation operators $\langle n_k - 1|\hat{a}_k|n_k\rangle = \langle n_k|\hat{a}_k^\dagger|n_k - 1\rangle = \sqrt{n_k}$.

By shifting the dummy index in Eq. (A9), we have already deployed the concentration of the probability distribution around the mean photon number in the moment-generating function. As stated below Eq. (A5), the photonic state shall also feature a well-defined phase. To account for this, we carry out Fourier transformations from the photon numbers $\boldsymbol{n}$ to their conjugate phases $\boldsymbol{\varphi}$, which are explicitly defined by

$$[\hat{U}^{(N,\mathrm{int})}(t)]_{\overline{\boldsymbol{n}},\overline{\boldsymbol{n}}-\boldsymbol{n}_1} = \frac{1}{(2\pi)^D} \int_{-\pi}^{\pi} d\boldsymbol{\varphi} \hat{U}^{(N)\dagger}_{\overline{\boldsymbol{n}},\boldsymbol{\varphi}}(t) e^{-i\boldsymbol{\varphi}\cdot\boldsymbol{n}_1}, \quad \rho^{(\mathrm{L})}_{\boldsymbol{n}_1,\boldsymbol{n}_2} = \frac{1}{(2\pi)^D} \iint_{-\pi}^{\pi} d\boldsymbol{\varphi}_1 d\boldsymbol{\varphi}_2 \rho^{(\mathrm{L})}_{\boldsymbol{\varphi}_1,\boldsymbol{\varphi}_2} e^{-i(\boldsymbol{\varphi}_1\cdot\boldsymbol{n}_1 - \boldsymbol{\varphi}_2\cdot\boldsymbol{n}_2)}. \tag{A11}$$

Inserting these Fourier transformations, the moment-generating function reads

$$\begin{aligned} M_{\boldsymbol{\chi}}(t) = \sum_{r=0}^{\infty} \sum_{\iota_1+\ldots\iota_{N_{\mathrm{D}}}} \frac{1}{(2\pi)^{3D}} \iiint\!\!\int \boldsymbol{\varphi}_1\boldsymbol{\varphi}_2\boldsymbol{\varphi}_3\boldsymbol{\varphi}_4 \sum_{\boldsymbol{n},\boldsymbol{n}_1,\boldsymbol{n}_2} \left\{ \partial_{\overline{n}_1}^{\iota_1} \cdots \partial_{\overline{n}_D}^{\iota_D} \langle \hat{U}^{(N)\dagger}_{\overline{\boldsymbol{n}},\boldsymbol{\varphi}_1}(t) \hat{U}^{(N)}_{\overline{\boldsymbol{n}},\boldsymbol{\varphi}_2}(t) \rangle_0 \right\} \frac{n_1^{\iota_1} \cdots n_{\mathrm{D}}^{\iota_D}}{\iota_1! \cdots \iota_D!} \\ \times \rho^{(\mathrm{L})}_{\boldsymbol{\varphi}_3,\boldsymbol{\varphi}_4} e^{i\boldsymbol{n}\cdot(\boldsymbol{\varphi}_4 - \boldsymbol{\chi} + \boldsymbol{\varphi}_3) + i\boldsymbol{n}_1\cdot(\boldsymbol{\varphi}_3 - \boldsymbol{\varphi}_1) - i\boldsymbol{n}_2\cdot(\boldsymbol{\varphi}_4 - \boldsymbol{\varphi}_2) + i\overline{\boldsymbol{n}}\cdot(\boldsymbol{\varphi}_4 - \boldsymbol{\chi} + \boldsymbol{\varphi}_3)}. \end{aligned} \tag{A12}$$

This form will allow us to evaluate the time-evolution operators $\hat{U}^{(N)\dagger}_{\overline{\boldsymbol{n}},\boldsymbol{\varphi}_1}$ at a well-defined phase later in the semiclassical approximation in Appendix A 3.

For illustration of the representation in terms of the phase, let us consider the photonic density matrix of the Gaussian state in Eq. (4). Carrying out the inverse Fourier transformation in Eq. (A11), we find

$$\rho^{(\mathrm{L})}_{\boldsymbol{\varphi}_1,\boldsymbol{\varphi}_2} = a_{\boldsymbol{\varphi}_1} a^*_{\boldsymbol{\varphi}_2}, \quad a_{\boldsymbol{\varphi}} = \frac{\sqrt{\det \sqrt{2}\boldsymbol{\Sigma}}}{(2\pi)^{\frac{N_{\mathrm{D}}}{4}}} e^{-(\boldsymbol{\varphi}-\overline{\boldsymbol{\varphi}})\boldsymbol{\Sigma}^2(\boldsymbol{\varphi}-\overline{\boldsymbol{\varphi}})} e^{i(\boldsymbol{\varphi}-\overline{\boldsymbol{\varphi}})\cdot\overline{\boldsymbol{n}}}. \tag{A13}$$

To reach the semiclassical limit in Appendix A 3, it will be crucial that we have a photonic state with photon numbers $\boldsymbol{n}$ and phases $\boldsymbol{\varphi}$ centered around their respective means. To make this limit precise, we assume that $\boldsymbol{\Sigma}^2 = \sigma \tilde{\boldsymbol{\Sigma}}^2$, where the matrix $\tilde{\boldsymbol{\Sigma}}^2$ shall be constant. The semiclassical limit can then be controlled by assuming $\overline{n}_k \to \infty$ and $\sigma \to \infty$ such that $\overline{n}_k/\sigma \to \infty$. For instance, this is true for a coherent state with $\sigma = \sqrt{\overline{n}_k}$.

The ongoing strategy is to deploy the identity

$$\frac{1}{2\pi} \sum_{-\infty}^{\infty} e^{-i\varphi n} = \delta(\varphi) \tag{A14}$$

to identify delta functions $\delta(\varphi)$ in Eq. (A12), which can then be used to evaluate some of the phase integrals. However, the photon numbers $n_k^{\iota_k}$ in Eq. (A12) prevent us from identifying the delta functions so far. For this reason, we express the photon numbers using derivatives with respect to the counting fields in the following way:

$$\begin{aligned} M_{\boldsymbol{\chi}}(t) &= \sum_{r=0}^{\infty} \sum_{\iota_1+\ldots+\iota_D=r} \frac{1}{(2\pi)^{3D}} \iiint\!\!\int \boldsymbol{\varphi}_1\boldsymbol{\varphi}_2\boldsymbol{\varphi}_3\boldsymbol{\varphi}_4 \sum_{\boldsymbol{n},\boldsymbol{n}_1,\boldsymbol{n}_2} \left\{ \partial_{\overline{n}_1}^{\iota_1} \cdots \partial_{\overline{n}_D}^{\iota_D} \langle \hat{U}^{(N)\dagger}_{\overline{\boldsymbol{n}},\boldsymbol{\varphi}_1}(t) \hat{U}^{(N)}_{\overline{\boldsymbol{n}},\boldsymbol{\varphi}_2}(t) \rangle_0 \right\} \\ &\quad \times \rho^{(\mathrm{L})}_{\boldsymbol{\varphi}_3,\boldsymbol{\varphi}_4} e^{i\boldsymbol{n}\cdot(\boldsymbol{\varphi}_4+\boldsymbol{\varphi}_3) + i\boldsymbol{n}_1\cdot(\boldsymbol{\varphi}_3-\boldsymbol{\varphi}_1) - i\boldsymbol{n}_2\cdot(\boldsymbol{\varphi}_4-\boldsymbol{\varphi}_2) + i\overline{\boldsymbol{n}}\cdot(\boldsymbol{\varphi}_4-\boldsymbol{\chi}+\boldsymbol{\varphi}_3)} \frac{\partial_{-i\chi_1}^{\iota_1} \cdots \partial_{-i\chi_D}^{\iota_D}}{\iota_1! \cdots \iota_D!} e^{-i\boldsymbol{n}\cdot\boldsymbol{\chi}} \\ &= \sum_{r=0}^{\infty} \sum_{\iota_1+\ldots+\iota_D=r} \frac{1}{(2\pi)^{3D}} e^{-i\overline{\boldsymbol{n}}\cdot\boldsymbol{\chi}} \frac{\partial_{-i\chi_1}^{\iota_1} \cdots \partial_{-i\chi_D}^{\iota_D}}{\iota_1! \cdots \iota_D!} \iiint\!\!\int \boldsymbol{\varphi}_1\boldsymbol{\varphi}_2\boldsymbol{\varphi}_3\boldsymbol{\varphi}_4 \sum_{\boldsymbol{n},\boldsymbol{n}_1,\boldsymbol{n}_2} \left\{ \partial_{\overline{n}_1}^{\iota_1} \cdots \partial_{\overline{n}_D}^{\iota_D} \langle \hat{U}^{(N)\dagger}_{\overline{\boldsymbol{n}},\boldsymbol{\varphi}_1}(t) \hat{U}^{(N)}_{\overline{\boldsymbol{n}},\boldsymbol{\varphi}_2}(t) \rangle_0 \right\} \\ &\quad \times \rho^{(\mathrm{L})}_{\boldsymbol{\varphi}_3,\boldsymbol{\varphi}_4} e^{i\boldsymbol{n}\cdot(\boldsymbol{\varphi}_4-\boldsymbol{\chi}+\boldsymbol{\varphi}_3) + i\boldsymbol{n}_1\cdot(\boldsymbol{\varphi}_3-\boldsymbol{\varphi}_1) - i\boldsymbol{n}_2\cdot(\boldsymbol{\varphi}_4-\boldsymbol{\varphi}_2) + i\overline{\boldsymbol{n}}\cdot(\boldsymbol{\varphi}_4+\boldsymbol{\varphi}_3)}. \end{aligned} \tag{A15}$$

In this form, we can now use the identity in Eq. (A14) to simplify the above expression. By evaluating the delta functions, we can cancel three of the four integrals over the phase $\boldsymbol{\varphi}_\alpha$, such that we obtain

$$M_{\boldsymbol{\chi}}(t) = \sum_{r=0}^{\infty} \sum_{\iota_1+\ldots+\iota_D=r} e^{-i\overline{\boldsymbol{n}}\cdot\boldsymbol{\chi}} \frac{\partial_{-i\chi_1}^{\iota_1}\cdots\partial_{-i\chi_D}^{\iota_D}}{\iota_1!\cdots\iota_D!} \int d\boldsymbol{\varphi} \times \left\{\partial_{\overline{n}_1}^{\iota_1}\cdots\partial_{\overline{n}_D}^{\iota_D}\left\langle \hat{U}^{(N)\dagger}_{\overline{\boldsymbol{n}},\boldsymbol{\varphi}-\frac{\boldsymbol{\chi}}{2}}(t)\hat{U}^{(N)}_{\overline{\boldsymbol{n}},\boldsymbol{\varphi}+\frac{\boldsymbol{\chi}}{2}}(t)\right\rangle_0\right\}\rho^{(\mathrm{L})}_{\boldsymbol{\varphi}+\frac{\boldsymbol{\chi}}{2},\boldsymbol{\varphi}-\frac{\boldsymbol{\chi}}{2}} e^{i\overline{\boldsymbol{n}}\cdot\boldsymbol{\chi}}. \tag{A16}$$

We emphasize that this is still an exact, yet formal, expression for the moment-generating function.

3. Semiclassical approximation

While exact, the expression in Eq. (A16) is impossible to evaluate. At this point, we recall the objective of this work to establish a theoretical framework that is capable of predicting the measurement statistics of spectroscopic experiments using only semiclassical methods. Motivated by this aim, we carry out a semiclassical approximation in Eq. (A16). As explained below Eq. (A13) in terms of a Gaussian state, the semiclassical approximation assumes that both the photon number and the phases of the photonic state are closely centered around their mean values. This semiclassical approach has a twofold effect:

(i) we replace the quantum optical time-evolution operators in Eq. (A16) by their semiclassical counterparts, i.e.,

$$\hat{U}^{(N)}_{\overline{\boldsymbol{n}},\boldsymbol{\varphi}} \to \hat{\mathcal{U}}^{(N)}_{\overline{\boldsymbol{n}},\boldsymbol{\varphi}}, \tag{A17}$$

which is defined in Eq. (7). We note that this replacement is exact, when representing the Hamiltonian in Eq. (1) in the Sambe space as shown in Ref. [61]. The Sambe space is closely related to the Fock space, but with the common photonic operators replaced by $\hat{a}_k^\dagger\hat{a}_k \to \sum_{n_k} n_k|n_k\rangle\langle n_k|$ and $\hat{a}_k \to \sum_{n_k}\sqrt{\overline{n}_k}|n_k\rangle\langle n_k+1|$, such that this approximation is well motivated in the large photon-number regime for which $\sqrt{n_k}$ becomes approximately constant in an interval $\sqrt{\overline{n}_k}-x/\sqrt{\overline{n}_k}, \sqrt{\overline{n}_k}+x/\sqrt{\overline{n}_k}$ [with an arbitrary scaling factor $x \in O(1)$].

(ii) The second simplification concerns the integral over the phase variables in Eq. (A16). As we work in the semiclassical limit, we assume that the phase of the photonic field should be clearly defined. Consequently, it is reasonable to assume that the photonic state $\rho^{(\mathrm{L})}_{\boldsymbol{\varphi}+\frac{\boldsymbol{\chi}}{2},\boldsymbol{\varphi}-\frac{\boldsymbol{\chi}}{2}}$ is strongly peaked around a specific mean phase $\overline{\boldsymbol{\varphi}}$, at which we evaluate the integral. For the Gaussian state in Eq. (A13), this limit can be uniquely defined by a diverging $\boldsymbol{\Sigma}\to\infty$. For non-Gaussian states, which we may encounter during the propagation of the laser pulse through the atom cloud, this replacement enters phenomenologically. Effectively, the semiclassical approximation thus means that

$$\hat{\mathcal{U}}^{(N)}_{\overline{\boldsymbol{n}},\boldsymbol{\varphi}} \to \hat{\mathcal{U}}^{(N)}_{\overline{\boldsymbol{n}},\overline{\boldsymbol{\varphi}}}, \tag{A18}$$

in the moment-generating function in Eq. (A16).

When applying the semiclassical approximation, the moment-generating function becomes

$$M_{\boldsymbol{\chi}}(t) = \sum_{r=0}^{\infty}\sum_{\iota_1+\ldots\iota_D} e^{-i\overline{\boldsymbol{n}}\cdot\boldsymbol{\chi}}\frac{\partial_{-i\chi_1}^{\iota_1}\cdots\partial_{-i\chi_D}^{\iota_D}}{\iota_1!\cdots\iota_D!} \times\left\{\partial_{\overline{n}_1}^{\iota_1}\cdots\partial_{\overline{n}_D}^{\iota_D}\left\langle\hat{\mathcal{U}}^{(N)\dagger}_{\overline{\boldsymbol{n}},\overline{\boldsymbol{\varphi}}-\frac{\boldsymbol{\chi}}{2}}(t)\hat{\mathcal{U}}^{(N)}_{\overline{\boldsymbol{n}},\overline{\boldsymbol{\varphi}}+\frac{\boldsymbol{\chi}}{2}}(t)\right\rangle_0\right\} \times e^{i\overline{\boldsymbol{n}}\cdot\boldsymbol{\chi}}\int d\boldsymbol{\varphi}\rho^{(\mathrm{L})}_{\boldsymbol{\varphi}+\frac{\boldsymbol{\chi}}{2},\boldsymbol{\varphi}-\frac{\boldsymbol{\chi}}{2}}. \tag{A19}$$

By setting $t=0$ in this expression, we can identify

$$M_{\boldsymbol{\chi}}(t=0) = \int d\boldsymbol{\varphi}\rho^{(\mathrm{L})}_{\overline{\boldsymbol{\varphi}}+\frac{\boldsymbol{\chi}}{2},\overline{\boldsymbol{\varphi}}-\frac{\boldsymbol{\chi}}{2}}, \tag{A20}$$

which is an exact expression.

To make progress, we use the defining relation between cumulant and moment-generating functions,

$$M_{\boldsymbol{\chi}}(0) = \exp[K_{\boldsymbol{\chi}}(0)]. \tag{A21}$$

Moreover, we introduce the dynamical cumulant-generating function describing the action of the ensemble of N atoms on the photonic fields

$$\begin{aligned}\mathcal{K}^{(N)}_{\boldsymbol{\chi}}(t) &\equiv \log\left\langle\hat{\mathcal{U}}^{(N)\dagger}_{\overline{\boldsymbol{n}},\overline{\boldsymbol{\varphi}}-\frac{\boldsymbol{\chi}}{2}}(t)\hat{\mathcal{U}}^{(N)}_{\overline{\boldsymbol{n}},\overline{\boldsymbol{\varphi}}+\frac{\boldsymbol{\chi}}{2}}(t)\right\rangle_0 \\ &= \log\left\langle\hat{\mathcal{U}}^{\dagger}_{\overline{\boldsymbol{n}},\overline{\boldsymbol{\varphi}}-\frac{\boldsymbol{\chi}}{2}}(t)\hat{\mathcal{U}}_{\overline{\boldsymbol{n}},\overline{\boldsymbol{\varphi}}+\frac{\boldsymbol{\chi}}{2}}(t)\right\rangle_0^N \\ &= N\log\left\langle\hat{\mathcal{U}}^{\dagger}_{\overline{\boldsymbol{n}},\overline{\boldsymbol{\varphi}}-\frac{\boldsymbol{\chi}}{2}}(t)\hat{\mathcal{U}}_{\overline{\boldsymbol{n}},\overline{\boldsymbol{\varphi}}+\frac{\boldsymbol{\chi}}{2}}(t)\right\rangle_0 \\ &= N\mathcal{K}_{\boldsymbol{\chi}}(t).\end{aligned} \tag{A22}$$

In the second line, we have assumed that the atoms are independent of each other, such that the expectation value of the ensemble is just the Nth power of the expectation value for an individual atom. In the last equality, we introduced the dynamical cumulant-generating function $\mathcal{K}_{\boldsymbol{\chi}}(t)$, which describes the impact of a single atom on the photonic modes.

In the following, we assume that these N atoms are confined in a volume with area $\mathcal{A}$ and infinitesimal length dz, i.e., $N=\rho_A\mathcal{A}dz$. Using these definitions, the moment-generating function in Eq. (A19) becomes

$$M_{\boldsymbol{\chi}}(t) = \sum_{r=0}^{\infty}\sum_{\iota_1+\ldots\iota_D} e^{-i\overline{\boldsymbol{n}}\cdot\boldsymbol{\chi}}\frac{\partial_{-i\chi_1}^{\iota_1}\cdots\partial_{-i\chi_D}^{\iota_D}}{\iota_1!\cdots\iota_D!} \times\left\{\partial_{\overline{n}_1}^{\iota_1}\cdots\partial_{\overline{n}_D}^{\iota_D}\exp[\rho_A\mathcal{A}dz\mathcal{K}_{\boldsymbol{\chi}}(t)]\right\}e^{K_{\boldsymbol{\chi}}(0)+i\overline{\boldsymbol{n}}\cdot\boldsymbol{\chi}}. \tag{A23}$$

The following scaling analysis will show how this expression can be simplified.

To this end, we first have to specify in which fashion we approach the semiclassical limit. As one can see from Eq. (6), the bare light-matter interaction parameters $g_{j,k}$ and mean photon numbers $\overline{n}_k$ appear only as the products $\Omega_{j,k}=g_{j,k}\sqrt{\overline{n}_k}$ (i.e., the Rabi frequencies) in the semiclassical Hamiltonian. Thus, the dynamical cumulant-generating function $\mathcal{K}_{\boldsymbol{\chi}}(t)$ is only a function of the Rabi frequencies. To reach the semiclassical limit in an unambiguous fashion, we

thus require that

$$\begin{aligned} \overline{n}_k &\to \infty, \\ g_{j,k} &\to 0, \\ \text{s.t. } g_{j,k}\sqrt{\overline{n}_k} &= \Omega_{j,k} = \text{const.} \end{aligned} \tag{A24}$$

Physically, the condition can be met by increasing the quantization volume of a laser pulse in the directions transversal to the propagation.

First, we investigate the scaling properties of the factor

$$\partial_{\overline{n}_1}^{\iota_1} \cdots \partial_{\overline{n}_D}^{\iota_D} \exp[\rho_A \mathcal{A} dz \mathcal{K}_{\boldsymbol{\chi}}(t)] \equiv \partial_{\overline{n}_1}^{\iota_1} \cdots \partial_{\overline{n}_D}^{\iota_D} g_{\boldsymbol{\chi}}(t), \tag{A25}$$

when the mean photon numbers approach infinity $\overline{n}_k \to \infty$. Using the scaling assumptions in Eq. (A24), we can thus conclude that

$$\begin{aligned} \partial_{\overline{n}_1}^{\iota_1} \cdots \partial_{\overline{n}_D}^{\iota_D} g_{\boldsymbol{\chi}}(t) &= \partial_{\Omega_1}^{\iota_1} \cdots \partial_{\Omega_D}^{\iota_D} g_{\boldsymbol{\chi}}(t) \big(\partial_{\overline{n}_1}^{\iota_1} \Omega_1\big) \cdots \big(\partial_{\overline{n}_D}^{\iota_D} \Omega_D\big) \\ &\propto \frac{g^r}{\sqrt{\overline{n}^r}} \propto \frac{1}{\overline{n}^r}, \quad r = \iota_1 + \cdots + \iota_D. \end{aligned} \tag{A26}$$

In the first equality, we have used the chain rule of differentiation. In the second line, we utilized g and $\overline{n}$ as measures for the $g_{j,k}$ and the $\overline{n}_k$. Importantly, note that the derivatives of $g_{\boldsymbol{\chi}}$ with respect to Ω_k are independent of the photon number, i.e., $g_{\boldsymbol{\chi}} \propto \overline{n}^0$ under the scaling assumptions in Eq. (A24), as $g_{\boldsymbol{\chi}}$ is only a function of the Rabi frequencies. Thus, the scaling properties are solely determined by the derivatives of the Rabi frequencies with respect to the mean-photon numbers, showing the terms vanish with $\overline{n}^{-r}$ in the Taylor order r.

Consequently, in order for the terms of order r to remain in Eq. (A23), we require additional factors which must jointly scale with $\overline{n}^r$. These factors can be delivered by the term $K_{\boldsymbol{\chi}}(0)$ in the exponential appearing in Eq. (A23). To this end, we make the reasonable assumption that

$$K_{\boldsymbol{\chi}}(0) \propto \overline{n}, \tag{A27}$$

which implies that all cumulants scale as $\propto \overline{n}$. This is definitely fulfilled for coherent states or states that are similar to coherent states, such as coherent squeezed states. More precisely, we have to repeatably bring down the factor $K_{\boldsymbol{\chi}}(0)$ from the exponent by deriving r times to produce the scaling $\propto \overline{n}^r$.

Taking all these scaling relations into account, we can express the moment-generating function in Eq. (A19) as

$$M_{\boldsymbol{\chi}}(t) = M_{\text{aux},\boldsymbol{\chi}}(t) M_{\boldsymbol{\chi}}(0), \tag{A28}$$

where

$$\begin{aligned} M_{\text{aux},\boldsymbol{\chi}}(t) &= \left\{1 + \rho_A \mathcal{A} \tilde{K}_{\text{aux},\boldsymbol{\chi}}(t) dz + O\left[(\rho_A \mathcal{A} dz)^2, \frac{1}{\overline{n}}\right]\right\} \\ &\quad \times e^{\rho_A \mathcal{A} \mathcal{K}_{\boldsymbol{\chi}}(t) dz}, \\ \tilde{K}_{\text{aux},\boldsymbol{\chi}}(t) &= \sum_{r=1}^{\infty} \sum_{\iota_1 + \ldots \iota_D = r} \left\{ \frac{\partial_{\overline{n}_1}^{\iota_1} \cdots \partial_{\overline{n}_D}^{\iota_D}}{\iota_1! \cdots \iota_D!} \mathcal{K}_{\boldsymbol{\chi}}(t) \right\} \\ &\quad \times \left\{ \left[\partial_{-i\chi_1} K_{\boldsymbol{\chi}}(0) - \overline{n}_1\right]^{\iota_1} \cdots \left[\partial_{-i\chi_D} K_{\boldsymbol{\chi}}(0) - \overline{n}_D\right]^{\iota_D} \right\} \end{aligned} \tag{A29}$$

will be denoted as the auxiliary moment-generating function in the following. Within the auxiliary moment-generating function, we have ordered the terms according to their powers of dz and $1/\overline{n}$. The terms with $1/\overline{n}^r$ with $r \geqslant 1$ will vanish in the semiclassical limit $\overline{n} \to \infty$. The terms dz^r with $r \geqslant 2$ will become irrelevant when constructing the cumulant flow equations in the next section.

4. Cumulant flow equation

In the previous section, we have derived an expression for the moment-generating function describing the occupation of the laser pulse modes after they have interacted with an ensemble of $N = \rho_A \mathcal{A} dz$ atoms for a time duration t. As explained below the Hamiltonian in Eq. (1), the interaction of a pulse with each atom is described by the time-dependent light-matter interaction parameters $g_{m,k}(t)$. For the following considerations, we assume that the train of pulses has a total duration of t_{M}, which we identify as the time of the light-matter interaction $t = t_{\text{M}}$ in Eq. (A28).

More precisely, we describe the propagation of a laser pulse (train) through the cloud of atoms as a sequential interaction of the pulse with each layer of the atom cloud as sketch in Fig. 2(a). After each layer of interaction, the moment-generating function describing the probability distribution is slightly modified according to Eq. (A28). For brevity, we consider the interaction duration $t = t_{\text{M}}$ as a fixed parameter and consider the moment and cumulant-generating functions as functions of position z, i.e., $K_{\boldsymbol{\chi}}(z) = \log M_{\boldsymbol{\chi}}(z)$, from now on.

We can thus interpret Eq. (A28) as the moment-generating function after interaction with the N atoms in the volume limited by z and $z + dz$. Taking the logarithm on both sides, we can formally write

$$K_{\boldsymbol{\chi}}(z + dz) = \log[M_{\text{aux},\boldsymbol{\chi}}] + K_{\boldsymbol{\chi}}(z), \tag{A30}$$

where $M_{\boldsymbol{\chi}}(0)$ in Eq. (A28) corresponds to $K_{\boldsymbol{\chi}}(z)$ and denotes the cumulant-generating function before the interaction with the next atom layer. To derive an effective equation of motion, we expand $\log[M_{\text{aux},\boldsymbol{\chi}}]$ up to the first order in dz. In doing so, we finally obtain

$$\frac{d}{dz} K_{\boldsymbol{\chi}}(z) = \rho_A \mathcal{A}[\mathcal{K}_{\boldsymbol{\chi}}(z) + \tilde{K}_{\text{aux},\boldsymbol{\chi}}(z)], \tag{A31}$$

which is equivalent to the equation of motion in Eq. (9). We note that $\tilde{K}_{\text{aux}}$ defined in Eq. (A29) and K_{aux} in Eq. (11) differ only in the start of the Taylor expansion.

5. Discussion of the cumulant flow equations

Here, we provide a technical discussion about the terms appearing in the flow equation of the cumulant-generating function in Eq. (9).

The $r = 0$ term in Eq. (10) equals the dynamical cumulant-generating function in Eq. (11). This term describes the photon statistics correctly when replacing the photonic operators in the Hamiltonian in Eq. (1) by their counterparts in Sambe space, as has been investigated in the original PRFT [61]. As the higher-order terms $r > 0$ are related to the deformation of the photonic state in phase space, we refer to them as phase-space terms.

In Sec. II C, we have established the flow equation for the means and the covariances of the photonic probability distribution. In a similar fashion, one can derive the flow

equations for higher-order cumulants. Inspection of Eq. (9) shows that the flow equation for a cumulant of order $l = l_1 + \cdots + l_D$ involves the Taylor expansion up to order $r = l - 1$ of the dynamical cumulant-generating function in Eq. (11). Consequently, a cumulant of order l cannot depend on a higher-order cumulant $l' > l$.

6. Relation to the Maxwell-Bloch theory

In this appendix, we discuss the relation of the cumulant flow equation in Eq. (9) to the celebrated Maxwell-Bloch theory [48]. To this end, we prove that the flow equation for the mean is equivalent to the semiclassical Maxwell-Bloch equation. For simplicity, we consider a monochromatic photonic field, but remark that the generalization to polychromatic photonic fields is straightforward. Recalling that the Rabi frequency is given by $\Omega = Ed/\hbar$ (electric field E, atomic dipole moment d), we express the single-quantum emitter Hamiltonian in Eq. (6) as

$$\hat{\mathcal{H}}_{m,\boldsymbol{\varphi}}(t) = \hat{H}_m + E(z_m, t)\hat{d}_m, \tag{A32}$$

where $\hat{d}_m$ denotes the dipole operator. The semiclassical electric field at the atomic position $z = z_m$ is given by

$$\begin{aligned} E_\varphi(z,t) &= E_z^{(0)} \cos(\omega t - kz + \varphi) \\ &= E_z^{(+)} e^{-i\omega t} + E_z^{(-)} e^{i\omega t}. \end{aligned} \tag{A33}$$

In the second line, we have distributed the electric field in positive- and negative-frequency contributions. For brevity, we neglect the index m in the following.

We recall that the flow equation of the first cumulant (i.e., the mean) reads

$$\frac{d}{dz}\overline{n}_z = I_{\overline{n}_z}, \tag{A34}$$

according to the PRFT. The total number of photons transversing an area $\mathcal{A}$ at position z can be expressed as

$$\overline{n}_z = \frac{\mathcal{A}c\epsilon_0}{\hbar\omega}\int_0^{t_M} E_\varphi^2(z,t)dt, \tag{A35}$$

where ϵ_0 is the vacuum permittivity, and c is the speed of light. To evaluate the right-hand-side of Eq. (A34), we use Eqs. (10) and (13), in which we represent the semiclassical time-evolution operator as

$$\begin{aligned} \hat{\mathcal{U}}_{\overline{\boldsymbol{n}},\varphi+\chi}(t) = \hat{\mathcal{U}}_{\overline{\boldsymbol{n}},\varphi}(t)\Big\{1 - \frac{i}{\hbar}\int_0^t \hat{d}(t')[E_{\varphi+\chi}(z,t') \\ - E_\varphi(z,t')]dt' + O(\chi^2)\Big\}, \end{aligned} \tag{A36}$$

where

$$\hat{d}(t) = \hat{\mathcal{U}}^\dagger_{\overline{\boldsymbol{n}},\varphi}(t)\hat{d}\hat{\mathcal{U}}_{\overline{\boldsymbol{n}},\varphi}(t) \tag{A37}$$

is the dipole operator time-evolved with the semiclassical time-evolution operator in Eq. (7). In doing so, we find

$$I_{\overline{\boldsymbol{n}}} = \frac{\rho_A\mathcal{A}}{\hbar}\int_0^{t_M}\langle\hat{d}(t)\rangle i(E_z^{(+)}e^{-i\omega t} - E_z^{(-)}e^{i\omega t})dt, \tag{A38}$$

where the $\langle\bullet\rangle$ refers to the expectation value in the initial state of the atomic system.

Comparing now the integrants of the left- and right-hand sites in Eq. (A34), we thus find

$$\begin{aligned} &\frac{c\epsilon_0}{\omega}E(z,t)\frac{d}{dz}E(z,t) \\ &\quad = i\rho_A\langle\hat{d}(t)\rangle(E_z^{(+)}e^{i\omega t} - E_z^{(-)}e^{-i\omega t}). \end{aligned} \tag{A39}$$

As the Maxwell-Bloch equation is typically represented in a rotating frame, we distribute the dipole operator as

$$\hat{d}(t) = \hat{d}^{(+)}(t) + \hat{d}^{(-)}(t), \tag{A40}$$

where $\hat{d}^{(+)}(t)$, $\hat{d}^{(-)}(t)$ denote the parts with positive and negative frequency contributions. Neglecting now rapidly oscillating terms, Eq. (A39) becomes

$$\begin{aligned} &E_z^{(+)}\left(\frac{d}{dz}E_z^{(-)}\right) + E_z^{(-)}\left(\frac{d}{dz}E_z^{(+)}\right) \\ &\quad = i\frac{\rho_A\hbar\omega}{c\epsilon_0}(E_z^{(+)}\langle\hat{d}^{(-)}(t)\rangle e^{i\omega t} - E_z^{(-)}\langle\hat{d}^{(+)}(t)\rangle e^{-i\omega t}), \end{aligned}$$

such that the corresponding complexified equation

$$\frac{d}{dz}E_z^{(-)} = i\frac{\rho_A\omega}{c\epsilon_0}\langle\hat{d}^{(-)}(t)e^{i\omega t}\rangle \tag{A41}$$

represents the desired Maxwell-Bloch equation in the semiclassical approximation [48].

Based on the considerations for the mean-value, we interpret the flow equation of the second cumulant (i.e., the variance) in terms of the semiclassical Maxwell-Bloch theory. Defining the energy-flow operator as

$$\hat{\mathcal{J}}(t) = \frac{d}{dt}\hat{H}(t) = i\omega\hat{d}(t)(E_z^{(+)}e^{-i\omega t} - E_z^{(-)}e^{i\omega t}), \tag{A42}$$

we can define the operator counting the number of photons that the matter systems have interchanged with the coherent driving field of frequency ω as

$$\Delta\hat{n} = \frac{1}{\hbar\omega}\int_0^{t_M}\hat{\mathcal{J}}(t')dt' \tag{A43}$$

during the laser pulse duration t_M. Using this operator, one can calculate the cumulants of the photonic probability distribution. Yet, the evaluation of higher-order cumulants is numerically cumbersome, as it requires high-dimensional integration of multitime correlation functions for $\hat{\mathcal{J}}(t)$. For instance, the diffusion coefficient is given by

$$D_{\overline{n}} = \frac{1}{\hbar^2\omega^2}\int_0^{t_M}\int_0^{t_M}\langle\Delta\hat{\mathcal{J}}(t_1)\Delta\hat{\mathcal{J}}(t_2)\rangle dt_1 dt_2, \tag{A44}$$

with $\Delta\hat{\mathcal{J}}(t) = \hat{\mathcal{J}}(t) - \langle\hat{\mathcal{J}}(t)\rangle$. We see that $D_{\overline{n}}$ encodes the temporal fluctuations of the matter system within a semiclassical description on the system, which is on the same footing as the semiclassical Maxwell-Bloch equations. It is also straightforward to see that $D_{\overline{n}} \propto t_M$ for $t_M \to \infty$ for dissipative dynamics.

Finally, we comment on the phase-space term in Eq. (15), which can be expressed as

$$C_{\overline{n}} = \frac{d}{d\overline{n}}\langle\Delta\hat{n}\rangle \propto \frac{1}{\sqrt{\overline{n}}}. \tag{A45}$$

This term is a consequence of the photon-number dependence of the creation and annihilation operators, and quantifies the

sensitivity of the mean photon number change with respect to a deviation of the photon number. As for a coherent photonic state the photon number varies on the order of $\Sigma \propto \sqrt{\overline{n}}$, we must respect this contribution in the flow equation in Eq. (14) to obtain an accurate account of the photon-number fluctuations induced by the light-matter interaction.

APPENDIX B: SPECTROSCOPIC OBSERVABLES

In this appendix, we provide details regarding the calculations of physical observables in Sec. III. In Appendix B 1, we briefly review the Faraday effect, and in Appendix B 2, we derive the representation of the flow equations in the rotated measurement basis.

1. Relation between polarization and phase measurements

Here, we briefly review how polarization measurements (Sec. III B) and phase measurements (Sec. III C) are mutually related via the Faraday effect [28]. The connection becomes clear when recalling that linearly polarized light can be considered as a superposition of two circularly polarized light modes. Using simple geometric considerations, one finds that a phase shift of one circularly polarized mode $\Delta\overline{\varphi}$ leads to a rotation of the resulting linearly polarized light $\Delta\overline{\theta}$, and the two angles are related by

$$\Delta\overline{\varphi} = 2\Delta\overline{\theta}. \tag{B1}$$

We can also discover this effect when comparing Eqs. (20) and (23). To this end, we assume that both modes are initially equally occupied according to Eq. (19). Deriving Eq. (20) with respect to the position z, we find

$$\frac{d}{dz}\overline{\theta} = \frac{\frac{d}{dz}\overline{n}_1 - \frac{d}{dz}\overline{n}_2}{2\overline{n}_+}, \tag{B2}$$

which is the differential change of the rotation axis induced by the light-matter interaction. Likewise, for the phase shift in Eq. (23), we assume that originally $\overline{n} = \overline{n}_{\mathrm{LO}}$ and $\overline{\varphi} = \overline{\varphi}_{\mathrm{LO}}$. Differentiating Eq. (23) with respect to z, we find

$$\frac{d}{dz}\overline{\varphi} = \frac{\frac{d}{dz}\overline{n}_1 - \frac{d}{dz}\overline{n}_2}{\overline{n}_+}, \tag{B3}$$

which describes the differential change of the measured phase due to the light-matter interaction.

Comparing Eq. (B2) with Eq. (B3), we readily find

$$\frac{d\overline{\varphi}}{dz} = 2\frac{d\overline{\theta}}{dz}, \tag{B4}$$

which is simply the differential form of Eq. (B1). This relation implies that we can formally map a phase-shift measurement to a polarization-direction measurement. The latter interpretation might be more appealing because the measured photonic operators already appear in the original Hamiltonian.

2. Rotated measurement frame

Here we provide additional information regarding the representation of the flow equations in the rotated measurement frame in Sec. III D. First, we shortly explain the advantages of integrating the flow equation in a rotated measurement frame:

(i) The PRFT is only valid if the photonic driving fields are highly occupied. For particular rotation angles, the occupation of one of the modes might vanish, which makes the integration of the flow equations invalid within the PRFT.

(ii) The matrices $C_{\overline{\boldsymbol{n}}}$ in Eq. (14) often dominate the time evolution of the covariance matrix. In a rotating measurement frame, these matrices will be rendered small, which enables a stable numerical integration and a theoretical analysis.

Next, we provide detailed derivations regarding the representation of the flow equation in a frame that rotates along with the polarization direction of the electromagnetic field, as explained in Sec. III D. To this end, we consider the variables

$$A_\alpha = \sqrt{n_\alpha} \tag{B5}$$

for $\alpha = 1, 2$, where n_α is the photon number of the occupation operators $\hat{a}_\alpha^\dagger \hat{a}_\alpha$. The observables A_1 and A_2 are proportional to the electromagnetic fields in the x and y directions. In addition, for a notational reason, we have introduced the variables A_α as they have more convenient transformation properties under rotations than the n_α. Next, we distribute these variables into their mean and fluctuation parts, i.e., $A_\alpha = \overline{A}_\alpha + dA_\alpha$. The same separation is also applied to $n_\alpha = \overline{n}_\alpha + dn_\alpha$.

First, we consider the mean values of the A_α. We transform them into a rotated measurement frame defined by the rotation angle of the electric-field polarization $\overline{\theta} = \overline{\theta}(z)$, such that

$$\begin{pmatrix} \overline{A}_{\mathrm{rot},1} \\ \overline{A}_{\mathrm{rot},2} \end{pmatrix} = e^{i\overline{\theta}\hat{\sigma}_y} \begin{pmatrix} \overline{A}_1 \\ \overline{A}_2 \end{pmatrix}. \tag{B6}$$

Clearly, the condition in Eq. (26) is equivalent to the relation

$$\overline{A}_{\mathrm{rot},1} = \overline{A}_{\mathrm{rot},2} \tag{B7}$$

for all positions, meaning that the electric field in the rotating frame always encloses an angle $\pi/4$ with the two measurement axes.

Using Eq. (B6), we find that the time evolution in the rotated frame is given by

$$\frac{d}{dz}\begin{pmatrix} \overline{A}_{\mathrm{rot},1} \\ \overline{A}_{\mathrm{rot},2} \end{pmatrix} = i\frac{d\overline{\theta}}{dz}\hat{\sigma}_y \begin{pmatrix} \overline{A}_{\mathrm{rot},1} \\ \overline{A}_{\mathrm{rot},2} \end{pmatrix} + \begin{pmatrix} \dot{\overline{A}}_{\mathrm{rot},1} \\ \dot{\overline{A}}_{\mathrm{rot},2} \end{pmatrix}, \tag{B8}$$

where $\dot{\overline{A}}_{\mathrm{rot},\alpha}$ denotes the position derivative in the fixed measurement frame. Using now Eqs. (B5), (B7), (B8), and $\overline{n}_+ = \overline{n}_1 + \overline{n}_2$, we find

$$\begin{aligned} \frac{d\overline{\theta}}{dz} &= \frac{\dot{\overline{A}}_{\mathrm{rot},2} - \dot{\overline{A}}_{\mathrm{rot},1}}{\overline{A}_{\mathrm{rot},2} + \overline{A}_{\mathrm{rot},1}}, \\ \dot{\overline{n}}_+ &= 2\overline{A}_{\mathrm{rot},2}\dot{\overline{A}}_{\mathrm{rot},2} + 2\overline{A}_{\mathrm{rot},1}\dot{\overline{A}}_{\mathrm{rot},1}, \end{aligned} \tag{B9}$$

which is equivalent to Eq. (27).

Next, we consider the covariance matrix $\boldsymbol{\Sigma}^2$, which can be expressed in terms of the fluctuations dn_α. In the rotated measurement basis, we find

$$dn_{\mathrm{rot},\alpha} = 2\overline{A}_{\mathrm{rot},\alpha} dA_{\mathrm{rot},\alpha}, \tag{B10}$$

where the amplitude fluctuations are related to fluctuations in the fixed measurement basis by

$$\begin{pmatrix} dA_{\mathrm{rot},1} \\ dA_{\mathrm{rot},2} \end{pmatrix} = e^{i\theta_z\hat{\sigma}_y} \begin{pmatrix} dA_1 \\ dA_2 \end{pmatrix}. \tag{B11}$$

Consequently, the amplitude fluctuations fulfill the same differential equations as their corresponding mean values, i.e.,

$$\frac{d}{dz}\begin{pmatrix} dA_{\mathrm{rot},1} \\ dA_{\mathrm{rot},2}\end{pmatrix} = i\frac{d\overline{\theta}}{dz}\hat{\sigma}_y\begin{pmatrix} dA_{\mathrm{rot},1} \\ dA_{\mathrm{rot},2}\end{pmatrix} + \begin{pmatrix} d\dot{A}_{\mathrm{rot},1} \\ d\dot{A}_{\mathrm{rot},2}\end{pmatrix}. \tag{B12}$$

Using now Eqs. (B8) and (B12), we can construct the flow equation in the rotated measurement frame for $\mathbf{\Sigma}^2$. For instance, we find

$$\begin{aligned}\frac{d}{dz}\left[\mathbf{\Sigma}^2_{\mathrm{rot}}\right]_{1,1} = \frac{d}{dz}\langle dn_{\mathrm{rot},1}dn_{\mathrm{rot},1}\rangle &= \left\langle\left(\frac{d}{dz}dn_{\mathrm{rot},1}\right)dn_{\mathrm{rot},1}\right\rangle + \left\langle dn_{\mathrm{rot},1}\left(\frac{d}{dz}dn_{\mathrm{rot},1}\right)\right\rangle = 4\langle\dot{\overline{A}}_{\mathrm{rot},1}\overline{A}_{\mathrm{rot},1}dA_{\mathrm{rot},1}dA_{\mathrm{rot},1}\rangle \\ &+ 4\langle\overline{A}_{\mathrm{rot},1}\dot{\overline{A}}_{\mathrm{rot},1}dA_{\mathrm{rot},1}dA_{\mathrm{rot},1}\rangle + 4\langle\overline{A}_{\mathrm{rot},1}\overline{A}_{\mathrm{rot},1}d\dot{A}_{\mathrm{rot},1}dA_{\mathrm{rot},1}\rangle + 4\langle\overline{A}_{\mathrm{rot},1}\overline{A}_{\mathrm{rot},1}dA_{\mathrm{rot},1}d\dot{A}_{\mathrm{rot},1}\rangle \\ &+ 4\frac{d\overline{\theta}}{dz}\langle\overline{A}_{\mathrm{rot},2}\overline{A}_{\mathrm{rot},1}dA_{\mathrm{rot},1}dA_{\mathrm{rot},1}\rangle + 4\frac{d\overline{\theta}}{dz}\langle\overline{A}_{\mathrm{rot},1}\overline{A}_{\mathrm{rot},2}dA_{\mathrm{rot},1}dA_{\mathrm{rot},1}\rangle \\ &+ 4\frac{d\overline{\theta}}{dz}\langle\overline{A}_{\mathrm{rot},1}\overline{A}_{\mathrm{rot},1}dA_{\mathrm{rot},2}dA_{\mathrm{rot},1}\rangle + 4\frac{d\overline{\theta}}{dz}\langle\overline{A}_{\mathrm{rot},1}\overline{A}_{\mathrm{rot},1}dA_{\mathrm{rot},1}dA_{\mathrm{rot},2}\rangle.\end{aligned} \tag{B13}$$

The first four terms represent the derivative of $\mathbf{\Sigma}^2$ in the fixed measurement basis. The second four terms can be simplified. Taking the fifth term as an example, we find

$$4\langle\overline{A}_{\mathrm{rot},2}\overline{A}_{\mathrm{rot},1}dA_{\mathrm{rot},1}dA_{\mathrm{rot},1}\rangle = 4\langle\overline{A}_{\mathrm{rot},1}\overline{A}_{\mathrm{rot},1}dA_{\mathrm{rot},1}dA_{\mathrm{rot},1}\rangle = \langle dn_{\mathrm{rot},1}dn_{\mathrm{rot},1}\rangle = \left[\mathbf{\Sigma}^2_{\mathrm{rot}}\right]_{1,1}, \tag{B14}$$

where we have used Eq. (B7). Putting everything together we finally obtain

$$\frac{d}{dz}\mathbf{\Sigma}^2_{\mathrm{rot}} = \dot{\mathbf{\Sigma}}^2_{\mathrm{rot}} + \frac{d\overline{\theta}}{dz}\left[\begin{pmatrix}1 & 1\\ -1 & -1\end{pmatrix}\mathbf{\Sigma}^2_{\mathrm{rot}} + \mathbf{\Sigma}^2_{\mathrm{rot}}\begin{pmatrix}1 & -1\\ 1 & -1\end{pmatrix}\right], \tag{B15}$$

where $\dot{\mathbf{\Sigma}}^2_{\mathrm{rot}}$ denotes the derivative of the covariance matrix in the instantaneous fixed measurement basis. This expression is equivalent to Eq. (29).

Finally, we explain how to transform the measurement statistics found in the rotated basis back into the fixed laboratory basis. Using that the mean amplitudes in the fixed measurement basis fulfill

$$\begin{pmatrix}\overline{A}_1\\ \overline{A}_2\end{pmatrix} = \sqrt{\frac{\overline{n}_+}{2}}e^{i\overline{\theta}\hat{\sigma}_y}\begin{pmatrix}1\\1\end{pmatrix}, \tag{B16}$$

it is straightforward to show that the mean photon numbers in the fixed measurement basis are given by Eq. (30). To find the relation between $\mathbf{\Sigma}^2_{\mathrm{rot}}$ and $\mathbf{\Sigma}^2$ we use that the differential of n_α is given by $dn_\alpha = 2\overline{A}_\alpha dA_\alpha$ for $\alpha = 1, 2$. Using the inverse relation of Eq. (B11), we can thus find, for example,

$$\begin{aligned}[\mathbf{\Sigma}^2]_{1,1} = \langle dn_x dn_x\rangle &+ 4\cos(\overline{\theta})\cos(\overline{\theta})\overline{A}_x\overline{A}_x\langle dA_{\mathrm{rot},1}dA_{\mathrm{rot},1}\rangle + 4\sin(\overline{\theta})\cos(\overline{\theta})\overline{A}_x\overline{A}_x\langle dA_{\mathrm{rot},1}dA_{\mathrm{rot},2}\rangle \\ &- 4\cos(\overline{\theta})\sin(\overline{\theta})\overline{A}_x\overline{A}_x\langle dA_{\mathrm{rot},2}dA_{\mathrm{rot},1}\rangle + 4\sin(\overline{\theta})\sin(\overline{\theta})\overline{A}_x\overline{A}_x\langle dA_{\mathrm{rot},2}dA_{\mathrm{rot},2}\rangle,\end{aligned} \tag{B17}$$

and similarly for the other entries of $\mathbf{\Sigma}^2$. Using Eq. (B16), we can carry out the inverse transformation from the rotated frame to the fixed laboratory by calculating

$$\mathbf{\Sigma}^2_{\alpha,\beta} = \frac{2\overline{A}_\alpha\overline{A}_\beta}{\overline{n}_+}\left(e^{i\overline{\theta}\hat{\sigma}_y}\mathbf{\Sigma}^2_{\mathrm{rot}}e^{-i\overline{\theta}\hat{\sigma}_y}\right)_{\alpha,\beta}. \tag{B18}$$

This is equivalent to the expression in Eq. (31).

Of note, using the relation between rotation and phase measurements in Appendix B 1, one can also transform a phase measurement into an adjusted measurement setup, which simplifies the flow equation. Physically, instead of rotating the measurement basis, we adjust the phase of the local oscillator such that Eq. (26) is fulfilled. This implies that $\overline{n} = \overline{n}_{\mathrm{LO}}$ and $\overline{\varphi} = \overline{\varphi}_{\mathrm{LO}}$. Thus, using the correspondence in Eq. (B1), we can interpret the phase measurement as a *virtual* polarization measurement. After calculating the virtual polarization change, we can then use Eq. (B1) to obtain the mean phase value. Moreover, the measurement statistics of the covariance matrix is the same in the phase and the polarization estimations.

APPENDIX C: DETAILS FOR THE DISSIPATIVE TWO-LEVEL SYSTEM

In this appendix, we provide details for the calculations in Sec. IV investigating the dissipative Tavis-Cummings model. In Appendix C 1, we briefly review a method that enables a straightforward analytical calculation of low-order cumulants as introduced in Ref. [62]. In Appendix C 2, we explicitly calculate the flow equation coefficients in Eqs. (13) and (15). In Appendix C 3, we provide details for the evaluation of the cumulant aptitudes in Eq. (55). In Appendix C 4, we physically interpret the diverging phase fluctuations.

1. Truncated polynomial approach

In this appendix, we review how to efficiently evaluate low-order cumulants in the long-time limit. We recall that in the long-time limit, the cumulant-generating function is given by Eq. (44) if the counting-field-dependent density matrix fulfills the quantum master equation in Eq. (43), where $\lambda_{0,\boldsymbol{\chi}}$ denotes

the dominating eigenvalue of the Liouvillian (i.e., with the largest real part). Crucially, it is not necessary to actually diagonalize the Hamiltonian, as the low-order cumulants can be directly obtained from the characteristic polynomial of the Liouvillian [62]:

$$\mathcal{P}_{\boldsymbol{\chi}}(z) \equiv \det[\mathcal{L}_{\bar{\boldsymbol{n}},\boldsymbol{\chi}} - z\mathbb{1}] = \sum_{j=0}^{N} a_j(\boldsymbol{\chi}) z^j, \tag{C1}$$

where the expansion coefficients $a_j(\boldsymbol{\chi})$ depend on the counting fields. When intending to evaluate an lth order cumulant, it is sufficient to consider the truncated polynomial

$$\mathcal{P}^{(l)}_{\boldsymbol{\chi}}(z) = \sum_{j=0}^{l} a_j(\boldsymbol{\chi}) z^j, \tag{C2}$$

as the derivatives of the dominating root of the full polynomial $\lambda_{0;\boldsymbol{\chi}}$ and of the truncated polynomial $\lambda^{(l)}_{0;\boldsymbol{\chi}}$ are equal, e.g.,

$$\frac{d^l}{d(-i\boldsymbol{\chi}_\alpha)^l}\lambda_{0;\boldsymbol{\chi}=0} = \frac{d^l}{d(-i\boldsymbol{\chi}_\alpha)^l}\lambda^{(l)}_{0;\boldsymbol{\chi}=0}. \tag{C3}$$

The same relations also hold true for mixed derivatives.

As we intend to calculate the first two cumulants, we use the dominant eigenvalue of the corresponding truncated polynomial, which reads

$$\lambda^{(2)}_{0;\boldsymbol{\chi}} = \frac{1}{2a_2}\big(-a_1 + \sqrt{a_1^2 - 4a_0a_2}\big),$$

where we have suppressed the dependence of the expansion coefficients on the counting fields. For brevity, we define the following short-hand notation for the derivatives of the polynomial coefficients

$$a_j^{(\alpha)} = \frac{d}{d\boldsymbol{\chi}_\alpha} a_j\bigg|_{\boldsymbol{\chi}=0},$$
$$a_j^{(\alpha\beta)} = \frac{d}{d\boldsymbol{\chi}_\alpha}\frac{d}{d\boldsymbol{\chi}_\beta} a_j\bigg|_{\boldsymbol{\chi}=0}. \tag{C4}$$

After some tedious but straightforward calculations, we find that the derivatives of the dominating eigenvalue with respect to the counting fields can be expressed as

$$\lambda^{(2)(\alpha)}_{0;\boldsymbol{\chi}=0} = -\frac{a_0^{(\alpha)}}{a_1}$$
$$\lambda^{(2)(\alpha\beta)}_{0;\boldsymbol{\chi}=0} = -\frac{a_0^{(\alpha\beta)}}{a_1} - \frac{a_0^{(\alpha)}a_2^{(\beta)} + a_0^{(\beta)}a_2^{(\alpha)}}{a_2a_1} + \frac{a_0^{(\alpha)}a_1^{(\beta)} + a_0^{(\beta)}a_1^{(\alpha)}}{a_1^2} - \frac{2a_2a_0^{(\alpha)}a_0^{(\beta)}}{a_1^3}, \tag{C5}$$

which can be used to directly evaluate the cumulants of first and second orders by just determining the expansion coefficients of the characteristic polynomial.

2. Coefficients of the flow equations

In this appendix, we calculate the coefficients of the flow equation in Eqs. (13) and (15) for the two-level system Liouvillian in Eq. (45). To this end, we use the truncated polynomial approach introduced in Appendix C 1. The coefficients of the characteristic polynomial are given by

$$a_4 = 1, \quad a_3 = 2\gamma, \quad a_2 = \frac{1}{2}\mathcal{A}_{\boldsymbol{\chi}} + \epsilon_\Delta^2 + \frac{5}{4}\gamma^2,$$
$$a_1 = \frac{\gamma}{2}[\mathcal{A}_{\boldsymbol{\chi}} - \mathcal{C}_{\boldsymbol{\chi}}] + \gamma\epsilon_\Delta^2 + \frac{\gamma^3}{4},$$
$$a_0 = \frac{1}{16}\mathcal{B}_{\boldsymbol{\chi}}^2 + \frac{\gamma^2}{8}(\mathcal{A}_{\boldsymbol{\chi}} - 2\mathcal{C}_{\boldsymbol{\chi}}) - i\frac{\epsilon_\Delta\gamma}{4}\mathcal{B}_{\boldsymbol{\chi}}, \tag{C6}$$

in which we have introduced

$$\mathcal{A}_{\boldsymbol{\chi}} = 2\Omega_1^2 + 2\Omega_2^2 + 4\Omega_1\Omega_2\cos(\overline{\varphi}_1 - \overline{\varphi}_2)\cos\Big(\frac{\chi_1}{2} - \frac{\chi_2}{2}\Big),$$
$$\mathcal{B}_{\boldsymbol{\chi}} = -4\Omega_1\Omega_2\sin(\overline{\varphi}_1 - \overline{\varphi}_2)\sin\Big(\frac{\chi_1}{2} - \frac{\chi_2}{2}\Big),$$
$$\mathcal{C}_{\boldsymbol{\chi}} = \Omega_1^2 e^{i\chi_1} + \Omega_2^2 e^{i\chi_2} + 2\Omega_1\Omega_2 e^{i\frac{\chi_1+\chi_2}{2}}\cos(\overline{\varphi}_1 - \overline{\varphi}_2). \tag{C7}$$

To evaluate the cumulants using Eq. (C5), we calculate the first and second derivatives of the expansion coefficients in Eq. (C6). A straightforward calculation gives

$$a_0 = 0,$$
$$a_0^{(1)} = -i\frac{\gamma^2}{4}\big[\Omega_1^2 + \Omega_1\Omega_2\cos(\tilde{\varphi})\big] + i\frac{\epsilon_\Delta\gamma}{4}2\Omega_1\Omega_2\sin(\tilde{\varphi}),$$
$$a_0^{(2)} = -i\frac{\gamma^2}{4}\big[\Omega_2^2 + \Omega_1\Omega_2\cos(\tilde{\varphi})\big] - i\frac{\epsilon_\Delta\gamma}{4}2\Omega_1\Omega_2\sin(\tilde{\varphi}),$$
$$a_0^{(11)} = \frac{1}{16}[2\Omega_1\Omega_2\sin(\tilde{\varphi})]^2 + \frac{\gamma^2}{8}\big[-\Omega_1\Omega_2\cos(\tilde{\varphi}) + 2\Omega_1^2 + \Omega_1\Omega_2\cos(\tilde{\varphi})\big],$$
$$a_0^{(22)} = \frac{1}{16}[2\Omega_1\Omega_2\sin(\tilde{\varphi})]^2 + \frac{\gamma^2}{8}\big[-\Omega_1\Omega_2\cos(\tilde{\varphi}) + 2\Omega_2^2 + \Omega_1\Omega_2\cos(\tilde{\varphi})\big],$$
$$a_0^{(12)} = -\frac{1}{16}[2\Omega_1\Omega_2\sin(\tilde{\varphi})]^2 + \frac{\gamma^2}{8}[\Omega_1\Omega_2\cos(\tilde{\varphi}) + \Omega_1\Omega_2\cos(\tilde{\varphi})],$$
$$a_0^{(21)} = a_0^{(12)},$$
$$a_1 = \frac{\gamma}{2}\big[\Omega_1^2 + \Omega_2^2 + 2\Omega_1\Omega_2\cos(\tilde{\varphi})\big] + \gamma\epsilon_\Delta^2 + \frac{\gamma^3}{4},$$
$$a_1^{(1)} = -i\frac{\gamma}{2}\big[\Omega_1^2 + \Omega_1\Omega_2\cos(\tilde{\varphi})\big],$$
$$a_1^{(2)} = -i\frac{\gamma}{2}\big[\Omega_2^2 + \Omega_1\Omega_2\cos(\tilde{\varphi})\big],$$
$$a_2 = \Omega_1^2 + \Omega_2^2 + 2\Omega_1\Omega_2\cos(\tilde{\varphi}) + \epsilon_\Delta^2 + \frac{5}{4}\gamma^2,$$
$$a_2^{(1)} = 0,$$
$$a_2^{(2)} = 0, \tag{C8}$$

where we have defined $\tilde{\varphi} = \overline{\varphi}_1 - \overline{\varphi}_2$. Consequently, the coefficients of the flow equations in Eqs. (13) and (15) are

given by

$$[\boldsymbol{I}_{\bar{\boldsymbol{n}}}]_{k_\alpha} = -i\rho_A \mathcal{A} t_{\mathrm{M}} \frac{a_0^{(\alpha)}}{a_1},$$
$$[\boldsymbol{D}_{\bar{\boldsymbol{n}}}]_{k_\alpha,k_\beta} = \rho_A \mathcal{A} t_{\mathrm{M}} \times \left(\frac{a_0^{(\alpha\beta)}}{a_1} - \frac{a_0^{(\alpha)} a_1^{(\beta)} + a_0^{(\beta)} a_1^{(\alpha)}}{a_1^2} + \frac{2a_2 a_0^{(\alpha)} a_0^{(\beta)}}{a_1^3} \right), \tag{C9}$$

where we recall that ρ_A denotes the atom density and $\mathcal{A}$ is the effective laser cross section.

3. Cumulant aptitudes

In a similar fashion, we can also evaluate the cumulant aptitudes introduced in Eq. (55). To this end, we first express the characteristic polynomial in the rotated measurement basis, in which $\Omega_1 = \Omega_2 = \frac{\Omega}{\sqrt{2}}$ with Ω being the Rabi frequency experienced by the atoms. In doing so, the first three expansion coefficients become

$$\begin{aligned} a_2 &= \Omega^2 + \frac{1}{4}\epsilon_\Delta^2 + \frac{5}{4}\gamma^2, \\ a_1 &= \frac{\gamma}{2}[2\Omega^2 - \Omega^2 e^{i\chi_+}\cos(\chi_-)] + \frac{\gamma}{4}\epsilon_\Delta^2 + \frac{\gamma^3}{4}, \\ a_0 &= \frac{1}{4}[\Omega^2 \sin(\chi_-)]^2 + \frac{\gamma^2}{4}[\Omega^2 - \Omega^2 e^{i\chi_+}\cos(\chi_-)] \\ &\quad + i\frac{\epsilon_\Delta \gamma}{4}\Omega^2 \sin(\chi_-), \end{aligned} \tag{C10}$$

where we have used the symmetric and antisymmetric representation of the counting fields $\chi_+ = \frac{1}{2}(\chi_1 + \chi_2)$ and $\chi_- = \frac{1}{2}(\chi_1 - \chi_2)$. Calculating the derivatives with respect to the counting fields χ_+ and χ_-, we obtain

$$\begin{aligned} &a_0^{(+)} = -i\frac{\gamma^2}{4}\Omega^2, \quad a_0^{(-)} = i\frac{\epsilon_\Delta \gamma}{2}\Omega^2, \\ &a_0^{(++)} = \frac{\gamma^2}{4}\Omega^2, \quad a_0^{(--)} = \frac{1}{2}\Omega^4 + \frac{1}{4}\gamma^2\Omega^2, \quad a_0^{(+-)} = 0, \\ &a_0^{(-+)} = 0, \quad a_1 = \frac{\gamma}{2}\Omega^2 + \gamma\epsilon_\Delta^2 + \frac{\gamma^3}{4}, \quad a_1^{(+)} = -i\frac{\gamma}{2}\Omega^2, \\ &a_1^{(-)} = 0, \quad a_2 = \Omega^2 + \epsilon_\Delta^2 + \frac{5}{4}\gamma^2. \end{aligned} \tag{C11}$$

Using Eq. (C5), we can readily obtain closed-form expressions for the cumulant aptitudes,

$$\begin{aligned} \kappa_+^{(\delta)} &= -\frac{\gamma\Omega^2}{4\epsilon_\Delta^2 + 2\Omega^2 + \gamma^2}, \\ \kappa_-^{(\delta)} &= \frac{2\epsilon_\Delta\Omega^2}{4\epsilon_\Delta^2 + 2\Omega^2 + \gamma^2}, \\ \kappa_{++}^{(\delta)} &= \frac{a_0^{(++)}}{a_1} - \frac{2a_0^{(+)}a_1^{(+)}}{a_1^2} + \frac{2a_2 a_0^{(+)} a_0^{(+)}}{a_1^3} \\ &= \frac{\gamma\Omega^2}{(4\epsilon_\Delta^2 + 2\Omega^2 + \gamma^2)} + \frac{\Omega^4\gamma(8\epsilon_\Delta^2 - 6\gamma^2)}{(4\epsilon_\Delta^2 + 2\Omega^2 + \gamma^2)^3}, \\ \kappa_{--}^{(\delta)} &= \frac{a_0^{(--)}}{a_1} + \frac{2a_2 a_0^{(-)} a_0^{(-)}}{a_1^3} \\ &= \frac{2\Omega^4 + \gamma^2\Omega^2}{\gamma(4\epsilon_\Delta^2 + 2\Omega^2 + \gamma^2)} - \frac{8\epsilon_\Delta^2\Omega^4(4\Omega^2 + 4\epsilon_\Delta^2 + 5\gamma^2)}{\gamma(4\epsilon_\Delta^2 + 2\Omega^2 + \gamma^2)^3}, \end{aligned} \tag{C12}$$

which are the same as in Eq. (56).

4. Diverging fluctuations

In this appendix, we explain the divergence of the second cumulant aptitude $\kappa_{--}^{(\delta)}$ in Eq. (56) for a vanishing dissipation, which is the origin of the huge uncertainty in phase measurements. As we see, this is related to a diverging correlation time, during which derivations from the mean value add up. The following considerations are valid for generic second cumulants $\kappa_2^{(\delta)}$.

First, we represent the generalized master equation in Eq. (43) in the eigenstate basis (labeled by μ in the following) of the two-level Hamiltonian in Eq. (46), which is approximately given by

$$\frac{d}{dt}\begin{pmatrix} p_1 \\ p_2 \end{pmatrix} \approx \boldsymbol{\mathcal{L}}_\chi \begin{pmatrix} p_1 \\ p_2 \end{pmatrix}, \tag{C13}$$

where p_μ with $\mu = 1, 2$ are the counting-field-dependent diagonal elements of the generalized density matrix. We thereby use that the coherences of the density matrix approximately decouple from the diagonal elements. The generalized rates are given by

$$\boldsymbol{\mathcal{L}}_\chi = \begin{pmatrix} \lambda_{\chi|1} - \gamma_1 & \gamma_2 \\ \gamma_1 & \lambda_{\chi|2} - \gamma_2 \end{pmatrix}, \tag{C14}$$

where the exact dependence of the rates γ_μ on the system parameters is not essential for the following discussion. The quantities,

$$\lambda_{\chi|\mu} = -i\big(\epsilon_{\frac{\chi}{2}|\mu} - \epsilon_{-\frac{\chi}{2},\mu}\big), \tag{C15}$$

where $\epsilon_{\varphi|\mu}$ denote the eigenvalues of the two-level system, can be interpreted as the cumulant-generating functions conditioned on the eigenstates μ. The φ dependence of $\epsilon_{\varphi|\mu}$ contains thereby the information about the desired statistics (e.g., the photon-number difference). Thus, we neglect a possible exchange of photons during the transitions between the eigenstates, which is negligible for a vanishing dissipation in comparison to the coherent photon transport represented by $\lambda_\chi^{(\mu)}$. Crucially, we find that

$$\frac{d^2}{d\chi^2}\lambda_{\chi=0|\mu} = 0, \tag{C16}$$

meaning that the noise vanishes exactly when the quantum system is an eigenstate, which is a particular prediction of the PRFT [61].

The photonic statistics in the long-time limit can be determined by the dominating eigenvalue of Eq. (C14), which

reads

$$\lambda_\chi = \tfrac{1}{2}(\lambda_{\chi|1} + \lambda_{\chi|2} - \gamma_1 - \gamma_2) + \tfrac{1}{2}\sqrt{(\lambda_{\chi|1} - \lambda_{\chi|2} - \gamma_1 + \gamma_2)^2 + 4\gamma_1\gamma_2}. \quad \text{(C17)}$$

Deriving the λ_χ with respect to χ, we find that the first cumulant aptitude is given by

$$\begin{aligned}\kappa_1^{(\delta)} &= \left(\frac{\gamma_2}{\gamma_1+\gamma_2}\kappa_{1|1}^{(\delta)} + \frac{\gamma_1}{\gamma_1+\gamma_2}\kappa_{1|2}^{(\delta)}\right) \\ &= \left(p_1\kappa_{1|1}^{(\delta)}\tau + p_2\kappa_{1|2}^{(\delta)}\tau\right)\frac{1}{\tau} \\ &= \exp(\hat{X})\frac{1}{\tau}, \end{aligned} \quad \text{(C18)}$$

where $\kappa_{1|\mu}^{(\delta)} = i\frac{d}{d\chi}\lambda_{\chi=0}^{(\mu)}$ is the first cumulant aptitude conditioned on the eigenstate μ. In the second line, we see that the mean value is an average over the cumulants conditioned on the eigenstates, where the stationary probabilities are given by $p_1 = \gamma_2/(\gamma_1+\gamma_2)$ and $p_2 = \gamma_1/(\gamma_1+\gamma_2)$. For later purposes, we have introduced the timescale τ, which will be specified below. In the third line, we have expressed this as an expectation value of a binomial random variables $\hat{X}$ taking the values $x_\mu = \tau\kappa_{1|\mu}^{(\delta)}$ depending on the eigenstate $\mu = 1, 2$.

For the second cumulant aptitude, we find

$$\begin{aligned}\kappa_2^{(\delta)} &= \frac{\gamma_1\gamma_2}{(\gamma_1+\gamma_2)^3}\left(\kappa_{1|1}^{(\delta)} - \kappa_{1|2}^{(\delta)}\right)^2 \\ &= p_1p_2\left(\kappa_{1|1}^{(\delta)}\tau - \kappa_{1|2}^{(\delta)}\tau\right)^2\frac{1}{\tau} \\ &= \mathrm{Var}(\hat{X})\frac{1}{\tau} \propto \tau. \end{aligned} \quad \text{(C19)}$$

In the second line, we have introduced the effective correlation time $\tau = 1/(\gamma_1+\gamma_2)$, which is an intrinsic value characterizing the temporal correlations of fluctuations.

In the third line, we show that $\kappa_2^{(\delta)}$ can be considered as the variance of $\hat{X}$, reflecting that only fluctuations within the coherence time τ are effectively correlated. Thus, deviation from the mean value adds up positively during the correlation time τ, i.e., the longer the correlation time, the larger the variance of the integrated photon number. Consequently, a vanishing dissipation $\gamma_1, \gamma_2 \to 0$ implies a diverging correlation time, which leads to a diverging variance of the integrated photon number.

Of note, for the calculation of $\kappa_{++}^{(\delta)}$ in Eq. (56), we would find that $\kappa_{1|1}^{(\delta)} = -\kappa_{1|2}^{(\delta)}$, such that $\mathrm{Var}(\hat{X}) = 0$. In this case, the approximation of the quantum master equation by the generalized rate equation in Eq. (C14) is insufficient, as it neglects the photon exchange appearing during the transition between eigenstates. For this reason $\kappa_{++}^{(\delta)}$ does not diverge for a vanishing dissipation.

[1] A. Zumbusch, G. R. Holtom, and X. S. Xie, Three-dimensional vibrational imaging by coherent anti-Stokes Raman scattering, Phys. Rev. Lett. **82**, 4142 (1999).

[2] Z. Movasaghi, S. Rehman, and I. U. Rehman, Raman spectroscopy of biological tissues, Appl. Spectrosc. Rev. **42**, 493 (2007).

[3] J. N. Anker, W. P. Hall, O. Lyandres, N. C. Shah, J. Zhao, and R. P. Van Duyne, Biosensing with plasmonic nanosensors, Nat. Mater. **7**, 442 (2008).

[4] C. L. Evans, E. O. Potma, M. Puoris'haag, D. Côté, C. P. Lin, and X. S. Xie, Chemical imaging of tissue *in vivo* with video-rate coherent anti-Stokes Raman scattering microscopy, Proc. Natl. Acad. Sci. USA **102**, 16807 (2005).

[5] J. H. Baraban, P. B. Changala, G. C. Mellau, J. F. Stanton, A. J. Merer, and R. W. Field, Spectroscopic characterization of isomerization transition states, Science **350**, 1338 (2015).

[6] J. E. Colley, N. J. Dynak, J. R. C. Blais, and M. A. Duncan, Photodissociation spectroscopy and photofragment imaging to probe Fe^+ $(benzene)_{1,2}$ dissociation energies, J. Phys. Chem. A **127**, 2795 (2023).

[7] W. Domcke and D. R. Yarkony, Role of conical intersections in molecular spectroscopy and photoinduced chemical dynamics, Annu. Rev. Phys. Chem. **63**, 325 (2012).

[8] Z. Zhang, S. Zhao, and D. Lei, Quantum statistical theory for an exciton-polariton condensate: Fluctuations and coherence, Phys. Rev. B **106**, L220306 (2022).

[9] M. Reitz, A. Koner, and J. Yuen-Zhou, Nonlinear semiclassical spectroscopy of ultrafast molecular polariton dynamics, Phys. Rev. Lett. **134**, 193803 (2025).

[10] K. E. Dorfman and S. Mukamel, Multidimensional photon correlation spectroscopy of cavity polaritons, Proc. Natl. Acad. Sci. USA **115**, 1451 (2018).

[11] G. Ferioli, A. Glicenstein, I. Ferrier-Barbut, and A. Browaeys, A non-equilibrium superradiant phase transition in free space, Nat. Phys. **19**, 1345 (2023).

[12] S. Agarwal, E. Chaparro, D. Barberena, A. P. Orioli, G. Ferioli, S. Pancaldi, I. Ferrier-Barbut, A. Browaeys, and A. M. Rey, Directional superradiance in a driven ultracold atomic gas in free space, PRX Quantum **5**, 040335 (2024).

[13] D. Goncalves, L. Bombieri, G. Ferioli, S. Pancaldi, I. Ferrier-Barbut, A. Browaeys, E. Shahmoon, and D. E. Chang, Driven-dissipative phase separation in free-space atomic ensembles, PRX Quantum **6**, 020303 (2025).

[14] C. L. Degen, F. Reinhard, and P. Cappellaro, Quantum sensing, Rev. Mod. Phys. **89**, 035002 (2017).

[15] L. Pezzè, A. Smerzi, M. K. Oberthaler, R. Schmied, and P. Treutlein, Quantum metrology with nonclassical states of atomic ensembles, Rev. Mod. Phys. **90**, 035005 (2018).

[16] J. Ye and P. Zoller, Essay: Quantum sensing with atomic, molecular, and optical platforms for fundamental physics, Phys. Rev. Lett. **132**, 190001 (2024).

[17] A. D. Ludlow, M. M. Boyd, J. Ye, E. Peik, and P. O. Schmidt, Optical atomic clocks, Rev. Mod. Phys. **87**, 637 (2015).

[18] J. M. Robinson, M. Miklos, Y. M. Tso, C. J. Kennedy, T. Bothwell, D. Kedar, J. K. Thompson, and J. Ye, Direct comparison of two spin-squeezed optical clock ensembles at the 10^{-17} level, Nat. Phys. **20**, 208 (2024).

[19] P. W. Graham, J. M. Hogan, M. A. Kasevich, and S. Rajendran, Resonant mode for gravitational wave detectors based on atom interferometry, Phys. Rev. D **94**, 104022 (2016).

[20] J. M. Hogan and M. A. Kasevich, Atom-interferometric gravitational-wave detection using heterodyne laser links, Phys. Rev. A **94**, 033632 (2016).

[21] C. D. Panda, M. J. Tao, M. Ceja, J. Khoury, G. M. Tino, and H. Müller, Measuring gravitational attraction with a lattice atom interferometer, Nature (London) **631**, 515 (2024).

[22] J. E. A. Wenxuan, Squeezing the quantum noise of a gravitational-wave detector below the standard quantum limit, Science **385**, 1318 (2024).

[23] T. Li, F. Li, X. Liu, V. V. Yakovlev, and G. S. Agarwal, Quantum-enhanced stimulated Brillouin scattering spectroscopy and imaging, Optica **9**, 959 (2022).

[24] Z. Zhang, X. Zhang, J. Liu, and H. Dong, Quantum-enhanced weak absorption estimation with correlated photons, Phys. Rev. Lett. **134**, 133604 (2025).

[25] K. E. Dorfman, S. Asban, B. Gu, and S. Mukamel, Hong-Ou-Mandel interferometry and spectroscopy using entangled photons, Commun. Phys. **4**, 49 (2021).

[26] Z. Zhang, T. Peng, X. Nie, G. S. Agarwal, and M. O. Scully, Entangled photons enabled time-frequency-resolved coherent Raman spectroscopy and applications to electronic coherences at femtosecond scale, Light Sci. Appl. **11**, 274 (2022).

[27] J. J. Fan, Z.-Y. Ou, and Z. Zhang, Entangled photons enabled ultrafast stimulated Raman spectroscopy for molecular dynamics, Light Sci. Appl. **13**, 163 (2024).

[28] *Optical Magnetometry*, edited by D. Budker and D. F. Jackson Kimball (Cambridge University Press, New York, 2013).

[29] F. Wolfgramm, A. Cerè, F. A. Beduini, A. Predojević, M. Koschorreck, and M. W. Mitchell, Squeezed-light optical magnetometry, Phys. Rev. Lett. **105**, 053601 (2010).

[30] Y. Ma, Y. Chen, M. Yu, Y. Wang, S. Lu, J. Guo, G. Luo, L. Zhao, P. Yang, Q. Lin, and Z. Jiang, Ultrasensitive SERF atomic magnetometer with a miniaturized hybrid vapor cell, Microsyst Nanoeng **10**, 121 (2024).

[31] M. Xu, M. Jiang, Y. Wang, H. Su, Y. Huang, and X. Peng, Cooperative spin amplifier for enhanced quantum sensing, Phys. Rev. Lett. **133**, 133202 (2024).

[32] Z. Ma, C. Han, Z. Tan, H. He, S. Shi, X. Kang, J. Wu, J. Huang, B. Lu, and C. Lee, Adaptive cold-atom magnetometry mitigating the trade-off between sensitivity and dynamic range, Sci. Adv. **11**, eadt3938 (2025).

[33] J. Wang, J. Lee, H. Loughlin, M. Hedges, and M. V. Romalis, Pulsed dual-axis alkali-metal–noble-gas comagnetometer, Phys. Rev. A **111**, 053103 (2025).

[34] C. Holloway, M. Simons, J. Gordon, A. Dienstfrey, D. Anderson, and G. Raithel, Electric field metrology for SI traceability: Systematic measurement uncertainties in electromagnetically induced transparency in atomic vapor, J. Appl. Phys. **121**, 233106 (2017).

[35] K. C. Cox, D. H. Meyer, F. K. Fatemi, and P. D. Kunz, Quantum-limited atomic receiver in the electrically small regime, Phys. Rev. Lett. **121**, 110502 (2018).

[36] D. H. Meyer, Z. A. Castillo, K. C. Cox, and P. D. Kunz, Assessment of Rydberg atoms for wideband electric field sensing, J. Phys. B: At. Mol. Opt. Phys. **53**, 034001 (2020).

[37] M. Jing, Y. Hu, J. Ma, H. Zhang, L. Zhang, L. Xiao, and S. Jia, Atomic superheterodyne receiver based on microwave-dressed Rydberg spectroscopy, Nat. Phys. **16**, 911 (2020).

[38] D. H. Meyer, P. D. Kunz, and K. C. Cox, Waveguide-coupled Rydberg spectrum analyzer from 0 to 20 GHz, Phys. Rev. Appl. **15**, 014053 (2021).

[39] C. L. Holloway, N. Prajapati, J. A. Sherman, A. Rüfenacht, A. B. Artusio-Glimpse, M. T. Simons, A. K. Robinson, D. S. La Mantia, and E. B. Norrgard, Electromagnetically induced transparency based Rydberg-atom sensor for traceable voltage measurements, AVS Quantum Sci. **4**, 034401 (2022).

[40] B. Liu, L.-H. Zhang, Z.-K. Liu, Z.-Y. Zhang, Z.-H. Zhu, W. Gao, G.-C. Guo, D.-S. Ding, and B.-S. Shi, Highly sensitive measurement of a megahertz rf electric field with a Rydberg-atom sensor, Phys. Rev. Appl. **18**, 014045 (2022).

[41] S. Borówka, U. Pylypenko, M. Mazelanik, and M. Parniak, Continuous wideband microwave-to-optical converter based on room-temperature Rydberg atoms, Nat. Photonics **18**, 32 (2024).

[42] A. Kumar, A. Suleymanzade, M. Stone, L. Taneja, A. Anferov, D. I. Schuster, and J. Simon, Quantum-enabled millimetre wave to optical transduction using neutral atoms, Nature (London) **615**, 614 (2023).

[43] D. Li, Z. Bai, X. Zuo, Y. Wu, J. Sheng, and H. Wu, Room temperature single-photon terahertz detection with thermal Rydberg atoms, Appl. Phys. Rev. **11**, 041420 (2024).

[44] D. Budker, P. W. Graham, M. Ledbetter, S. Rajendran, and A. O. Sushkov, Proposal for a cosmic axion spin precession experiment (CASPEr), Phys. Rev. X **4**, 021030 (2014).

[45] D. Aybas, H. Bekker, J. W. Blanchard, D. Budker, G. P. Centers, N. L. Figueroa, A. V. Gramolin, D. F. Jackson Kimball, A. Wickenbrock, and A. O. Sushkov, Quantum sensitivity limits of nuclear magnetic resonance experiments searching for new fundamental physics, Quantum Sci. Technol. **6**, 034007 (2021).

[46] I. M. Bloch, G. Ronen, R. Shaham, O. Katz, T. Volansky, and O. Katz, New constraints on axion-like dark matter using a Floquet quantum detector, Sci. Adv. **8**, eabl8919 (2022).

[47] S. Ghosh, E. Graham, S. Getz, A. Giman, and R. Maruyama, Advancing Rydberg atom-based axion detection, Proc. SPIE Int. Soc. Opt. Eng. **12912**, 86 (2024).

[48] M. O. Scully and M. S. Zubairy, *Quantum Optics* (Cambridge University Press, Cambridge, 1997).

[49] K. Hammerer, A. S. Sørensen, and E. S. Polzik, Quantum interface between light and atomic ensembles, Rev. Mod. Phys. **82**, 1041 (2010).

[50] S. Mukamel, *Principles of Nonlinear Optical Spectroscopy* (Oxford University Press, New York, 1995).

[51] H. M. Wiseman and G. J. Milburn, Quantum theory of field-quadrature measurements, Phys. Rev. A **47**, 642 (1993).

[52] C. W. Gardiner and M. J. Collett, Input and output in damped quantum systems: Quantum stochastic differential equations and the master equation, Phys. Rev. A **31**, 3761 (1985).

[53] A. Pusch, S. Wuestner, J. M. Hamm, K. L. Tsakmakidis, and O. Hess, Coherent amplification and noise in gain-enhanced nanoplasmonic metamaterials: A Maxwell-Bloch Langevin approach, ACS Nano **6**, 2420 (2012).

[54] M. Fang, Z. Huang, W. E. I. Sha, and C. M. Soukoulis, Modelling of the fluctuation and coherent dynamics in active metamaterial devices, IEEE Trans. Nanotechnol. **20**, 543 (2021).

[55] Z. Zhang, X. Nie, D. Lei, and S. Mukamel, Multidimensional coherent spectroscopy of molecular polaritons: Langevin approach, Phys. Rev. Lett. **130**, 103001 (2023).

[56] K. Mølmer and L. B. Madsen, Estimation of a classical parameter with Gaussian probes: Magnetometry with collective atomic spins, Phys. Rev. A **70**, 052102 (2004).

[57] G. I. Petrov, R. Arora, V. V. Yakovlev, X. Wang, A. V. Sokolov, and M. O. Scully, Comparison of coherent and spontaneous Raman microspectroscopies for noninvasive detection of single bacterial endospores, Proc. Natl. Acad. Sci. USA **104**, 7776 (2007).

[58] C. Zhang and K. Mølmer, Estimating a fluctuating magnetic field with a continuously monitored atomic ensemble, Phys. Rev. A **102**, 063716 (2020).

[59] H. F. Hofmann and O. Hess, Quantum Maxwell-Bloch equations for spatially inhomogeneous semiconductor lasers, Phys. Rev. A **59**, 2342 (1999).

[60] G. Engelhardt, S. Choudhury, and W. V. Liu, Unified light-matter Floquet theory and its application to quantum communication, Phys. Rev. Res. **6**, 013116 (2024).

[61] G. Engelhardt, J. Y. Luo, V. M. Bastidas, and G. Platero, Photon-resolved Floquet theory. I. Full counting statistics of the driving field in Floquet systems, Phys. Rev. A **110**, 063707 (2024).

[62] G. Engelhardt, J. Y. Luo, V. M. Bastidas, and G. Platero, Photon-resolved Floquet theory. II. Open quantum systems, Phys. Rev. A **110**, 063708 (2024).

[63] L. S. Levitov, H. Lee, and G. B. Lesovik, Electron counting statistics and coherent states of electric current, J. Math. Phys. **37**, 4845 (1996).

[64] G. Platero and R. Aguado, Photon-assisted transport in semiconductor nanostructures, Phys. Rep. **395**, 1 (2004).

[65] K. Schönhammer, Full counting statistics for noninteracting fermions: Exact results and the Levitov-Lesovik formula, Phys. Rev. B **75**, 205329 (2007).

[66] M. C. Baldiotti, Waiting times and noise in single particle transport, Ann. Phys. **520**, 450 (2008).

[67] M. Esposito, U. Harbola, and S. Mukamel, Nonequilibrium fluctuations, fluctuation theorems, and counting statistics in quantum systems, Rev. Mod. Phys. **81**, 1665 (2009).

[68] R. Hussein and S. Kohler, Quantum transport, master equations, and exchange fluctuations, Phys. Rev. B **89**, 205424 (2014).

[69] C. Flindt, C. Fricke, F. Hohls, T. Novotný, K. Netočný, T. Brandes, and R. J. Haug, Universal oscillations in counting statistics, Proc. Natl. Acad. Sci. USA **106**, 10116 (2009).

[70] M. Ridley, M. Galperin, E. Gull, and G. Cohen, Numerically exact full counting statistics of the energy current in the Kondo regime, Phys. Rev. B **100**, 165127 (2019).

[71] F. A. Pollock, E. Gull, K. Modi, and G. Cohen, Reduced dynamics of full counting statistics, SciPost Phys. **13**, 027 (2022).

[72] E. Kleinherbers, P. Stegmann, and J. König, Revealing attractive electron–electron interaction in a quantum dot by full counting statistics, New J. Phys. **20**, 073023 (2018).

[73] M. Benito, M. Niklas, and S. Kohler, Full-counting statistics of time-dependent conductors, Phys. Rev. B **94**, 195433 (2016).

[74] G. Schaller, J. Cerrillo, G. Engelhardt, and P. Strasberg, Electronic Maxwell demon in the coherent strong-coupling regime, Phys. Rev. B **97**, 195104 (2018).

[75] J. Xu, S. Wang, J. Wu, Y. Yan, J. Hu, G. Engelhardt, and J. Y. Luo, Noise suppression of transport through double quantum dots by feedback control, Phys. Rev. B **107**, 125113 (2023).

[76] G. T. Landi, M. J. Kewming, M. T. Mitchison, and P. P. Potts, Current fluctuations in open quantum systems: Bridging the gap between quantum continuous measurements and full counting statistics, PRX Quantum **5**, 020201 (2024).

[77] C. Wang, J. Ren, and J. Cao, Unifying quantum heat transfer in a nonequilibrium spin-boson model with full counting statistics, Phys. Rev. A **95**, 023610 (2017).

[78] J. Cerrillo, M. Buser, and T. Brandes, Nonequilibrium quantum transport coefficients and transient dynamics of full counting statistics in the strong-coupling and non-Markovian regimes, Phys. Rev. B **94**, 214308 (2016).

[79] S. Restrepo, J. Cerrillo, P. Strasberg, and G. Schaller, From quantum heat engines to laser cooling: Floquet theory beyond the Born–Markov approximation, New J. Phys. **20**, 053063 (2018).

[80] A. Soret and M. Esposito, Thermodynamics of coherent energy exchanges between lasers and two-level systems, Phys. Rev. A **111**, 062205 (2025).

[81] X. Zhang, Y. Liu, X. Cao, and D. He, Thermodynamic precision in nonequilibrium critical quantum systems, Phys. Rev. B **111**, 235401 (2025).

[82] A. Fick, Ueber diffusion, Ann. Phys. **170**, 59 (1855).

[83] A. Einstein, Über die von der molekularkinetischen theorie der wärme geforderte bewegung von in ruhenden flüssigkeiten suspendierten teilchen, Ann. Phys. (Berlin, Ger.) **322**, 549 (1905).

[84] C. R. Rao, Information and the accuracy attainable in the estimation of statistical parameters, in *Breakthroughs in Statistics. Springer Series in Statistics*, edited by S. Kotz and N. L. Johnson (Springer, New York, NY, 1992), pp. 235–247.

[85] H. Cramér, *Mathematical Methods of Statistics* (Princeton University Press, Princeton, 1946).

[86] S. M. Kay, *Fundamentals of Statistical Signal Processing: Estimation Theory* (Prentice-Hall, Inc., USA, 1993).

[87] E. Robertson, N. Šibalić, R. Potvliege, and M. Jones, Arc 3.0: An expanded Python toolbox for atomic physics calculations, Comput. Phys. Commun. **261**, 107814 (2021).

[88] V. Weisskopf and E. Wigner, Berechnung der natürlichen Linienbreite auf Grund der Diracschen Lichttheorie, Z. Phys. **63**, 54 (1930).

[89] A. Nitzan, *Chemical Dynamics in Condensed Phases: Relaxation, Transfer and Reactions in Condensed Molecular Systems* (Oxford University Press, 2006).

[90] M. Radaelli, G. T. Landi, K. Modi, and F. C. Binder, Fisher information of correlated stochastic processes, New J. Phys. **25**, 053037 (2023).

[91] A. G. Dijkstra and Y. Tanimura, The role of the environment time scale in light-harvesting efficiency and coherent oscillations, New J. Phys. **14**, 073027 (2012).

[92] D. Xu and J. Cao, Non-canonical distribution and non-equilibrium transport beyond weak system-bath coupling regime: A polaron transformation approach, Front. Phys. **11**, 110308 (2016).

[93] G. Engelhardt and J. Cao, Unusual dynamical properties of disordered polaritons in microcavities, Phys. Rev. B **105**, 064205 (2022).

[94] G. Engelhardt, A. Bhoonah, and W. V. Liu, Detecting axion dark matter with Rydberg atoms via induced electric dipole transitions, Phys. Rev. Res. **6**, 023017 (2024).

[95] S. E. Harris, Electromagnetically induced transparency, Phys. Today **50**(7), 36 (1997).

[96] M. D. Lukin, M. Fleischhauer, M. O. Scully, and V. L. Velichansky, Intracavity electromagnetically induced transparency, Opt. Lett. **23**, 295 (1998).

[97] Numerical data and source code are available at: https://www.georg-engelhardt-research.de.